Generalized Continuum Modelling of Crystal Plasticity

Samuel Forest
MINES ParisTech
Centre des Matériaux
CNRS UMR 7633
BP 87 91003 Evry Cedex, France

1 Cosserat crystal plasticity

The classical theory of continuum crystal plasticity is first recalled and then generalized to incorporate the effect of lattice curvature on material hardening. The specific notations used in this chapter are summarized in section 1.6.

1.1 Dislocation densities and classical continuum crystal plasticity

Elements from a statistical theory of dislocations The yielding and hardening behaviour of crystals mainly depends on the growth of the dislocation population and on the development of dislocation structures inside the volume element V of continuum mechanics. A precise account of the evolution of dislocation distribution in V still lies beyond current computing capacity, although promising results in that field are available Fivel et al. (1998). The incomplete information about the dislocation state permits probability predictions and suggests the use of statistical mechanics. Kröner proposed that the information be given in terms of n-point dislocation correlation tensor functions Kröner (1969, 1971). If the vectors $\underline{\boldsymbol{\xi}}(\underline{\boldsymbol{x}})$ and $\underline{\boldsymbol{b}}(\underline{\boldsymbol{x}})$ describe the line vector and Burgers vector of a dislocation located at $\underline{\boldsymbol{x}}$, the first correlation function reads :

$$\underset{\sim}{\boldsymbol{\alpha}} = < \underline{\boldsymbol{b}} \otimes \underline{\boldsymbol{\xi}} > \tag{1}$$

where the brackets denote ensemble averaging. The next correlation function then is :

$$\underset{\sim}{\boldsymbol{\alpha}}(\underline{\boldsymbol{x}}, \underline{\boldsymbol{x}}') = < (\underline{\boldsymbol{b}} \otimes \underline{\boldsymbol{\xi}})(\underline{\boldsymbol{x}}) \otimes (\underline{\boldsymbol{b}} \otimes \underline{\boldsymbol{\xi}})(\underline{\boldsymbol{x}}') > = \underset{\sim}{\boldsymbol{\alpha}}(\underline{\boldsymbol{x}} - \underline{\boldsymbol{x}}') \tag{2}$$

C. Sansour et al. (eds.), *Generalized Continua and Dislocation Theory*

if statistical uniformity is assumed. Second and fourth rank tensors $\underset{\sim}{\boldsymbol{\alpha}}$ and $\underset{\approx}{\boldsymbol{\alpha}}$ are indeed related to classical plastic state indicators used in classical crystal plasticity. For a large enough volume element V, it is resorted to the ergodic hypothesis so that ensemble averaging is replaced by volume averaging over V. In that case, $\underset{\sim}{\boldsymbol{\alpha}}$ turns out to be identical to the so-called dislocation density tensor, or Nye's tensor, which is the basic variable of the continuum theory of dislocations Nye (1953). On the other hand, one invariant of the tensor $\underset{\approx}{\boldsymbol{\alpha}}$ can be shown to be

$$\alpha_{ijij}(\underline{\mathbf{0}}) = L/V \tag{3}$$

where L is the length of dislocation lines inside V. The dislocation density ϱ well-known in the field of metallurgy.

Classical thermomechanics of single crystals Classical crystal plasticity theory is the paradigm of the model for anisotropic finite deformation plasticity. It has been founded in the original references Teodosiu (1970); Mandel (1971, 1973); Rice (1971); Teodosiu and Sidoroff (1976). More recent accounts of this continuum approach show the success of this approach based on multiplicative decomposition and the use of scalar dislocation densities ϱ Maugin (1992); Teodosiu (1997); Gumbsch and Pippan (2005); Bertram (2005). It is useful to recall the basis of this theory before generalizing it to include the effect of the dislocation density tensor.

The main field equations of continuum thermomechanics are:

- energy principle (local form)

$$\rho\dot{\epsilon} = \underset{\sim}{\boldsymbol{\sigma}} : \underset{\sim}{\boldsymbol{D}} + \rho r - div\, \underline{\boldsymbol{q}}$$

  where $\underset{\sim}{\boldsymbol{D}}$ is the strain rate tensor, $\underset{\sim}{\boldsymbol{\sigma}}$ the Cauchy stress and $\underline{\boldsymbol{q}}$ the heat flux vector.
- entropy principle (local form)

$$\rho\dot{\eta} + div\left(\frac{\underline{\boldsymbol{q}}}{T}\right) - \frac{\rho r}{T} \geq 0$$

  where η is the specific entropy function.
- Clausius-Duhem inequality

$$-\rho(\dot{e} - T\dot{\eta}) + \underset{\sim}{\boldsymbol{\sigma}} : \underset{\sim}{\boldsymbol{D}} - \frac{\underline{\boldsymbol{q}}}{T}.grad\, T \geq 0$$

  The Helmholtz free energy density $\psi = \epsilon - Ts$ is introduced:

$$-\rho(\dot{\psi} + \eta\dot{T}) + \underset{\sim}{\boldsymbol{\sigma}} : \underset{\sim}{\boldsymbol{D}} - \frac{\underline{\boldsymbol{q}}}{T}.grad\, T \geq 0$$

- intrinsic and thermal dissipation

$$D^{th} = -\frac{\boldsymbol{q}}{T}.grad\,T$$

$$D^{i} = -\rho(\dot{\psi} + s\dot{T}) + \underset{\sim}{\boldsymbol{\sigma}} : \underset{\sim}{\boldsymbol{D}}$$

The gradient of the transformation is called the deformation gradient $\underset{\sim}{\boldsymbol{F}}$. It is decomposed into elastic and plastic parts as shown in figure 1(a):

$$\underset{\sim}{\boldsymbol{F}} = \underset{\sim}{\boldsymbol{F}}^{e}.\underset{\sim}{\boldsymbol{F}}^{p} \tag{4}$$

The uniqueness of this decomposition is ensured in the case of the single crystal material element if the orientation of the intermediate configuration is such that the lattice vectors do not rotate from the initial to the intermediate configuration. This unique intermediate configuration is called isoclinic by Mandel (1973). The elastic strain and a stress tensor are defined with respect to the isoclinic configuration:

$$\underset{\sim}{\boldsymbol{E}}^{e} = \frac{1}{2}(\underset{\sim}{\boldsymbol{F}}^{e}.\underset{\sim}{\boldsymbol{F}}^{eT} - \underset{\sim}{\mathbf{1}}), \quad \underset{\sim}{\boldsymbol{\Pi}}^{e} = \frac{\rho_i}{\rho}\underset{\sim}{\boldsymbol{F}}^{e-1}.\underset{\sim}{\boldsymbol{\sigma}}.\underset{\sim}{\boldsymbol{F}}^{e-T} \tag{5}$$

The power of internal forces makes the link between the different stress tensors:

$$\frac{1}{\rho}\underset{\sim}{\boldsymbol{\sigma}} : (\dot{\underset{\sim}{\boldsymbol{F}}}.\underset{\sim}{\boldsymbol{F}}^{-1}) = \frac{1}{\rho_i}(\underset{\sim}{\boldsymbol{\Pi}}^{e} : \dot{\underset{\sim}{\boldsymbol{E}}}^{e} + (\underset{\sim}{\boldsymbol{F}}^{eT}.\underset{\sim}{\boldsymbol{F}}^{e}.\underset{\sim}{\boldsymbol{\Pi}}^{e}) : (\dot{\underset{\sim}{\boldsymbol{F}}}^{p}.\underset{\sim}{\boldsymbol{F}}^{p-1})) \tag{6}$$

The Clausius–Duhem inequality takes now the form

$$\rho(\frac{\underset{\sim}{\boldsymbol{\Pi}}^{e}}{\rho_i} - \frac{\partial\Psi}{\partial\underset{\sim}{\boldsymbol{E}}^{e}}) : \dot{\underset{\sim}{\boldsymbol{E}}}^{e} - \rho(s + \frac{\partial\Psi}{\partial T})\dot{T} - \rho\frac{\partial\Psi}{\partial\alpha} : \dot{\alpha} + D^{res} \geq 0 \tag{7}$$

The state variables are $(\underset{\sim}{\boldsymbol{E}}^{e}, T, \alpha)$ with additional internal variables α. The state functions are the internal energy density $e(\underset{\sim}{\boldsymbol{E}}^{e}, \eta, \alpha)$ and the Helmholtz free energy density $\psi(\underset{\sim}{\boldsymbol{E}}^{e}, T, \alpha)$. The exploitation of the second principle à la Coleman–Noll provides the state laws

$$\underset{\sim}{\boldsymbol{\Pi}}^{e} = \rho_i\frac{\partial\Psi}{\partial\underset{\sim}{\boldsymbol{E}}^{e}}, \quad X = \rho_i\frac{\partial\Psi}{\partial\alpha}, \quad s = -\frac{\partial\Psi}{\partial T} \tag{8}$$

The residual dissipation then reads

$$D^{res} = \underset{\sim}{\boldsymbol{M}} : (\dot{\underset{\sim}{\boldsymbol{F}}}^{p}.\underset{\sim}{\boldsymbol{F}}^{p-1}) - X\dot{\alpha} \geq 0 \tag{9}$$

This leads to the definition of the so–called Mandel stress tensor:

$$\underset{\sim}{\boldsymbol{M}} := \underset{\sim}{\boldsymbol{F}}^{eT}.\underset{\sim}{\boldsymbol{F}}^{e}.\underset{\sim}{\boldsymbol{\Pi}}^{e} = \underset{\sim}{\boldsymbol{C}}^{e}.\underset{\sim}{\boldsymbol{\Pi}}^{e} \tag{10}$$

We assume the existence of a convex dissipation potential $\Omega(\underset{\sim}{\boldsymbol{M}}, X)$ from which the flow rule and evolution equations for internal variables are derived:

$$\dot{\underset{\sim}{\boldsymbol{F}}}^p . \underset{\sim}{\boldsymbol{F}}^{p-1} = \frac{\partial \Omega}{\partial \underset{\sim}{\boldsymbol{M}}}, \quad \dot{\alpha} = -\frac{\partial \Omega}{\partial X} \tag{11}$$

We present now a template model for single crystal behaviour introducing the specific internal variables: "dislocation density" ϱ^s, internal structure α^s. Take the free energy function as

$$\rho^i \psi(\underset{\sim}{\boldsymbol{E}}^e, \varrho^s, \alpha^s) = \frac{1}{2} \underset{\sim}{\boldsymbol{E}}^e : \underset{\approx}{\boldsymbol{c}} : \underset{\sim}{\boldsymbol{E}}^e + r_0 \sum_{s=1}^{N} \varrho^s + \frac{1}{2} q \sum_{r,s=1}^{N} h^{rs} \varrho^r \varrho^s + \frac{1}{2} \sum_{s=1}^{N} \alpha^{s2} \tag{12}$$

The state laws then read

$$\begin{aligned} \underset{\sim}{\boldsymbol{\Pi}}^e &= \rho^i \frac{\partial \psi}{\partial \underset{\sim}{\boldsymbol{E}}^e} = \underset{\approx}{\boldsymbol{c}} : \underset{\sim}{\boldsymbol{E}}^e \\ r^s &= \rho^i \frac{\partial \psi}{\partial \varrho^s} = r_0 + q \sum_{r=1}^{N} h^{sr} \varrho^s \\ x^s &= \rho^i \frac{\partial \psi}{\partial \alpha^s} = c \alpha^s \end{aligned}$$

The driving force for plastic slip is the resolved shear stress on slip system s

$$\tau^s = (\underset{\sim}{\boldsymbol{M}} . \underline{\boldsymbol{n}}^s) . \underline{\boldsymbol{m}}^s = \underset{\sim}{\boldsymbol{M}} : (\underline{\boldsymbol{m}}^s \otimes \underline{\boldsymbol{n}}^s) \tag{13}$$

The multimechanism crystal plasticity yield criterion for single crystal is Schmid's law:

$$f^s = |\tau^s - x^s| - r^s \tag{14}$$

The yield threshold is r^s. An internal stress (back–stress) x^s is introduced for each system s. Take the dissipation potential

$$\Omega(\underset{\sim}{\boldsymbol{M}}, r^s, x^s) = \frac{K}{n+1} \sum_{s=1}^{N} \langle \frac{f^s}{K} \rangle^{n+1} \tag{15}$$

from which flow and hardening rules are derived

$$\dot{\underset{\sim}{\boldsymbol{\varepsilon}}}^p = \frac{\partial \Omega}{\partial \underset{\sim}{\boldsymbol{\sigma}}} = \sum_{s=1}^{N} \dot{\gamma}^s \underline{\boldsymbol{m}}^s \overset{sym}{\otimes} \underline{\boldsymbol{n}}^s, \quad \dot{\varrho}^s = -\frac{\partial \Omega}{\partial r^s} = \dot{v}^s, \quad \dot{\alpha}^s = -\frac{\partial \Omega}{\partial x^s} = \dot{\gamma}^s \tag{16}$$

with

$$\dot{v}^s = \langle \frac{f^s}{K} \rangle^n, \quad \dot{\gamma}^s = \dot{v}^s \, sign(\tau^s - r^s) \tag{17}$$

Nonlinear hardening rules are more realistic for actual materials in the form:

- nonlinear isotropic hardening

$$\varrho^s = 1 - \exp(-bv^s), \quad r^s = r_0 + q\sum_{r=1} h^{sr}(1 - \exp(-bv^s)) \tag{18}$$

- nonlinear kinematic hardening

$$\dot{\alpha}^s = \dot{\gamma}^s - d\dot{v}^s\alpha^s \tag{19}$$

For monotonic loading, this equation integrates in

$$x^s = \frac{c}{d}(\pm 1 - \exp(-dv^s)) \tag{20}$$

The isotropic hardening involves an interaction matrix between slip systems. This corresponds to the notion of latent hardening Besson et al. (2001); Fivel and Forest (2004). The general form of this matrix for FCC crystals is

	$B4$	$B2$	$B5$	$D4$	$D1$	$D6$	$A2$	$A6$	$A3$	$C5$	$C3$	$C1$
$B4$	h_1	h_2	h_2	h_4	h_5	h_5	h_5	h_6	h_3	h_5	h_3	h_6
$B2$		h_1	h_2	h_5	h_3	h_6	h_4	h_5	h_5	h_5	h_6	h_3
$B5$			h_1	h_5	h_6	h_3	h_5	h_3	h_6	h_4	h_5	h_5
$D4$				h_1	h_2	h_2	h_6	h_5	h_3	h_6	h_3	h_5
$D1$					h_1	h_2	h_3	h_5	h_6	h_5	h_5	h_4
$D6$						h_1	h_5	h_4	h_5	h_3	h_6	h_5
$A2$							h_1	h_2	h_2	h_6	h_5	h_3
$A6$								h_1	h_2	h_3	h_5	h_6
$A3$									h_1	h_5	h_4	h_5
$C5$										h_1	h_2	h_2
$C3$											h_1	h_2
$C1$												h_1

A simplified form of the matrix is $h_1 = 1, \quad h_2 = h_3 = h_4 = h_5 = h_6 = h$. If additionally $h = 1$, we obtain Taylor hardening.

Improved evolution equations for continuum crystal plasticity are obtained by comparing continuum and discrete dislocation dynamics methods Šiška et al. (2009).

1.2 A Cosserat theory for elastoviscoplastic single crystals at finite deformation

Mandel Mandel (1973) introduced the notion of oriented microelements characterized by some hidden directors into the theory of elastoviscoplasticity. The epoch-making expression "trièdre directeur" is directly taken

from the Cosserat brothers' well-known work Cosserat and Cosserat (1909). The relative rotation of neighbouring microelements may induce local couple stresses. To a first approximation Mandel neglects them and regards the single crystal and the polycrystal as a classical continuum. We propose here the strict treatment of the single crystal as a Cosserat continuum.

Nye noticed that after bending or torsion a crystal contains excess dislocations of a definite sign that give rise to lattice curvature Nye (1953). In a modelling of single crystals with more reference to dislocations, this additional deformation possibility should be taken into account. Kröner claimed that the macroscopic response of a medium to lattice curvature is the existence of actual Cosserat couple stresses Kröner (1963). The couple-stresses may be of the same order of magnitude as force-stresses under some circumstances Hehl and Kröner (1958); McClintock et al. (1958). In these early works Kröner regards the dislocated crystal as a Cosserat medium. However, his theory deals with symmetric force-stresses and he suggests later that there may be fundamental differences between dislocation theory and Cosserat theory Kröner, E. (1967).

The reason for such a misunderstanding stems from the frequent use in literature of the Cosserat continuum as the medium in which single dislocations may be embedded. Kessel computes the force and couple stress fields around a screw and an edge dislocation in a Cosserat continuum Kessel (1970). In this chapter, we claim that the continuum containing a large number of dislocations in the sense of the continuum theory of dislocations, can be modelled as a Cosserat continuum. Kröner argues that the rotation of the crystal lattice with dislocations is not the eigenrotation of physical particles but the rotation of a structure. This pleads against the constrained Cosserat theory that is usually used in the continuum theory of dislocations. As a result, in the Cosserat theory presented here, the rotational degrees of freedom are independent of the displacement field. Whereas the definition of the Cosserat directors involved in the continuum theory of dislocation is left unspecified, the "trièdre directeur" in this work is clearly made of three orthogonal lattice vectors attached to each volume element. As for them, Claus and Eringen also erect a lattice triad at every point of the continuum Eringen and Claus (1970). A most interesting point in their work is that they resort to a micromorphic continuum. They also propose a phenomenological treatment of micromorphic elastoplasticity but they do not derive the crystallographic expressions of plastic slip and curvature nor the necessary constitutive equations.

The characteristic size of the volume element must be such that it contains a large number of dislocations and that a mean crystal orientation can be unambiguously defined at each time. The elements of the presented

theory have been proposed in Forest et al. (1997). They have been recently extended and implemented in finite element code by Clayton et al. (2006); Mayeur et al. (2011).

Kinematics of the Cosserat continuum A material point $M \in \mathrm{V}$ at time t_0 is described by its position $\underline{\boldsymbol{X}}$ and its inner state, for an arbitrary initial placement, chosen as the reference configuration. At time t, its position is $\underline{\boldsymbol{x}}\,(\underline{\boldsymbol{X}}\,,t)$ and its inner state $\underset{\sim}{\boldsymbol{R}}(\underline{\boldsymbol{X}}\,,t)$, in a given reference frame E. If $(\underline{\boldsymbol{d}}_i)_{i=1,3}$ are three orthogonal lattice vectors in a released state at t and $(\underline{\boldsymbol{d}}_i^{\,0})_{i=1,3}$ their initial position in E, then the rotation $\underline{\boldsymbol{R}}$ is defined through

$$\underline{\boldsymbol{d}}_i \;=\; \underset{\sim}{\boldsymbol{R}}.\underline{\boldsymbol{d}}_i^{\,0}, \quad \textit{with} \quad \underset{\sim}{\boldsymbol{R}}.\underset{\sim}{\boldsymbol{R}}^T \;=\; \underset{\sim}{\mathbf{1}}, \quad \underset{\sim}{\boldsymbol{R}}(\underline{\boldsymbol{X}}\,,t_0) \;=\; \underset{\sim}{\mathbf{1}} \;\textit{and}\; \textit{Det}\,\underset{\sim}{\boldsymbol{R}} \;=\; 1 \tag{21}$$

A rotating frame $E^\sharp(M)$ is attached to the lattice structure at each point $M \in \mathrm{V}$ and each tensor variable y considered with respect to $E^\sharp$ will be denoted ${}^\sharp y$.

The rotation field $\underset{\sim}{\boldsymbol{R}}(\underline{\boldsymbol{X}}\,,t)$ can be replaced by the vector field $\underline{\boldsymbol{\Phi}}\,(\underline{\boldsymbol{X}}\,,t)$ given by equation (118). The three components of $\underline{\boldsymbol{\Phi}}$ are three degrees of freedom of the continuum in addition to the three components of the displacement field

$$\underline{\boldsymbol{u}}\,(\underline{\boldsymbol{X}}\,,t) \;=\; \underline{\boldsymbol{x}}\,(\underline{\boldsymbol{X}}\,,t) \;-\; \underline{\boldsymbol{X}} \tag{22}$$

Here, $\underline{\boldsymbol{u}}$ and $\underline{\boldsymbol{\Phi}}$ are regarded as independent kinematic variables which can be connected only on the balance or constitutive level or by some constraint.

The deformation gradient classically links a current infinitesimal material segment $d\underline{\boldsymbol{x}}$ with its initial position $d\underline{\boldsymbol{X}}$

$$d\underline{\boldsymbol{x}} \;=\; \underset{\sim}{\boldsymbol{F}}.d\underline{\boldsymbol{X}} \tag{23}$$

so that

$$\underset{\sim}{\boldsymbol{F}} \;=\; \underline{\boldsymbol{u}} \otimes \boldsymbol{\nabla} \;=\; u_{i,j}\;\underline{\boldsymbol{e}}_i \otimes \underline{\boldsymbol{e}}_j \tag{24}$$

(in the absence of other indication, partial derivatives are taken with respect to the X_j).

Similarly, we compute the variation $d\underset{\sim}{\boldsymbol{R}}$ of microrotation along a material segment $d\underline{\boldsymbol{X}}$. Defining $\delta\underline{\boldsymbol{\Phi}}$ by

$$(d\underset{\sim}{\boldsymbol{R}}).\underset{\sim}{\boldsymbol{R}}^T \;=\; \underset{\sim}{\mathbf{1}} \times \delta\underline{\boldsymbol{\Phi}} \;=\; \underset{\approx}{\boldsymbol{\epsilon}}.\delta\underline{\boldsymbol{\Phi}} \tag{25}$$

we derive

$$\delta\underline{\boldsymbol{\Phi}} \;=\; -\frac{1}{2}\,\underset{\approx}{\boldsymbol{\epsilon}} : (d\underset{\sim}{\boldsymbol{R}}.\underset{\sim}{\boldsymbol{R}}^T) \;=\; \underset{\sim}{\boldsymbol{\Gamma}}\; d\underline{\boldsymbol{X}} \tag{26}$$

with

$$\underset{\sim}{\boldsymbol{\Gamma}} \;=\; \frac{1}{2}\,\underset{\approx}{\boldsymbol{\epsilon}} : (\underset{\sim}{\boldsymbol{R}}.(\underset{\sim}{\boldsymbol{R}}^T \otimes \boldsymbol{\nabla})) \tag{27}$$

The notation $\delta\underline{\boldsymbol{\Phi}}$ means that $\delta\underline{\boldsymbol{\Phi}}$ is not a total differential, as can be seen from (26). Contrary to $\underset{\sim}{\boldsymbol{F}}$, $\underset{\sim}{\boldsymbol{\Gamma}}$ generally is not invertible. With respect to the local space frame $E^\sharp$,

$$^\sharp d\underline{\boldsymbol{x}} \;=\; {}^\sharp\underset{\sim}{\boldsymbol{F}}.d\underline{\boldsymbol{X}} \quad \textit{and} \quad {}^\sharp\delta\underline{\boldsymbol{\Phi}} \;=\; {}^\sharp\underset{\sim}{\boldsymbol{\Gamma}}.d\underline{\boldsymbol{X}} \tag{28}$$

where $^\sharp d\underline{\boldsymbol{x}} \;=\; \underset{\sim}{\boldsymbol{R}}^T.d\underline{\boldsymbol{x}}$ and $^\sharp\delta\underline{\boldsymbol{\Phi}} \;=\; \underset{\sim}{\boldsymbol{R}}^T.\delta\underline{\boldsymbol{\Phi}}$ and

$$^\sharp\underset{\sim}{\boldsymbol{F}} \;=\; \underset{\sim}{\boldsymbol{R}}^T.\underset{\sim}{\boldsymbol{F}}, \quad {}^\sharp\underset{\sim}{\boldsymbol{\Gamma}} \;=\; \underset{\sim}{\boldsymbol{R}}^T.\underset{\sim}{\boldsymbol{\Gamma}} \tag{29}$$

It can be seen that the relative measures $^\sharp\underset{\sim}{\boldsymbol{F}}$ and $^\sharp\underset{\sim}{\boldsymbol{\Gamma}}$ are invariant under any Euclidean transformation Kafadar and Eringen (1971). Accordingly they are natural Cosserat strains for the development of constitutive equations. They are called respectively the Cosserat deformation tensor and the wryness (or bend-twist, or torsion-curvature) tensor. An alternative expression of the wryness tensor is then

$$^\sharp\underset{\sim}{\boldsymbol{\Gamma}} \;=\; -\frac{1}{2}\,\underline{\underline{\boldsymbol{\epsilon}}} : (\underset{\sim}{\boldsymbol{R}}^T.(\underset{\sim}{\boldsymbol{R}} \otimes \boldsymbol{\nabla})) \tag{30}$$

One defines next the velocity and the gyration tensor Stojanović (1970); Eringen (1976)

$$\underline{\boldsymbol{v}} \;=\; \underline{\dot{\boldsymbol{u}}} \;=\; \dot{u}_i\,\underline{\boldsymbol{e}}_i \quad \textit{and} \quad \underset{\sim}{\boldsymbol{v}} \;=\; \dot{\underset{\sim}{\boldsymbol{R}}}.\underset{\sim}{\boldsymbol{R}}^T \tag{31}$$

which can be replaced by the associated gyration vector

$$\overset{\times}{\underline{\boldsymbol{v}}} \;=\; -\frac{1}{2}\,\underline{\underline{\boldsymbol{\epsilon}}} : \underset{\sim}{\boldsymbol{v}} \tag{32}$$

since it is antisymmetric. The time derivative of the Cosserat strains can be related to the gradient of the latter quantities:

$$^\sharp\dot{\underset{\sim}{\boldsymbol{F}}}.{}^\sharp\underset{\sim}{\boldsymbol{F}}^{-1} \;=\; \underset{\sim}{\boldsymbol{R}}^T.(\underline{\boldsymbol{v}} \otimes \boldsymbol{\nabla}^c \;-\; \underset{\sim}{\boldsymbol{1}} \times \overset{\times}{\underline{\boldsymbol{v}}}).\underset{\sim}{\boldsymbol{R}} \tag{33}$$

$$^\sharp\dot{\underset{\sim}{\boldsymbol{\Gamma}}}.{}^\sharp\underset{\sim}{\boldsymbol{F}}^{-1} \;=\; \underset{\sim}{\boldsymbol{R}}^T.(\overset{\times}{\underline{\boldsymbol{v}}} \otimes \boldsymbol{\nabla}^c).\underset{\sim}{\boldsymbol{R}} \tag{34}$$

where $\boldsymbol{\nabla}^c \;=\; \dfrac{\partial}{\partial x_i}\,\underline{\boldsymbol{e}}_i \;=\; \underset{\sim}{\boldsymbol{F}}^{-T}\,\boldsymbol{\nabla}$ (Euclidean representation, c stands for current).
$\underline{\boldsymbol{v}} \otimes \boldsymbol{\nabla}^c \;-\; \underset{\sim}{\boldsymbol{v}}$ is the relative velocity gradient and describes the local motion of the material element with respect to the microstructure.

Sthenics In order to introduce forces and stresses and to deduce the equilibrium equations, we resort to the method of virtual power developed by Germain in the case of micromorphic media Germain (1973b). The virtual motions are the velocity $\underline{\boldsymbol{v}}$ and the gyration $\overset{\times}{\underline{\boldsymbol{v}}}$ (or microrotation rate vector). The next step is to choose the form of the virtual power of a system of forces. Within the framework of a first gradient theory, the virtual power of the internal forces is a linear form of the virtual motions and their gradient. The principle of material frame indifference requires that this linear form should be invariant under any Euclidean transformation. That is why we will work with the objective quantities $\underline{\boldsymbol{v}} \otimes \boldsymbol{\nabla}^c - \underset{\sim}{\boldsymbol{v}}$ and $\overset{\times}{\underline{\boldsymbol{v}}} \otimes \boldsymbol{\nabla}^c$. The dual quantities involved in the linear form of the virtual power of the internal forces are denoted $\underset{\sim}{\boldsymbol{\sigma}}$ and $\underset{\sim}{\boldsymbol{\mu}}$ respectively and are assumed to be objective tensors. For objectivity reasons the dual variable associated with $\underline{\boldsymbol{v}}$ is zero. For any subdomain $D \subset V$

$$
\begin{aligned}
P^{(i)} &= -\int_D \left(\underset{\sim}{\boldsymbol{\sigma}} : (\underline{\boldsymbol{v}} \otimes \boldsymbol{\nabla}^c - \underset{\sim}{\boldsymbol{v}}) + \underset{\sim}{\boldsymbol{\mu}} : (\overset{\times}{\underline{\boldsymbol{v}}} \otimes \boldsymbol{\nabla}^c) \right) dV \\
&= -\int_D \left(\sigma_{ij}\, v_{i,j} + \mu_{ij}\, \overset{\times}{v}_{i,j} - \sigma_{ij}\, v_{ij} \right) dV \\
&= -\int_D \left(\sigma_{ij}\, v_i + \mu_{ij} \overset{\times}{v}_i \right)_{,j} dV \qquad (35) \\
&+ \int_D \left(\sigma_{ij,j}\, v_i + (\mu_{ij,j} - \epsilon_{ikl}\, \sigma_{kl})\, \overset{\times}{v}_i \right) dV \qquad (36) \\
&= -\int_{\partial D} \left(\underline{\boldsymbol{v}}\, \underset{\sim}{\boldsymbol{\sigma}} + \overset{\times}{\underline{\boldsymbol{v}}}\, \underset{\sim}{\boldsymbol{\mu}} \right) . \underline{\boldsymbol{n}}\, dS \\
&+ \int_D \left(\underline{\boldsymbol{v}} . div\, \underset{\sim}{\boldsymbol{\sigma}} + \overset{\times}{\underline{\boldsymbol{v}}} . (div\, \underset{\sim}{\boldsymbol{\mu}} + 2 \overset{\times}{\underline{\boldsymbol{\sigma}}}) \right) dV \qquad (37)
\end{aligned}
$$

(in this section the partial derivatives are taken with respect to the current configuration). The virtual power of external forces reads

$$
P^{(e)} = \int_D \left(\underline{\boldsymbol{f}} . \underline{\boldsymbol{v}} + \underline{\boldsymbol{c}} . \overset{\times}{\underline{\boldsymbol{v}}} \right) dS \qquad (38)
$$

The virtual power of contact forces must then be defined

$$
P^{(c)} = \int_{\partial D} \left(\underline{\boldsymbol{t}} . \underline{\boldsymbol{v}} + \underline{\boldsymbol{m}} . \overset{\times}{\underline{\boldsymbol{v}}} \right) dS \qquad (39)
$$

The dual quantities of the velocity and microrotation rate in $P^{(e)}$ and $P^{(i)}$ have the dimensions of force and moment respectively. The principle of

virtual power then states that

$$\forall D \subset V, \forall (\underline{\boldsymbol{v}}, \overset{\times}{\underline{\boldsymbol{v}}}) \quad P^{(i)} + P^{(e)} + P^{(c)} = 0 \tag{40}$$

In particular

$$\forall D \subset V, \forall (\underline{\boldsymbol{v}}, \overset{\times}{\underline{\boldsymbol{v}}}) \; / \; \underline{\boldsymbol{v}} = \overset{\times}{\underline{\boldsymbol{v}}} = 0 \;\; on \; \partial D, \tag{41}$$

$$\int_D \left(\underline{\boldsymbol{v}} . (div \; \underset{\sim}{\boldsymbol{\sigma}} + \underline{\boldsymbol{f}}) + \overset{\times}{\underline{\boldsymbol{v}}} . (div \; \underset{\sim}{\boldsymbol{\mu}} + 2 \overset{\times}{\underline{\boldsymbol{\sigma}}} + \underline{\boldsymbol{c}}) \right) dV = 0 \tag{42}$$

Assuming that the quantities are continuous on V, the local equilibrium equations follow from (42)

$$\left\{ \begin{array}{l} div \; \underset{\sim}{\boldsymbol{\sigma}} + \underline{\boldsymbol{f}} = 0 \\ div \; \underset{\sim}{\boldsymbol{\mu}} + 2 \overset{\times}{\underline{\boldsymbol{\sigma}}} + \underline{\boldsymbol{c}} = 0 \end{array} \right. \tag{43}$$

As a result, the principle of virtual power becomes

$$\forall D \subset V, \forall (\underline{\boldsymbol{v}}, \overset{\times}{\underline{\boldsymbol{v}}}) \quad \int_{\partial D} \left((\underset{\sim}{\boldsymbol{\sigma}} . \underline{\boldsymbol{n}} - \underline{\boldsymbol{t}}) . \underline{\boldsymbol{v}} + (\underset{\sim}{\boldsymbol{\mu}} . \underline{\boldsymbol{n}} - \underline{\boldsymbol{m}}) . \overset{\times}{\underline{\boldsymbol{v}}} \right) dV = 0 \tag{44}$$

from which the boundary conditions are deduced

$$\left\{ \begin{array}{l} \underset{\sim}{\boldsymbol{\sigma}} . \underline{\boldsymbol{n}} = \underline{\boldsymbol{t}} \\ \underset{\sim}{\boldsymbol{\mu}} . \underline{\boldsymbol{n}} = \underline{\boldsymbol{m}} \end{array} \right. \tag{45}$$

$\underset{\sim}{\boldsymbol{\sigma}}$ is called the Cauchy force stress tensor and $\underset{\sim}{\boldsymbol{\mu}}$ the couple-stress tensor. They are generally not symmetric.

Hyperelasticity

Energy balance Let ϵ be the internal energy per unit mass, $\underline{\boldsymbol{q}}$ the heat flux vector, ρ the current density. The energy balance equation reads then

$$\rho \, \dot{\epsilon} = \underset{\sim}{\boldsymbol{\sigma}} : (\underline{\boldsymbol{v}} \otimes \boldsymbol{\nabla}^c - \underset{\sim}{\boldsymbol{v}}) + \underset{\sim}{\boldsymbol{\mu}} : (\overset{\times}{\underline{\boldsymbol{v}}} \otimes \boldsymbol{\nabla}^c) - div \; \underline{\boldsymbol{q}} \tag{46}$$

(any other inner heat supply is excluded).

According to the thermodynamics of irreversible processes, the entropy principle is written

$$\rho \, \dot{\eta} + div \left(\frac{\underline{\boldsymbol{q}}}{T} \right) \geq 0 \tag{47}$$

where T denotes the temperature and η the entropy per unit mass.

Introducing the free energy $\psi = \epsilon - \eta\, T$ and combining the energy and entropy equations, one derives the Clausius-Duhem inequality

$$-\rho\,(\dot{\psi} + \eta\dot{T}) + {}^\sharp\underset{\sim}{\boldsymbol{\sigma}} : ({}^\sharp\dot{\underset{\sim}{\boldsymbol{F}}}.{}^\sharp\underset{\sim}{\boldsymbol{F}}^{-1}) + {}^\sharp\underset{\sim}{\boldsymbol{\mu}} : ({}^\sharp\dot{\underset{\sim}{\boldsymbol{\Gamma}}}.{}^\sharp\underset{\sim}{\boldsymbol{F}}^{-1}) - \frac{1}{T}\,\underline{\boldsymbol{q}}.T\boldsymbol{\nabla}^c \geq 0 \quad (48)$$

where

$$\left\{\begin{array}{l} {}^\sharp\underset{\sim}{\boldsymbol{\sigma}} = \underset{\sim}{\boldsymbol{R}}^T.\underset{\sim}{\boldsymbol{\sigma}}.\underset{\sim}{\boldsymbol{R}} \\ {}^\sharp\underset{\sim}{\boldsymbol{\mu}} = \underset{\sim}{\boldsymbol{R}}^T.\underset{\sim}{\boldsymbol{\mu}}.\underset{\sim}{\boldsymbol{R}} \end{array}\right. \quad (49)$$

are rotated stress tensors with respect to the space frame $E^\sharp$ attached to the microstructure.

A material is said to be hyperelastic if its free energy and entropy are functions of ${}^\sharp\underset{\sim}{\boldsymbol{F}}$, ${}^\sharp\underset{\sim}{\boldsymbol{\Gamma}}$ and temperature only. The Clausius-Duhem inequality (48) becomes

$$-\left(\rho\,\frac{\partial\psi}{\partial^\sharp\underset{\sim}{\boldsymbol{F}}} - {}^\sharp\underset{\sim}{\boldsymbol{\sigma}}.{}^\sharp\underset{\sim}{\boldsymbol{F}}^{-T}\right) : {}^\sharp\dot{\underset{\sim}{\boldsymbol{F}}} \qquad -\left(\rho\,\frac{\partial\psi}{\partial^\sharp\underset{\sim}{\boldsymbol{\Gamma}}} - {}^\sharp\underset{\sim}{\boldsymbol{\mu}}.{}^\sharp\underset{\sim}{\boldsymbol{F}}^{-T}\right) : {}^\sharp\dot{\underset{\sim}{\boldsymbol{\Gamma}}}$$
$$-\left(\rho\,\eta + \rho\,\frac{\partial\psi}{\partial T}\right)\dot{T} - \frac{1}{T}\,\underline{\boldsymbol{q}}.T\boldsymbol{\nabla}^c \geq 0$$

Since this expression is linear in ${}^\sharp\dot{\underset{\sim}{\boldsymbol{F}}}$, ${}^\sharp\dot{\underset{\sim}{\boldsymbol{\Gamma}}}$ and $\dot{T}$, the last inequality implies

$$\eta = -\frac{\partial\psi}{\partial T} \quad (50)$$

and

$$\left\{\begin{array}{l} {}^\sharp\underset{\sim}{\boldsymbol{\sigma}} = \rho\,\dfrac{\partial\psi}{\partial^\sharp\underset{\sim}{\boldsymbol{F}}}.{}^\sharp\underset{\sim}{\boldsymbol{F}}^T \\ {}^\sharp\underset{\sim}{\boldsymbol{\mu}} = \rho\,\dfrac{\partial\psi}{\partial^\sharp\underset{\sim}{\boldsymbol{\Gamma}}}.{}^\sharp\underset{\sim}{\boldsymbol{F}}^T \end{array}\right. \quad (51)$$

Linear case; isotropic elasticity Strain and torsion-curvature are small if $\|{}^\sharp\underset{\sim}{\boldsymbol{F}} - \underset{\sim}{\mathbf{1}}\| \ll 1$ and $\|{}^\sharp\underset{\sim}{\boldsymbol{\Gamma}}\|\, l \ll 1$, where l is a characteristic length. If, in addition, microrotations remain small, i.e. if $\|\underline{\boldsymbol{\Phi}}\| \ll 1$, then

$$\left\{\begin{array}{l} \underset{\sim}{\boldsymbol{R}} \simeq \underset{\sim}{\mathbf{1}} + \underset{\sim}{\mathbf{1}} \times \underline{\boldsymbol{\Phi}} = \underset{\sim}{\mathbf{1}} - \underset{\sim}{\boldsymbol{\epsilon}}.\underline{\boldsymbol{\Phi}} \\ {}^\sharp\underset{\sim}{\boldsymbol{F}} \simeq \underset{\sim}{\mathbf{1}} + \underline{\boldsymbol{u}} \otimes \boldsymbol{\nabla} + \underset{\sim}{\boldsymbol{\epsilon}}.\underline{\boldsymbol{\Phi}} = \underset{\sim}{\mathbf{1}} + \underset{\sim}{\boldsymbol{e}} \\ {}^\sharp\underset{\sim}{\boldsymbol{\Gamma}} \simeq \underline{\boldsymbol{\Phi}} \otimes \boldsymbol{\nabla} = \underset{\sim}{\boldsymbol{\kappa}} \end{array}\right. \quad (52)$$

Furthermore, ${}^\sharp\underset{\sim}{\boldsymbol{\sigma}} \simeq \underset{\sim}{\boldsymbol{\sigma}}$ and ${}^\sharp\underset{\sim}{\boldsymbol{\mu}} \simeq \underset{\sim}{\boldsymbol{\mu}}$. Accordingly, for linear elasticity, two four-rank elasticity tensors are introduced

$$\left\{\begin{array}{l} \underset{\sim}{\boldsymbol{\sigma}} = \underset{\approx}{\boldsymbol{E}} : \underset{\sim}{\boldsymbol{e}} \\ \underset{\sim}{\boldsymbol{\mu}} = \underset{\approx}{\boldsymbol{C}} : \underset{\sim}{\boldsymbol{\kappa}} \end{array}\right. \quad (53)$$

(No coupling between strain and torsion-curvature is possible as soon as point symmetry is assumed even for the less symmetric solid Kessel (1964)). Some symmetry properties of these tensors are derived from the hyperelasticity conditions (51)

$$E_{ijkl} \;=\; E_{klij} \;\; and \;\; C_{ijkl} \;=\; C_{klij} \tag{54}$$

Further symmetry conditions can be gained if material symmetries are taken into account. The form of the Cosserat elasticity tensors for all symmetry classes has been established by Kessel Kessel (1964). For a triclinic solid, 90 independent constants are necessary instead of 21 in the classical case (for a solid without point symmetry, Kessel found 171 constants!). We now consider the example of isotropic elasticity. The two classical Lamé constants λ, μ are complemented by 4 additional parameters according to

$$\left\{ \begin{array}{rcl} \underset{\sim}{\boldsymbol{\sigma}} & = & \lambda \, \underset{\sim}{\mathbf{1}} \, Tr \, \underset{\sim}{\boldsymbol{e}} \;+\; 2\mu \, \{\underset{\sim}{\boldsymbol{e}}\} \;+\; 2\mu_c \, \}\underset{\sim}{\boldsymbol{e}}\{ \\ \underset{\sim}{\boldsymbol{\mu}} & = & \alpha \, \underset{\sim}{\mathbf{1}} \, Tr \, \underset{\sim}{\boldsymbol{\kappa}} \;+\; 2\beta \, \{\underset{\sim}{\boldsymbol{\kappa}}\} \;+\; 2\gamma \, \}\underset{\sim}{\boldsymbol{\kappa}}\{ \end{array} \right. \tag{55}$$

Elastoplastic Cosserat single crystals The works of Sawczuk, Lippmann and Besdo are the first milestones in the plasticity theory of Cosserat continua at small strains Sawczuk (1967); Lippmann (1969); Besdo (1974). In the case of single crystals we resort to recent results in Cosserat theory at large strains Sievert (1992); Sansour (1998b).

Strain decomposition In single crystals, non-homogeneous plastic deformations induce non-homogeneous permanent lattice rotations, which are associated with plastic lattice curvature. That is why elastic and plastic Cosserat deformations and curvatures are introduced: ${}^\sharp\underset{\sim}{\boldsymbol{F}}^e, {}^\sharp\underset{\sim}{\boldsymbol{F}}^p, {}^\sharp\underset{\sim}{\boldsymbol{\Gamma}}^e$ *and* ${}^\sharp\underset{\sim}{\boldsymbol{\Gamma}}^p$. Strain partition rules must then be proposed.

The multiplicative decomposition proposed in Mandel (1971) is adopted here but only for the Cosserat deformation gradient

$${}^\sharp\underset{\sim}{\boldsymbol{F}} \;=\; {}^\sharp\underset{\sim}{\boldsymbol{F}}^e . {}^\sharp\underset{\sim}{\boldsymbol{F}}^p \tag{56}$$

The expression

$${}^\sharp\dot{\underset{\sim}{\boldsymbol{F}}} . {}^\sharp\underset{\sim}{\boldsymbol{F}}^{-1} \;=\; {}^\sharp\dot{\underset{\sim}{\boldsymbol{F}}}^e . {}^\sharp\underset{\sim}{\boldsymbol{F}}^{e-1} \;+\; {}^\sharp\underset{\sim}{\boldsymbol{F}}^e . {}^\sharp\dot{\underset{\sim}{\boldsymbol{F}}}^p . {}^\sharp\underset{\sim}{\boldsymbol{F}}^{p-1} . {}^\sharp\underset{\sim}{\boldsymbol{F}}^{e-1} \tag{57}$$

has to be substituted in the Clausius-Duhem inequality (48). The most natural assumption is that the hyperelastic relations still have the form

$$\left\{ \begin{array}{rcl} {}^\sharp\underset{\sim}{\boldsymbol{\sigma}} & = & \rho \, \dfrac{\partial \psi}{\partial {}^\sharp\underset{\sim}{\boldsymbol{F}}^e} . {}^\sharp\underset{\sim}{\boldsymbol{F}}^{eT} \\ {}^\sharp\underset{\sim}{\boldsymbol{\mu}} & = & \rho \, \dfrac{\partial \widetilde{\psi}}{\partial {}^\sharp\underset{\sim}{\boldsymbol{\Gamma}}^e} . {}^\sharp\underset{\sim}{\boldsymbol{F}}^{eT} \end{array} \right. \tag{58}$$

It has been proved in Sievert (1992) that the multiplicative decomposition (56) results from the hyperelastic relation (58)a. Similarly, for the relations (58) to hold the form of the decomposition of the overall curvature tensor cannot be arbitrary. One must have :

$$^{\sharp}\underset{\sim}{\boldsymbol{\Gamma}} \;=\; ^{\sharp}\underset{\sim}{\boldsymbol{\Gamma}}^{e}.^{\sharp}\underset{\sim}{\boldsymbol{F}}^{p} \;+\; ^{\sharp}\underset{\sim}{\boldsymbol{\Gamma}}^{p} \tag{59}$$

An elastic-plastic decomposition of displacement or rotation like in Steinmann (1994) is not recommended, because these non-objective variables can not be connected with the quantities energy and dissipation. Such a connection is possible only on the level of strains. The form of the decomposition (59) is similar to that used by Eringen and Kafadar for the symmetry transformation of a Cosserat fluid. The decomposition (59) has been assumed in Dluzewski (1991). Then the elastic constitutive equations (58) follow necessarily.

The previous decompositions of total deformation and curvature, together with the hyperelastic relations (58) make it possible to define a unique intermediate isoclinic configuration for which force and couple stresses are simultaneously released. This is illustrated by the actualized picture of Cosserat crystal plasticity in figure 1(b).

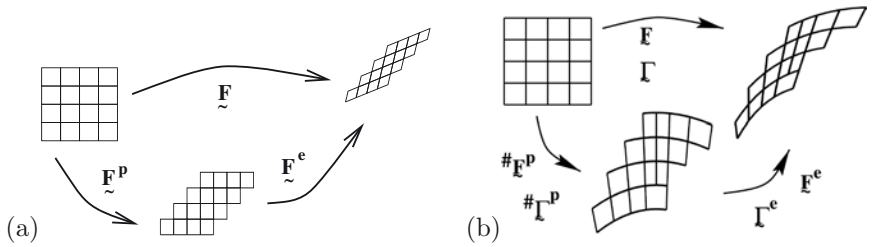

Figure 1. Kinematics of classical crystal plasticity (a) and Cosserat crystal crystal plasticity (b).

Kinematics of elastoplastic Cosserat single crystals The plastic deformation of single crystals is the result of slip processes on slip systems. For each slip system s, we define

$$\underline{\boldsymbol{m}}^{s} \;=\; \underline{\boldsymbol{b}}^{s}/\|\underline{\boldsymbol{b}}^{s}\| \tag{60}$$

where $\underline{\boldsymbol{b}}^s$ is the Burgers vector. $\underline{\boldsymbol{n}}^s$ is the unit vector normal to the slip plane. As a result, the plastic strain rate takes the form

$$ {}^\sharp\dot{\underset{\sim}{\boldsymbol{F}}}^p.{}^\sharp\underset{\sim}{\boldsymbol{F}}^{p-1} \;=\; \sum_{s\in S} \dot\gamma^s \; {}^\sharp\underset{\sim}{\boldsymbol{P}}^s \tag{61} $$

γ^s is the amount of slip for the system s. ${}^\sharp\underset{\sim}{\boldsymbol{P}}^s$ is given by the kinematics of slip

$$ {}^\sharp\underset{\sim}{\boldsymbol{P}}^s \;=\; {}^\sharp\underline{\boldsymbol{m}}^s \otimes {}^\sharp\underline{\boldsymbol{n}}^s \tag{62} $$

If we go back to the Eulerian representation

$$ \underline{\boldsymbol{v}} \otimes \boldsymbol{\nabla}^c \;=\; \dot{\underset{\sim}{\boldsymbol{F}}}.\underset{\sim}{\boldsymbol{F}}^{-1} \;=\; \dot{\underset{\sim}{\boldsymbol{R}}}.\underset{\sim}{\boldsymbol{R}}^T \;+\; \underset{\sim}{\boldsymbol{R}}.{}^\sharp\dot{\underset{\sim}{\boldsymbol{F}}}^e.{}^\sharp\underset{\sim}{\boldsymbol{F}}^{e-1}.\underset{\sim}{\boldsymbol{R}}^T \tag{63} $$

$$ +\quad \underset{\sim}{\boldsymbol{R}}.{}^\sharp\underset{\sim}{\boldsymbol{F}}^e.{}^\sharp\dot{\underset{\sim}{\boldsymbol{F}}}^p.{}^\sharp\underset{\sim}{\boldsymbol{F}}^{p-1}.{}^\sharp\underset{\sim}{\boldsymbol{F}}^{e-1}.\underset{\sim}{\boldsymbol{R}}^T, \tag{64} $$

we can split the last expression into its symmetric and skew–symmetric parts:

$$ {}^{\{}\underline{\boldsymbol{v}} \otimes \boldsymbol{\nabla}^{c\}} \;=\; {}^{\{}\underset{\sim}{\boldsymbol{R}}.{}^\sharp\dot{\underset{\sim}{\boldsymbol{F}}}^e.{}^\sharp\underset{\sim}{\boldsymbol{F}}^{e-1}.\underset{\sim}{\boldsymbol{R}}^{T\}} \;+\; \sum_{s\in S} \dot\gamma^s \; {}^{\{}\,{}^\star\underline{\boldsymbol{m}}^s \otimes {}^\star\underline{\boldsymbol{n}}^{s\}} \tag{65} $$

and

$$ {}^{\}}\underline{\boldsymbol{v}} \otimes \underline{\boldsymbol{\nabla}}^{c\{} - \dot{\underset{\sim}{\boldsymbol{R}}}.\underset{\sim}{\boldsymbol{R}}^T \;=\; {}^{\}}\underset{\sim}{\boldsymbol{R}}.{}^\sharp\dot{\underset{\sim}{\boldsymbol{F}}}^e.{}^\sharp\underset{\sim}{\boldsymbol{F}}^{e-1}.\underset{\sim}{\boldsymbol{R}}^{T\{} + \sum_{s\in S} \dot\gamma^s \; {}^{\}}\,{}^\star\underline{\boldsymbol{m}}^s \otimes {}^\star\underline{\boldsymbol{n}}^{s\{} \tag{66} $$

where we have noted

$$ {}^\star\underline{\boldsymbol{m}}^s \;=\; \underset{\sim}{\boldsymbol{R}}.{}^\sharp\underset{\sim}{\boldsymbol{F}}^e.{}^\sharp\underline{\boldsymbol{m}}^s \;\; \textit{and} \;\; {}^\star\underline{\boldsymbol{n}}^s \;=\; \underset{\sim}{\boldsymbol{R}}.{}^\sharp\underset{\sim}{\boldsymbol{F}}^{e-T}.{}^\sharp\underline{\boldsymbol{n}}^s \tag{67} $$

Equation (66) clearly shows that the relative rotation rate of material lines with respect to the microstructure is due to the lattice rotation associated with slip processes, if elastic contributions are neglected.

We would like to compare the proposed formulation with Mandel's work. We are working with invariant tensors written in the microstructure space frame in order to get rid of undetermined rotations. An equivalent method is to deal with the so-called isoclinic configuration introduced by Teodosiu and Mandel Teodosiu (1970); Mandel (1971). Their description reads

$$ \underset{\sim}{\boldsymbol{F}} \;=\; \underset{\sim}{\boldsymbol{E}}.\underset{\sim}{\boldsymbol{P}} \tag{68} $$

where the rotation $\underset{\sim}{\boldsymbol{R}}^{isoclinic}$ appearing in the polar decomposition of $\underset{\sim}{\boldsymbol{E}}$ links the isoclinic reference frame to the working space frame. As a result comparing (56) and (68) one can think of the equivalence

$$ \underset{\sim}{\boldsymbol{E}} \;=\; \underset{\sim}{\boldsymbol{R}}\,{}^\sharp\underset{\sim}{\boldsymbol{F}}^e \tag{69} $$

However, considering the respective polar decompositions

$$\underset{\sim}{\boldsymbol{E}} \;=\; \underset{\sim}{\boldsymbol{R}}^{isoclinic}\,\underset{\sim}{\boldsymbol{U}}^{e} \quad and \quad {}^{\sharp}\underset{\sim}{\boldsymbol{F}}^{e} \;=\; \underset{\sim}{\boldsymbol{R}}^{e}\,\underset{\sim}{\boldsymbol{U}}^{e} \tag{70}$$

we should have then

$$\underset{\sim}{\boldsymbol{R}}^{isoclinic} \;=\; \underset{\sim}{\boldsymbol{R}}.\underset{\sim}{\boldsymbol{R}}^{e} \tag{71}$$

Regarding the elastic behaviour in the classical case, lattice vectors are material vectors with respect to the intermediate configuration. Within the proposed framework this is not exactly true any more. There is an additional rotation $\underset{\sim}{\boldsymbol{R}}^{e}$ of material fibres with respect to the microstructure, that could be attributed to the presence of heterogeneities. Nevertheless the constitutive theory must be such that $\underset{\sim}{\boldsymbol{R}}^{e}$ remains a corrective term. The equivalence of the two theories is established if ${}^{\sharp}\underset{\sim}{\boldsymbol{F}}^{e}$ is symmetric.

The plastic lattice curvature and torsion are due to the presence of dislocations with a non-vanishing resulting Burgers vector. The curvature planes and torsion axes are therefore related to crystallographic directions. They can be represented by the effect of continuous edge and screw dislocations for each slip system. That is why we propose the following kinematics for the plastic wryness

$${}^{\sharp}\dot{\underset{\sim}{\boldsymbol{\Gamma}}}^{p}.{}^{\sharp}\underset{\sim}{\boldsymbol{F}}^{p-1} \;=\; \sum_{s\in S}\frac{\dot{\theta}^{s}}{l}\,{}^{\sharp}\underset{\sim}{\boldsymbol{Q}}^{s} \tag{72}$$

The θ^{s} are angles that measure the plastic curvature and torsion over a characteristic length l. Explicit forms for ${}^{\sharp}\underset{\sim}{\boldsymbol{Q}}^{s}$ are given in section 4.1. In section 3.4.2 an alternative more simple treatment for the plastic curvature is proposed.

Dissipation In the Clausius-Duhem inequality (48), a contribution to the overall entropy production is due to the development of rotation gradients. If no hardening variables are introduced, the intrinsic dissipation rate is

$$\begin{aligned}\dot{D} \;&=\; \underset{\sim}{\boldsymbol{\sigma}} \;:\; \underset{\sim}{\boldsymbol{R}}.{}^{\sharp}\underset{\sim}{\boldsymbol{F}}^{e}.{}^{\sharp}\dot{\underset{\sim}{\boldsymbol{F}}}^{p}.{}^{\sharp}\underset{\sim}{\boldsymbol{F}}^{p-1}.{}^{\sharp}\underset{\sim}{\boldsymbol{F}}^{e-1}.\underset{\sim}{\boldsymbol{R}}^{T}\\ &+\; \underset{\sim}{\boldsymbol{\mu}} \;:\; \underset{\sim}{\boldsymbol{R}}.{}^{\sharp}\underset{\sim}{\boldsymbol{\Gamma}}^{e}.{}^{\sharp}\dot{\underset{\sim}{\boldsymbol{F}}}^{p}.{}^{\sharp}\underset{\sim}{\boldsymbol{F}}^{p-1}.{}^{\sharp}\underset{\sim}{\boldsymbol{F}}^{e-1}\;\underset{\sim}{\boldsymbol{R}}^{T} + \underset{\sim}{\boldsymbol{\mu}} \;:\; \underset{\sim}{\boldsymbol{R}}.{}^{\sharp}\dot{\underset{\sim}{\boldsymbol{\Gamma}}}^{p}.{}^{\sharp}\underset{\sim}{\boldsymbol{F}}^{-1}.\underset{\sim}{\boldsymbol{R}}^{T}\end{aligned} \tag{73}$$

Taking (61) and (72) into account,

$$\dot{D} \;=\; \sum_{s\in S}\dot{\gamma}^{s}\,\underset{\sim}{\boldsymbol{\sigma}} \;:\; {}^{\star}\underset{\sim}{\boldsymbol{P}}^{s} + \sum_{s\in S}\dot{\theta}^{s}\,\underset{\sim}{\boldsymbol{\mu}} \;:\; {}^{\star}\underset{\sim}{\boldsymbol{Q}}^{s} + \underset{\sim}{\boldsymbol{\mu}} \;:\; \underset{\sim}{\boldsymbol{R}}.{}^{\sharp}\underset{\sim}{\boldsymbol{\Gamma}}^{e}.{}^{\sharp}\dot{\underset{\sim}{\boldsymbol{F}}}^{p}.{}^{\sharp}\underset{\sim}{\boldsymbol{F}}^{p-1}.{}^{\sharp}\underset{\sim}{\boldsymbol{F}}^{e-1}.\underset{\sim}{\boldsymbol{R}}^{T} \tag{74}$$

where

$$\left\{\begin{array}{lcl} {}^{\star}\underset{\sim}{\boldsymbol{P}}^{s} &=& \underset{\sim}{\boldsymbol{R}}.{}^{\sharp}\underset{\sim}{\boldsymbol{F}}^{e}.{}^{\sharp}\underset{\sim}{\boldsymbol{P}}^{s}.{}^{\sharp}\underset{\sim}{\boldsymbol{F}}^{e-1}.\underset{\sim}{\boldsymbol{R}}^{T}\\ {}^{\star}\underset{\sim}{\boldsymbol{Q}}^{s} &=& \underset{\sim}{\boldsymbol{R}}.{}^{\sharp}\underset{\sim}{\boldsymbol{F}}^{e}.{}^{\sharp}\underset{\sim}{\boldsymbol{Q}}^{s}.{}^{\sharp}\underset{\sim}{\boldsymbol{F}}^{e-1}.\underset{\sim}{\boldsymbol{R}}^{T}\end{array}\right.$$

Three terms appear in the dissipation. The first one is the classical one: slip processes due to irreversible dislocation motion are dissipative. The second one is due to the evolution of plastic curvature and torsion. It is clear that homogeneous lattice rotation is definitely not a dissipative process but plastic curvature due to non-homogeneous lattice rotation is related to the existence of accommodation dislocations and therefore must be associated with dissipation. The last term reveals the independence of the elastic curvature-torsion measure from plastic changes of the material lines in the intermediate configuration. This is due to the lattice concept, which means that the elastic behaviour, established in (58), is primary not influenced by plastic straining. Thus, the elastic strain measures are related to lattice line-elements and the referring to material lines produces an additional term in the plastic wryness rate. However, at small elastic strains, this term vanishes.

1.3 Closure of the continuum theory of dislocations

Closure problem of the continuum theory of dislocations The origin of the continuum theory of dislocations goes back to Nye's epoch-making work Nye (1953). He introduced the dislocation density tensor $\underset{\sim}{\boldsymbol{\alpha}}$ and he established a link between $\underset{\sim}{\boldsymbol{\alpha}}$ and the lattice curvature. Kröner proposed a general presentation of the theory and gave the set of partial differential equations to be solved in the linear static case for a given distribution of dislocations and here for an infinite body Kröner (1958)

$$\left\{\begin{array}{l} \underset{\sim}{\boldsymbol{\beta}} \;=\; \underset{\sim}{\boldsymbol{\beta}}^{e} \;+\; \underset{\sim}{\boldsymbol{\beta}}^{p} \\ \underset{\sim}{\boldsymbol{\sigma}} \;=\; \underset{\approx}{\boldsymbol{E}} : \{\underset{\sim}{\boldsymbol{\beta}}^{e}\} \\ div\, \underset{\sim}{\boldsymbol{\sigma}} \;=\; 0 \\ curl\, \underset{\sim}{\boldsymbol{\beta}}^{e} \;=\; \underset{\approx}{\boldsymbol{\alpha}} \end{array}\right.$$

where $\underset{\sim}{\boldsymbol{\beta}} = \underline{\boldsymbol{u}} \otimes \boldsymbol{\nabla} = u_{i,j}\ \underline{\boldsymbol{e}}_i \otimes \underline{\boldsymbol{e}}_j$. In this part, we use Kröner's notations for historical reasons. It must be noted that strictly speaking the non-objective quantity $\underset{\sim}{\boldsymbol{\beta}}$ cannot be decomposed entirely into an elastic and plastic part but the usual notations of the continuum theory of dislocations and of classical plasticity theory can be reconciled by the concept of isoclinic configuration. The continuum theory of dislocations is a way to think of dislocation theory as a physical field theory. Despite the fact that the system (75) enables us to find the stress strain field around dislocations in some given arrangement, such a theory cannot bridge the gap between dislocation theory and plasticity theory since it does not predict the motion of dislocations: the dislocation distribution must be known at each step. In the dynamic theory of continuous distributions of dislocations, Kröner

and Mura, T. (1963) introduce the dislocation velocity tensor $\underset{\sim}{\underline{\boldsymbol{V}}}$ which is related to the plastic deformation rate $\underset{\sim}{\dot{\boldsymbol{\beta}}}^{p}$ by

$$\underset{\sim}{\dot{\boldsymbol{\beta}}}^{p} \;=\; -\left(\underset{\sim}{\underline{\boldsymbol{\epsilon}}} : \underset{\sim}{\underline{\boldsymbol{V}}}\right)^{T} \tag{75}$$

and we still have

$$\dot{\underset{\sim}{\boldsymbol{\alpha}}} \;=\; -curl\ \underset{\sim}{\dot{\boldsymbol{\beta}}}^{p} \tag{76}$$

For a single dislocation

$$\underset{\approx}{\underline{\underline{\boldsymbol{V}}}} \;=\; \underline{\boldsymbol{v}} \otimes \underline{\boldsymbol{\xi}} \otimes \underline{\boldsymbol{b}} \tag{77}$$

$\underline{\boldsymbol{v}}$ is the dislocation velocity vector, $\underline{\boldsymbol{\xi}}$ is the dislocation line vector (notation of Hirth and Lothe (1982)) and $\underline{\boldsymbol{b}}$ the Burgers vector. In this case stress and strain can be obtained provided that $\underset{\sim}{\boldsymbol{\alpha}}$ and $\underset{\sim}{\underline{\boldsymbol{V}}}$ are given at each time, which is of no help to derive a plasticity theory. For, the continuum theory of dislocations does not provide constitutive equations. As pointed out by Hahn and Jaunzemis (1973), in a complete theory of dislocations, the density and motion of dislocations should be derivable from the knowledge of initial conditions (and boundary conditions) only. This is what we call the closure problem of the continuum theory of dislocations.

Two attempts to derive the missing constitutive equations must be mentioned. On the one hand Mura showed how the von Mises yield criterion and Prandtl-Reuss relations can be explained in terms of the dislocation velocity tensor and a so-called "gliding force" Mura, T. (1965). The underlying constitutive assumption is a linear relation between $\underset{\sim}{\underline{\boldsymbol{V}}}$ and the gliding force. According to Lardner (1969); Eisenberg (1970), constitutive equations are also necessary to link plasticity and dislocation theories. On the other hand Hahn and Jaunzemis distinguish mobile dislocations (M) from immobile ones (I) with common line and Burgers vectors. $A^{ab} = A_I^{ab} + A_M^{ab}$ is the number of dislocations of Burgers vector $\underline{\boldsymbol{b}}^{a}$ and line vector $\underline{\boldsymbol{\xi}}^{b}$. Using a large strain formulation, (75) combined with (77) yields

$$\underset{\sim}{\dot{\boldsymbol{F}}}^{p}\ \underset{\sim}{\boldsymbol{F}}^{p-1} \;=\; \sum_{a,b} \underline{\boldsymbol{b}}^{a} \otimes (\underline{\boldsymbol{\xi}}^{b} \times \underline{\boldsymbol{v}}^{ab})\ A_M^{ab} \;=\; \sum_{a} A^a V^a\ \underline{\boldsymbol{b}}^{a} \otimes \underline{\boldsymbol{n}}^{a} \tag{78}$$

where $A^a V^a\ \underline{\boldsymbol{n}}^{a} = \sum_{b} A_M^{ab}\ \underline{\boldsymbol{\xi}}^{b} \times \underline{\boldsymbol{v}}^{ab}$ is normal to the slip plane. Evolution equations are proposed for A_I^a and A_M^a. Isotropic and kinematic hardening and a viscous stress are also introduced in the modelling.

Recent advances have been reported in the development of a dynamic continuum theory of dislocations Acharya (2010). Applications to continuum modelling of pile-ups around particles can be found in Taupin et al.

(2010). A common feature of such generalized continuum dislocations theories is that they are associated with the existence of lattice curvature induced back-stress and corresponding kinematic hardening Steinmann (1996); Forest (2008); Cordero et al. (2010).

Statistical description of dislocation distribution The dislocation network and the distribution of dislocation sources within a volume element of single crystal often is or becomes so intricate that an exact description of all dislocation lines and Burgers vectors must be abandoned. Instead some overall and statistical information about the distribution may be sufficient for the modelling of the plastic behaviour of the element. The only known attempts to develop a complete statistical theory of dislocations goes back to Zorski (1968) and Kröner (1969). The systematic approach comes up against tremendous difficulties which are still not overcome. This explains why the concepts reviewed in this section are only rudimentary tools which do not exhaust the complexity of dislocation structures.

Dislocation density tensor and the continuum theory of dislocations Within the framework of the continuum theory of dislocations, the characteristic size l of the volume element is taken large enough for the effects of the dislocations within it to be averaged. The distribution of dislocations is made continuous by letting $b = \|\underline{\boldsymbol{b}}\|$ approach zero and increasing the number n of dislocations of each kind so as to keep nb constant Nye (1953). The definition of the Burgers vector can be extended to continuous distributions of dislocations. For that purpose one refers to the kinematic description proposed by Mandel making use of the isoclinic configuration and of the strain partition given by (68). In (68), $\underset{\sim}{\boldsymbol{E}}$ relates the infinitesimal vectors $d\underline{\boldsymbol{\zeta}}$ and $d\underline{\boldsymbol{x}}$, where $d\underline{\boldsymbol{\zeta}}$ results from the cutting and releasing operations from the infinitesimal current lattice vector $d\underline{\boldsymbol{x}}$

$$d\underline{\boldsymbol{\zeta}} \;=\; \underset{\sim}{\boldsymbol{E}}^{-1}\, d\underline{\boldsymbol{x}} \tag{79}$$

From this, it can be seen that the decomposition (68) actually goes back to Bilby et al. (1957).

Accordingly, if S is a smooth surface containing $\underline{\boldsymbol{x}}$ in the current configuration and bounded by the closed line c, the true Burgers vector is defined as

$$\underline{\boldsymbol{b}} \;=\; \oint_c \underset{\sim}{\boldsymbol{E}}^{-1}.d\underline{\boldsymbol{x}} \tag{80}$$

The application of Stokes' formula (125) leads to the definition of the so-

called true dislocation density tensor

$$\underset{\sim}{\boldsymbol{\alpha}} \;=\; -curl^c\ \underset{\sim}{\boldsymbol{E}}^{-1} \;=\; \underset{\sim}{\boldsymbol{E}}^{-1} \times \boldsymbol{\nabla}^c \;=\; -\epsilon_{jkl}\ E^{-1}_{ik,l}\ \underline{\boldsymbol{e}}_i \otimes \underline{\boldsymbol{e}}_j \tag{81}$$

such that

$$\underline{\boldsymbol{b}} \;=\; \int_S \underset{\sim}{\boldsymbol{\alpha}}.\underline{\boldsymbol{n}}\ dS \tag{82}$$

If the surface is infinitesimal of normal $\underline{\boldsymbol{n}}$, $d\underline{\boldsymbol{b}} = \underset{\sim}{\boldsymbol{\alpha}}.\underline{\boldsymbol{n}}\ dS$ is the resulting true Burgers vector of dislocations crossing the surface dS. It is convenient to associate each component α_{ij} of the dislocation density tensor with a (super)dislocation characterized by its line vector $\underline{\boldsymbol{e}}_j$ and its Burgers vector $b_i\ \underline{\boldsymbol{e}}_i$ (no summation). As a result, the diagonal components of $\underset{\sim}{\boldsymbol{\alpha}}$ represent screw dislocations and the out-of-diagonal ones edge dislocations. For n dislocations per unit surface of Burgers vector $\underline{\boldsymbol{b}}$ and line vector $\underline{\boldsymbol{\xi}}$, we have

$$\underset{\sim}{\boldsymbol{\alpha}} \;=\; n\ \underline{\boldsymbol{b}} \otimes \underline{\boldsymbol{\xi}} \tag{83}$$

Scalar dislocation densities and crystal plasticity In the classical continuum theory of dislocations, the description of the dislocation distribution is restricted to the dislocation density tensor. It enables one to compute stress-strain fields for special distributions and even discrete dislocations for which $\underset{\sim}{\boldsymbol{\alpha}}$ becomes the sum of Dirac's functions. However the classical continuum theory of dislocations has failed to describe the elastoplastic behaviour of single crystals. The main reason is that the dislocation density tensor is not the relevant variable to explain the hardening processes. In Hahn and Jaunzemis (1973), the kinematics of plastic deformation are derived from the dislocation velocity tensor and corresponds exactly to the purely mechanical description of slip processes proposed by Mandel. The next step is the introduction of hardening variables as in the classical macroscopic plasticity theory. They are related to usual scalar dislocation densities that are commonly used by metal physicists and which represent the total length of dislocation lines within a volume element. The multiplication and interaction of dislocations is responsible for the hardening of single crystals and the scalar densities are reliable measures for it. This type of description culminates with the work of Mandel, Zarka and Teodosiu and Sidoroff Mandel (1971); Zarka (1972); Teodosiu and Sidoroff (1976). In these theories the dislocation density tensor is not even mentioned since it is not the relevant quantity any more. Constitutive equations for hardening variables are proposed in a more or less phenomenological way and several elementary dislocation interaction processes are taken into account.

The main successes of these theories are the modelling of the tensile behaviour of single crystals, the lattice rotations and the cyclic behaviour of single and polycrystals Cailletaud (1992).

Proposed description In this work we claim that both types of descriptions are required for the modelling of non-homogeneous deformation of single crystals. That is why the statistical description of dislocation distribution must contain at least:

• the dislocation density tensor $\underset{\sim}{\boldsymbol{\alpha}}$ which accounts for the resulting Burgers vector across any infinitesimal surface,

and

• scalar dislocation densities ρ^s or the associated hardening variables, for instance r^s and x^s already used in Méric and Cailletaud (1991). The kinematic hardening variables x_s are a measure for microscopically non-homogeneous spatial dislocation distributions that give rise to a vanishing resulting Burgers vector (dislocation cells...). Additional variables (densities of mobile and immobile dislocations...) may also be necessary.

It must be noted that the dislocation density tensor and the scalar dislocation densities are related respectively to the one-point and two-point dislocation correlations introduced by Kröner Kröner (1969), as explained in section 1.1.

The scalar dislocation densities are necessary to account for the hardening or softening behaviour of the material whereas the dislocation density tensor may play a significant role when strong lattice incompatibilities are present.

Link between the dislocation density tensor and the lattice torsion-curvature tensor

Classical analysis at small strains and small rotations Nye introduces the rotation vector $\underline{\boldsymbol{\Phi}}$ of the lattice and the curvature tensor $\underset{\sim}{\boldsymbol{\kappa}} = \underline{\boldsymbol{\Phi}} \otimes \boldsymbol{\nabla}$ At small strains and small rotations, the strain and rotation rate decomposition into elastic and plastic parts reads

$$\begin{aligned} \underset{\sim}{\dot{\boldsymbol{\beta}}} &= \underset{\sim}{\dot{\boldsymbol{\beta}}}^{e} + \underset{\sim}{\dot{\boldsymbol{\beta}}}^{p} = \underset{\sim}{\dot{\boldsymbol{\varepsilon}}} + \underset{\sim}{\boldsymbol{\omega}} \\ &= \underset{\sim}{\dot{\boldsymbol{\varepsilon}}}^{e} + \underset{\sim}{\boldsymbol{\omega}}^{e} + \underset{\sim}{\dot{\boldsymbol{\varepsilon}}}^{p} + \underset{\sim}{\boldsymbol{\omega}}^{p} \end{aligned}$$

$\underset{\sim}{\boldsymbol{\omega}}^{p} = \underset{\sim}{\boldsymbol{\omega}} - \underset{\sim}{\boldsymbol{\omega}}^{e} = \underset{\sim}{\boldsymbol{\omega}} - \underset{\sim}{\mathbf{1}} \times \underline{\dot{\boldsymbol{\Phi}}}^{e}$ represents the relative rotation of material lines with respect to the lattice. As a result, relation (76) becomes

$$\underset{\sim}{\dot{\boldsymbol{\alpha}}} = curl\ \underset{\sim}{\dot{\boldsymbol{\beta}}}^{e} = curl\ \underset{\sim}{\dot{\boldsymbol{\varepsilon}}}^{e} + curl\ \underset{\sim}{\boldsymbol{\omega}}^{e} \tag{84}$$

In a way similar to Kröner (1958), we derive

$$\begin{aligned} curl\ \underset{\sim}{\boldsymbol{\omega}}^e &= \epsilon_{jkl}\ \omega_{ik,l}\ \underline{\boldsymbol{e}}_i \otimes \underline{\boldsymbol{e}}_j \\ &= -\epsilon_{jkl}\ \epsilon_{ikm}\ \dot{\Phi}_{m,l}\ \underline{\boldsymbol{e}}_i \otimes \underline{\boldsymbol{e}}_j \\ &= -\epsilon_{klj}\epsilon_{kmi}\ \dot{\kappa}_{ml}\ \underline{\boldsymbol{e}}_i \otimes \underline{\boldsymbol{e}}_j \\ &= -(\delta_{ml}\delta_{ij}\ -\ \delta_{il}\delta_{mj})\ \dot{\kappa}_{ml}\underline{\boldsymbol{e}}_i \otimes \underline{\boldsymbol{e}}_j \\ &= \dot{\underset{\sim}{\boldsymbol{\kappa}}}^T\ -\ Tr\,\dot{\underset{\sim}{\boldsymbol{\kappa}}}\ \underset{\sim}{\mathbf{1}} \end{aligned}$$

Neglecting the elastic strain, one obtains the expression proposed by Nye and its inverse form

$$\underset{\sim}{\boldsymbol{\alpha}} = \underset{\sim}{\boldsymbol{\kappa}}^T\ -\ Tr\,\underset{\sim}{\boldsymbol{\kappa}}\ \underset{\sim}{\mathbf{1}}, \quad \underset{\sim}{\boldsymbol{\kappa}} = \underset{\sim}{\boldsymbol{\alpha}}^T\ -\ \frac{1}{2}\ Tr\,\underset{\sim}{\boldsymbol{\alpha}}\ \underset{\sim}{\mathbf{1}} \tag{85}$$

Keeping the elastic term

$$\underset{\sim}{\boldsymbol{\alpha}} = curl\ \underset{\sim}{\boldsymbol{\varepsilon}}^e\ +\ \underset{\sim}{\boldsymbol{\kappa}}^T\ -\ Tr\,\underset{\sim}{\boldsymbol{\kappa}}\ \underset{\sim}{\mathbf{1}} \tag{86}$$

Analysis for the Cosserat theory Within the framework of the Cosserat theory for single crystals presented in part 2, we propose the following definition for the true dislocation density tensor

$$\underset{\sim}{\boldsymbol{\alpha}} = -curl^c\ (^\sharp\underset{\sim}{\boldsymbol{F}}^{e-1}.\underset{\sim}{\boldsymbol{R}}^T) \tag{87}$$

We try now to link the dislocation density tensor and the wryness tensor. Equation (87) becomes

$$\underset{\sim}{\boldsymbol{\alpha}} = -\left(\epsilon_{jkl}\ \frac{\partial^\sharp F^{e-1}_{im}}{\partial x_l}\ R_{km}\ +\ ^\sharp F^{e-1}_{im}\ \epsilon_{jkl}\ R^T_{mk,L}\ F^{-1}_{Ll}\right)\ \underline{\boldsymbol{e}}_i \otimes \underline{\boldsymbol{e}}_j \tag{88}$$

(the comma denotes again a derivative with respect to the reference configuration). Note that,

$$\underset{\sim}{\boldsymbol{\Gamma}} = \frac{1}{2}\ \underline{\underline{\boldsymbol{\epsilon}}} : (\underset{\sim}{\boldsymbol{R}}.(\underset{\sim}{\boldsymbol{R}}^T \otimes \boldsymbol{\nabla})) \implies \underset{\sim}{\boldsymbol{R}}.(\underset{\sim}{\boldsymbol{R}}^T \otimes \boldsymbol{\nabla}) = \underline{\underline{\boldsymbol{\epsilon}}}.\underset{\sim}{\boldsymbol{\Gamma}} \tag{89}$$

or, in components,

$$R^T_{mk,l} = -R^T_{mu}\ \epsilon_{ukv}\ \Gamma_{vl} \tag{90}$$

As a result (87) can now be written

$$\begin{aligned} \underset{\sim}{\boldsymbol{\alpha}} &= \underset{\sim}{\boldsymbol{A}}^{el}\ -\ ^\sharp F^{e-1}_{im}\ R^T_{mu}\ \epsilon_{klj}\ \epsilon_{kvu}\ \Gamma_{vL}\ F^{-1}_{Ll}\ \underline{\boldsymbol{e}}_i \otimes \underline{\boldsymbol{e}}_j \\ &= \underset{\sim}{\boldsymbol{A}}^{el}\ +\ ^\sharp\underset{\sim}{\boldsymbol{F}}^{e-1}.\underset{\sim}{\boldsymbol{R}}^T.\left((\underset{\sim}{\boldsymbol{\Gamma}}.\underset{\sim}{\boldsymbol{F}}^{-1})^T\ -\ Tr\,(\underset{\sim}{\boldsymbol{\Gamma}}.\underset{\sim}{\boldsymbol{F}}^{-1})\ \underset{\sim}{\mathbf{1}}\right) \\ &= \underset{\sim}{\boldsymbol{A}}^{el}\ +\ ^\sharp\underset{\sim}{\boldsymbol{F}}^{e-1}.\left((^\sharp\underset{\sim}{\boldsymbol{\Gamma}}.^\sharp\underset{\sim}{\boldsymbol{F}}^{-1})^T\ -\ Tr\,(^\sharp\underset{\sim}{\boldsymbol{\Gamma}}.^\sharp\underset{\sim}{\boldsymbol{F}}^{-1})\ \underset{\sim}{\mathbf{1}}\right)\ \underset{\sim}{\boldsymbol{R}}^T \end{aligned}$$

where $\underset{\sim}{\boldsymbol{A}}^{el} = \epsilon_{jkl} \dfrac{\partial^\sharp F^{e-1}_{im}}{\partial x_l} R_{km}\, \underline{\boldsymbol{e}}_i \otimes \underline{\boldsymbol{e}}_j$. It can be checked that equation (86) is retrieved for small strains and rotations. We define

$$^\sharp\underset{\sim}{\boldsymbol{\alpha}} = \underset{\sim}{\boldsymbol{\alpha}}.\underset{\sim}{\boldsymbol{R}} \tag{91}$$

and $\underset{\sim}{\boldsymbol{R}}.^\sharp\underset{\sim}{\boldsymbol{F}}^e\ \underset{\sim}{\boldsymbol{\alpha}}$ can be interpreted as the Cosserat counterpart of the local dislocation density tensor introduced in the classical continuum theory of dislocations.

Geometrically necessary dislocations and statistically stored dislocations According to Ashby (1971), dislocations become stored in a plastically non-homogeneous solid for two reasons: dislocations are either required for the compatible deformation of various parts of the specimen or they accumulate by trapping each other in a random way. This gives rise on the one hand to the density ρ_G of so-called geometrically necessary dislocations and on the other hand to the density ρ_S of statistically stored dislocations. The density ρ_G can be computed approximately in some situations like plastic bending or punching. This variable comes directly from the continuum theory of dislocations and corresponds to the components of the dislocation density tensor $\underset{\sim}{\boldsymbol{\alpha}}$. In contrast, the density ρ_S belongs to the second group of variables that have been listed and called hardening variables. However, as shown by Ashby in the case of two-phase alloys, geometrically necessary dislocations may lead to additional hardening. In the following, we will try to model this coupling effect between the two types of variables that describe the dislocation distribution. The relative importance of ρ_G and ρ_S depends on the amount of overall plastic deformation, and on the type of solicitation. Clearly ρ_G can dominate in the case of strong deformation gradients.

1.4 Explicit constitutive equations

We propose a complete set of constitutive equations for the elastoviscoplastic deformation and intrinsic curvature of metal single crystals.

Kinematics of plastic deformation and curvature The plastic flow due to slip on various slip systems is given by equation (61). Similarly an expression of the plastic curvature evolution has been proposed (equation (72)). An expression of $^\sharp\underset{\sim}{\boldsymbol{Q}}^s$ is now derived from the analysis of the dislocation density tensor. The scalar γ^s represent the amount of slip due to the passage of dislocations of type s through the volume element. As for them the scalars θ^s represent the plastic curvature due to dislocations trapped in

the volume element of characteristic length l. We will assume that the curvature axes or say the expression ${}^\sharp\underset{\sim}{\boldsymbol{F}}^{e-1}.\left(({}^\sharp\underset{\sim}{\boldsymbol{\Gamma}}^{p}.{}^\sharp\underset{\sim}{\boldsymbol{F}}^{-1})^T \;-\; Tr\,({}^\sharp\underset{\sim}{\boldsymbol{\Gamma}}^{p}.{}^\sharp\underset{\sim}{\boldsymbol{F}}^{-1})\;\underset{\sim}{\mathbf{1}}\right)$ are given by the dislocation density tensor ${}^\sharp\underset{\sim}{\boldsymbol{\alpha}}$. Conversely, the curvature axes ${}^\sharp\underset{\sim}{\boldsymbol{\Gamma}}^{p}.{}^\sharp\underset{\sim}{\boldsymbol{F}}^{p-1}$ are then given by $\left(({}^\sharp\underset{\sim}{\boldsymbol{F}}^{e}.{}^\sharp\underset{\sim}{\boldsymbol{\alpha}})^T \;-\; \frac{1}{2}\,Tr\,({}^\sharp\underset{\sim}{\boldsymbol{F}}^{e}.{}^\sharp\underset{\sim}{\boldsymbol{\alpha}})\;\underset{\sim}{\mathbf{1}}\right).{}^\sharp\underset{\sim}{\boldsymbol{F}}^{e}$ for each type of dislocation. The amount of curvature θ^s will be computed using constitutive equations proposed in the next section. Furthermore we drop the factors ${}^\sharp\underset{\sim}{\boldsymbol{F}}^{e}$ for simplicity (small elastic strains). We must now distinguish :

Curvature due to edge dislocations ($\perp$)

For edge dislocations, ${}^\sharp\underset{\sim}{\boldsymbol{\alpha}} \;=\; b\;{}^\sharp\underline{\boldsymbol{m}} \;\otimes{}^\sharp\underline{\boldsymbol{\xi}}$.
$\underline{\boldsymbol{\xi}}$ is the dislocation line vector and the normal to the glide plane is defined as

$$\underline{\boldsymbol{n}} \;=\; \underline{\boldsymbol{m}} \times \underline{\boldsymbol{\xi}} \tag{92}$$

The associated curvature is then $b\;{}^\sharp\underline{\boldsymbol{\xi}} \;\otimes{}^\sharp\underline{\boldsymbol{m}}$, so that we take

$${}^\sharp\underset{\sim}{\boldsymbol{Q}}_{\perp} \;=\; {}^\sharp\underline{\boldsymbol{\xi}} \;\otimes{}^\sharp\underline{\boldsymbol{m}} \tag{93}$$

Arrays of edge dislocations of the same type give rise to lattice curvature in the plane $(\underline{\boldsymbol{m}}\,,\underline{\boldsymbol{b}}\,)$. The rotation vector $\underline{\boldsymbol{\Phi}}$ has the same direction as the dislocation line vector.

Torsion due to screw dislocations ($\odot$)

For a screw dislocation, ${}^\sharp\underset{\sim}{\boldsymbol{\alpha}} \;=\; b\;{}^\sharp\underline{\boldsymbol{m}} \;\otimes{}^\sharp\underline{\boldsymbol{m}}$
The associated curvature is then $b\;({}^\sharp\underline{\boldsymbol{m}} \;\otimes{}^\sharp\underline{\boldsymbol{m}} \;-\; \frac{1}{2}\;\underset{\sim}{\mathbf{1}})$, so that we take

$${}^\sharp\underset{\sim}{\boldsymbol{Q}}_{\odot} \;=\; {}^\sharp\underline{\boldsymbol{m}} \;\otimes{}^\sharp\underline{\boldsymbol{m}} \;-\; \frac{1}{2}\;\underset{\sim}{\mathbf{1}} \tag{94}$$

As a result screw dislocations cause lattice torsion about the three reference axes. Kröner Kröner (1958) noticed that a planar array of crossed screw dislocations with perpendicular Burgers vectors produces a twist of the lattice about the third direction. This is equivalent to a grain boundary of the second kind. Grain boundaries of the first kind are generated by an array of edge dislocations with parallel Burgers and line vectors. Note that the result (94) is different from that proposed in Dluzewski (1992),

$$\underset{\sim}{\boldsymbol{\Gamma}}^{Dluzewski} \;=\; b\;({}^\sharp\underline{\boldsymbol{m}} \otimes{}^\sharp\underline{\boldsymbol{m}} \;-\; \underset{\sim}{\mathbf{1}}) \tag{95}$$

which gives no torsion with respect to the dislocation line axis. This seems to hold only when the couple that can be derived from the classical stress

field around a screw dislocation is not released Friedel (1964); Hirth and Lothe (1982).

At last we give the proposed kinematics of the plastic lattice torsion-curvature

$$ {}^\sharp\dot{\underset{\sim}{\boldsymbol{\Gamma}}}^p . {}^\sharp\underset{\sim}{\boldsymbol{F}}^{p-1} \;=\; \sum_{s\in S} \left(\frac{\dot\theta^s_\perp}{l}\, {}^\sharp\underline{\boldsymbol{\xi}}^{\,s} \otimes {}^\sharp\underline{\boldsymbol{m}}^{\,s} \;+\; \frac{\dot\theta^s_\odot}{l}\, ({}^\sharp\underline{\boldsymbol{m}}^{\,s} \otimes {}^\sharp\underline{\boldsymbol{m}}^{\,s} \;-\; \frac{1}{2}\,\underset{\sim}{\mathbf{1}}) \right) \tag{96} $$

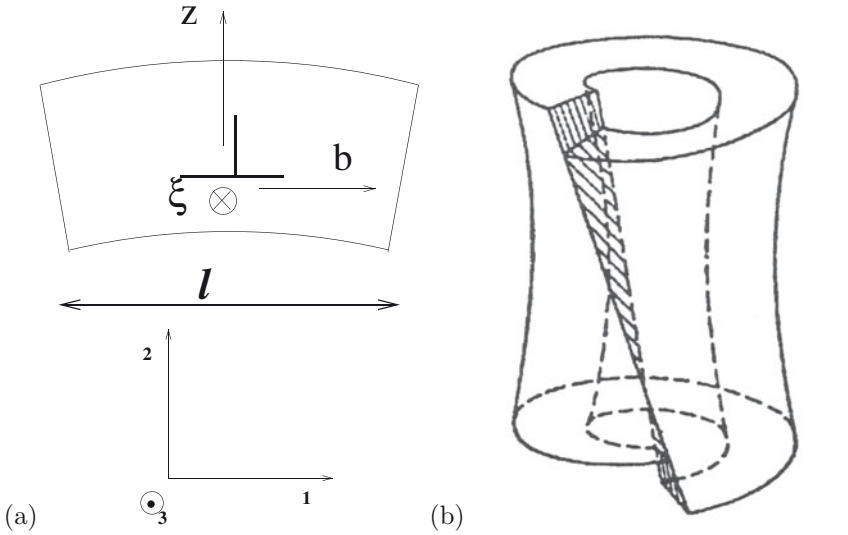

Figure 2. Lattice curvature induced by edge dislocations (a); lattice torsion induced by screw dislocations (b).

Generalized Schmid's law

Peach and Koehler's force Kröner shows that Peach and Koehler's formula giving the force on a dislocation $(\underline{\boldsymbol{b}}, \underline{\boldsymbol{\xi}})$ due to a stress field $\underset{\sim}{\boldsymbol{\sigma}}$ applies also for a non-symmetric stress tensor Kröner (1956). But it is important to derive again the formula taking care of any transposition. The force $\underline{\boldsymbol{f}}$ per unit length of dislocation is defined through

$$ \underline{\boldsymbol{f}}\,.d\underline{\boldsymbol{x}} \;=\; \underline{\boldsymbol{b}}\,.(\underset{\sim}{\boldsymbol{\sigma}}\;\underline{\boldsymbol{n}})\; dS \;=\; ((\underline{\boldsymbol{b}}\;\underset{\sim}{\boldsymbol{\sigma}}) \times \underline{\boldsymbol{\xi}}\,).d\underline{\boldsymbol{x}} \tag{97} $$

where

$$ \underline{\boldsymbol{n}}\; dS \;=\; \underline{\boldsymbol{\xi}} \times d\underline{\boldsymbol{x}} \tag{98} $$

The dislocation can move in its plane only if the component of the force in the glide plane

$$b\tau \;=\; \underline{\boldsymbol{f}}\,.(\underline{\boldsymbol{n}} \times \underline{\boldsymbol{\xi}}) \;=\; \underset{\sim}{\boldsymbol{\sigma}} : (\underline{\boldsymbol{b}} \otimes \underline{\boldsymbol{n}}) \tag{99}$$

reaches a threshold. This is the physical meaning of Schmid's criterion. We will use this criterion to compute the slip rate on slip system s

$$\dot{\gamma}^s \;=\; \left(\frac{Max(0, \mid \tau^s \;-\; x^s \mid \;-\; r^s)}{k^s} \right)^{n^s} \; sign\ (\tau^s \;-\; x^s) \tag{100}$$

where $\tau^s \;=\; {}^{\sharp}\underset{\sim}{\boldsymbol{\sigma}} \;:{}^{\sharp}\underset{\sim}{\boldsymbol{P}}^s$ according to (99), and x^s and r^s are internal kinematic and isotropic hardening variables. x^s and r^s represent respectively a back-stress and the yield threshold, which are supposed to describe with sufficient accuracy the dislocation structure with a view to modelling the hardening behaviour.

Evolution law for the viscoplastic torsion-curvature variables We consider an array of edge dislocations with $\underline{\boldsymbol{b}} \;=\; b\ \underline{\boldsymbol{e}}_1$, the normal to the glide plane $\underline{\boldsymbol{n}} \;=\; \underline{\boldsymbol{e}}_2$ *and* $\underline{\boldsymbol{\xi}} \;=\; -\underline{\boldsymbol{e}}_3$ (see figure 2). At small strains they produce a curvature

$$\underset{\sim}{\boldsymbol{\kappa}}^p \;=\; -nb\ \underline{\boldsymbol{e}}_3 \otimes \underline{\boldsymbol{e}}_1 \;=\; \kappa^p_{31}\ \underline{\boldsymbol{e}}_3 \otimes \underline{\boldsymbol{e}}_1 \tag{101}$$

We will assume that such geometrically necessary dislocations are produced by local dislocation sources if the local moment $\underset{\sim}{\boldsymbol{\mu}} \;=\; m\ \underline{\boldsymbol{e}}_3 \otimes \underline{\boldsymbol{e}}_1$ ($m < 0$ *here*) is so high that the imposed curvature cannot be accommodated elastically any longer.

Generalizing the previous example, we propose the following expression of the viscoplastic curvature rate

$$\dot{\theta}^s \;=\; \left(\frac{Max(0, \mid {}^{\sharp}\underset{\sim}{\boldsymbol{\mu}} : {}^{\sharp}\underset{\sim}{\boldsymbol{Q}}^s \mid \;-\; l\ r^s_c)}{l\ k_c} \right)^{n_c} \; sign\ ({}^{\sharp}\underset{\sim}{\boldsymbol{\mu}} : {}^{\sharp}\underset{\sim}{\boldsymbol{Q}}^s) \tag{102}$$

where r^s_c denotes the threshold and k_c and n_c is a viscosity parameter. The formula is to be applied successively for edge and screw dislocations belonging to the same system. Equations (100) and (102) and the hardening rules of the next section close the theory based on multicriteria and associative flow rules. Accordingly this theory is part of associative generalized plasticity.

Expression of the free energy and hardening rules The key-point of the thermodynamical analysis of a constitutive model for a dissipative

system is the choice of the relevant internal variables on which the free energy may depend. We propose such a formulation of the previous model in the linear case for simplicity. In addition to the observable variables deformation, curvature and temperature ($\underset{\sim}{\boldsymbol{e}}$, $\underset{\sim}{\boldsymbol{\kappa}}$, T) or equivalently ($\underset{\sim}{\boldsymbol{e}}^e$, $\underset{\sim}{\boldsymbol{\kappa}}^e$, T), the free energy is assumed to depend on the following internal variables:

- the variables ϱ_S^s, which are similar to the densities of statistically stored dislocations, and which are defined by

$$\dot{\varrho}_S^s = \mid \dot{\gamma}^s \mid \tag{103}$$

- the variables ϱ_G^s, which are similar to the densities of geometrically necessary dislocations, and which are defined by

$$\varrho_G^s = \mid \frac{b\theta^s}{l} \mid \tag{104}$$

- the kinematic hardening variables α^s.

We postulate then that the free energy is a quadratic form of these variables according to

$$\begin{aligned}
\rho\psi(\underset{\sim}{\boldsymbol{e}}^e, \underset{\sim}{\boldsymbol{\kappa}}^e, T, \alpha^s, \varrho_S^s, \varrho_G^s) &= \tfrac{1}{2}\, \underset{\sim}{\boldsymbol{e}}^e : \underset{\approx}{\boldsymbol{E}} : \underset{\sim}{\boldsymbol{e}}^e + \tfrac{1}{2}\, \underset{\sim}{\boldsymbol{\kappa}}^e : \underset{\approx}{\boldsymbol{C}} : \underset{\sim}{\boldsymbol{\kappa}}^e \;+\; \tfrac{1}{2} \sum_{s\in S}\; c\alpha^{s2} \\
&+ \quad r_0 \;\sum_{s\in S} \varrho_S^s \;+\; \tfrac{1}{2} \;\sum_{r,s\in S}\; h^{sr}\varrho_S^s\varrho_S^r \\
&+ \quad r_{c0} \;\sum_{s\in S} \varrho_G^s \;+\; \tfrac{1}{2} \;\sum_{r,s\in S}\; h_c^{sr}\varrho_G^s\varrho_G^r \\
&+ \quad \sum_{r,s\in S}\; h_I^{sr}\varrho_S^s\varrho_G^r \;+\; f(T)
\end{aligned}$$

Hardening matrices h^{rs} and h_c^{rs} have been introduced for each population of dislocations following Mandel (1965), but a coupling term associated with the matrix h_I^{sr} must be added.

Assuming then that the thermodynamical forces corresponding to the variables ϱ_S^s, ϱ_G^s and α^s respectively are r^s, r_c^s and x^s, the following hardening rules are derived :

Isotropic hardening

$$r^s \;=\; \rho\frac{\partial\psi}{\partial\varrho_S^s} \;=\; r_0 \;+\; \sum_{r\in S}\; h^{sr}\varrho_S^r \;+\; \sum_{r\in S}\; h_I^{sr}\varrho_G^r \tag{105}$$

$$r_c^s \;=\; \rho\frac{\partial\psi}{\partial\varrho_G^s} \;=\; r_{c0} \;+\; \sum_{r\in S}\; h_c^{sr}\varrho_G^r \;+\; \sum_{r\in S}\; h_I^{sr}\varrho_S^r \tag{106}$$

Note that, for simplicity, we have omitted to split the terms $h_c^{sr}\varrho_G^r$ into $h_{c\perp}^{sr}\varrho_{G\perp}^r + h_{c\odot}^{sr}\varrho_{G\odot}^r$ in order to distinguish the contributions of edge and screw dislocations. The same holds for the terms involving matrix h_I^{sr}. Furthermore, a similar thermodynamical formulation can be worked out for non-linear isotropic hardening. It can be seen that a coupling between plastic deformation and curvature naturally arises from our choice of the free energy. The existence of additional hardening due to plastic curvature must be investigated experimentally.

Kinematic hardening

$$x^s \;=\; \rho\frac{\partial\psi}{\partial\alpha^s} \;=\; c^s\;\alpha^s \tag{107}$$

We refer to Méric and Cailletaud (1991) for the expression of the non-linear evolution law for kinematic hardening:

$$\dot{\alpha}^s \;=\; \dot{\gamma}^s \;-\; d\;\mid\dot{\gamma}^s\mid\;\alpha^s \tag{108}$$

Dissipation Introducing now the internal variables in the expression of the intrinsic dissipation rate derived in 2.5, one obtains

$$\begin{aligned}\dot{D} \;=\; \sum_{r\in S}\Big(&\tau^s\;\dot{\gamma}^s \;-\; x^s\dot{\alpha}^s \;-\; r^s\dot{\varrho}_S^s \;+\; \nu_\perp^s\;\dot{\theta}_\perp^s \;+\; \nu_\odot^s\;\dot{\theta}_\odot^s \;-\; r_{c\perp}^s\dot{\varrho}_{G\perp}^s\\ &-\; r_{c\odot}^s\dot{\varrho}_{G\odot}^s\Big)\end{aligned} \tag{109}$$

where

$$\nu_\perp^s \;=\; \frac{1}{l}\;{}^\sharp\underset{\sim}{\boldsymbol{\mu}} : {}^\sharp\underset{\sim}{\boldsymbol{Q}}_\perp^s \quad and \quad \nu_\odot^s \;=\; \frac{1}{l}\;{}^\sharp\underset{\sim}{\boldsymbol{\mu}} : {}^\sharp\underset{\sim}{\boldsymbol{Q}}_\odot^s \tag{110}$$

The multiplication and motion of dislocations are dissipative processes. The three first terms in (109) account for dissipation due to slip activity whereas the remaining terms account for multiplication of geometrically necessary dislocations. In many cases the last terms can be neglected. But when strong lattice rotation gradients develop, they may well be the leading terms.

Some conditions on the material parameters can then be derived from the entropy principle. Taking the flow rules (100) and (102) and the definitions (103) and (104) into account, equation (109) can be rewritten under the form

$$\begin{aligned}\dot{D} \;=\;& \textstyle\sum_{r\in S}\;\Big(\big((\tau^s - x^s)\;sign(\dot{\gamma}^s) - r^s \;+\; cd\alpha^{s2}\big)\mid\dot{\gamma}^s\mid\\ +\;& \dot{\theta}_\perp^s\;(\nu_\perp^s - r_{c\perp}^s\;sign(\theta_{G\perp}^s)) \;+\; \dot{\theta}_\odot^s(\nu_\odot^s - r_{c\odot}^s\;sign(\theta_{G\odot}^s))\Big)\end{aligned}$$

It can be checked that the positivity of the intrinsic dissipation rate is ensured if $c\ d\ >\ 0$ and if the marix $h^{rs}_{c\perp,\odot}$ is such that $r^{s}_{c\perp,\odot}$ is always positive.

1.5 Conclusions

Recent advances in the mechanics of generalized continua have been used to develop a Cosserat theory for single crystals at finite deformation and curvature. The decomposition of the relative deformation gradient into an elastic and plastic part is multiplicative as usual, whereas the wryness tensor admits a mixed additive-multiplicative decomposition. We have assumed that the plastic lattice curvature and torsion are accommodated respectively by edge and screw dislocations belonging to each slip system. The curvature and torsion angles over a characteristic length due to each type of dislocation are internal variables in addition to the cumulative amounts of slip for each slip system. Explicit constitutive equations have been proposed in the case of elastoviscoplasticity. An important consequence of the theory is that the plastic lattice curvature and torsion as well as the plastic spin are associated with dissipation. The production of geometrically necessary dislocations is clearly a dissipative process. There is an overwhelming tendency to include these microstructural features of dislocated crystals into the framework of generalized continua. Since the pioneering work of Günther, Claus and Eringen Eringen and Claus (1970) resorted to a micromorphic continuum. As for them, Smyshlyaev and Fleck (1996) prefer to develop a strain gradient theory of slip. However they replace this plasticity problem by a problem of non-linear elasticity at small strains. In contrast our theory has the tremendous advantage to provide a set of kinematic and constitutive equations in elastoviscoplasticity at finite deformation on a physical and thermodynamical basis. Finally Lachner et al. (1994) have shown that polycrystals also can be regarded as Cosserat media. Homogenization techniques should enable one to derive a polycrystal model from the present theory.

Only a precise enough description of dislocation distribution within a volume element can enable one to model the plastic behaviour of single crystals. For that purpose, the continuum theory of dislocations resorts to the dislocation density tensor. In contrast, macroscopic elastoplasticity theory involves hardening variables which are related to scalar dislocation densities. In both theories, the expression "dislocation density" is seen to have a very different meaning. The dislocation density tensor and the scalar dislocation densities are independent measures of the dislocation distribution. The most important advantage of the proposed theory is to combine

both descriptions within a single constitutive framework.

It must be noticed that only slip processes have been taken into account in the present work. Further developments are necessary to include climb processes, which may play a significant role during creep.

A coupling between plastic curvature and plastic deformation has been introduced on the level of the hardening rule to represent the influence of slip plane curvature on further dislocation motion. Experimental evidence of such hardening effects have been provided for instance in Jaoul (1965).

It is clear that the difference between the classical theory and the Cosserat theory can appear only if deformation and more precisely lattice rotation is not homogeneous. The theory can therefore be applied to the prediction and the simulation of localized deformation modes like shear bands in single crystals. A theoretical analysis of such material instabilities is presented in Petryk (1992). The case of single crystals is investigated in Asaro and Rice (1977); Duszek-Perzyna and Perzyna (1993). An analysis and numerical simulations of localization phenomena in single crystals are presented in Forest and Cailletaud (1995) for the classical theory. In Forest (1998) we have performed a bifurcation analysis for single crystals undergoing single slip using the Cosserat theory. Some crucial differences with respect to the classical case have been pointed out. For instance, according to the classical theory, slip bands and kink bands can occur for the same critical hardening modulus. This is no longer true for the Cosserat theory, which is strongly supported by experimental evidence.

1.6 Appendix: Notations

In this work, $\underline{\boldsymbol{a}}$ denotes a vector of the Euclidean space E, $\underline{\underline{\boldsymbol{A}}}$ a second-rank Euclidean tensor, and $\underset{\sim}{\underline{\underline{\boldsymbol{A}}}}$ (resp. $\underset{\sim}{\underline{\boldsymbol{A}}}$) a third-rank tensor when operating on a vector (resp. a second-rank tensor). The same third-rank tensor is denoted $\underline{\underline{\underline{\boldsymbol{A}}}}$ when regarded as a 3-linear form. The tensor product of two vectors $\underline{\boldsymbol{a}}, \underline{\boldsymbol{b}}$ is such that, for all $\underline{\boldsymbol{x}} \in E$,

$$\begin{aligned} \underline{\boldsymbol{x}}.(\underline{\boldsymbol{a}} \otimes \underline{\boldsymbol{b}}) &= \underline{\boldsymbol{x}}.\underline{\boldsymbol{a}}\ \underline{\boldsymbol{b}} \\ (\underline{\boldsymbol{a}} \otimes \underline{\boldsymbol{b}}).\underline{\boldsymbol{x}} &= \underline{\boldsymbol{b}}.\underline{\boldsymbol{x}}\ \underline{\boldsymbol{a}} \end{aligned}$$

where the dot denotes the inner product on E.

Let $(\underline{\boldsymbol{e}}_1, \underline{\boldsymbol{e}}_2, \underline{\boldsymbol{e}}_3)$ be a positive oriented orthonormal basis of oriented E with dimension 3. When written in components, the double contraction of second-rank tensors reads

$$\underline{\underline{\boldsymbol{A}}} : \underline{\underline{\boldsymbol{B}}} = A_{ij} B_{ij} \tag{111}$$

We note $\underline{\underline{\underline{\boldsymbol{\epsilon}}}}$ the Levi-Civita tensor

$$\underline{\underline{\underline{\boldsymbol{\epsilon}}}} = Det(\underline{\boldsymbol{e}}_j, \underline{\boldsymbol{e}}_k, \underline{\boldsymbol{e}}_l)\ \underline{\boldsymbol{e}}_j \otimes \underline{\boldsymbol{e}}_k \otimes \underline{\boldsymbol{e}}_l \tag{112}$$

Notice the useful identity

$$\epsilon_{ijk}\ \epsilon_{ilm} = \delta_{jl}\ \delta_{km} - \delta_{jm}\ \delta_{kl} \tag{113}$$

The following result concerning third-rank tensors is used,

$$\begin{array}{ll} If & \underset{\sim}{\boldsymbol{B}} \;=\; \frac{1}{2}\,\underset{\sim}{\boldsymbol{\epsilon}} \,:\, \underset{\approx}{\boldsymbol{A}} \;=\; \frac{1}{2}\,\epsilon_{ikl}\,A_{klj}\,\underline{\boldsymbol{e}}_i \otimes \underline{\boldsymbol{e}}_j \\ and & A_{ijk} \;=\; -A_{jik} \\ then & \underset{\approx}{\boldsymbol{A}} \;=\; \underset{\sim}{\boldsymbol{\epsilon}} \,.\, \underset{\sim}{\boldsymbol{B}} \;=\; \epsilon_{ijm}\,B_{mk}\,\underline{\boldsymbol{e}}_i \otimes \underline{\boldsymbol{e}}_j \otimes \underline{\boldsymbol{e}}_k \end{array}$$

The cross product is defined by

$$\underline{\boldsymbol{a}} \times \underline{\boldsymbol{b}} \;=\; \underset{\sim}{\boldsymbol{\epsilon}} : (\underline{\boldsymbol{a}} \otimes \underline{\boldsymbol{b}}) \;=\; \epsilon_{ijk}\,a_j b_k\,\underline{\boldsymbol{e}}_i \tag{114}$$

The symmetric and antisymmetric parts of tensor $\underset{\approx}{\boldsymbol{A}}$ are respectively denoted $^{\{}\underset{\approx}{\boldsymbol{A}}^{\}}$ and $^{\}}\underset{\approx}{\boldsymbol{A}}^{\{}$. There is then one and only one vector $\overset{\times}{\underline{\boldsymbol{A}}}$ such that, for all $\underline{\boldsymbol{x}}$,

$$^{\}}\underset{\approx}{\boldsymbol{A}}^{\{}\,.\underline{\boldsymbol{x}} \;=\; \overset{\times}{\underline{\boldsymbol{A}}} \times \underline{\boldsymbol{x}}, \quad \overset{\times}{\underline{\boldsymbol{A}}} \;=\; -\frac{1}{2}\,\underset{\sim}{\boldsymbol{\epsilon}} : \underset{\approx}{\boldsymbol{A}} \;=\; -\frac{1}{2}\,\epsilon_{klm}\,A_{lm}\,\underline{\boldsymbol{e}}_k \tag{115}$$

Following Trostel [56], we define a cross product between a second-rank tensor and a vector

$$\begin{array}{l} (\underline{\boldsymbol{a}} \otimes \underline{\boldsymbol{b}}) \times \underline{\boldsymbol{c}} \;=\; \underline{\boldsymbol{a}} \otimes (\underline{\boldsymbol{b}} \times \underline{\boldsymbol{c}}) \\ \underline{\boldsymbol{a}} \times (\underline{\boldsymbol{b}} \otimes \underline{\boldsymbol{c}}) \;=\; (\underline{\boldsymbol{a}} \times \underline{\boldsymbol{b}}) \otimes \underline{\boldsymbol{c}} \end{array}$$

so that

$$\underset{\approx}{\boldsymbol{A}} \times \underline{\boldsymbol{c}} \;=\; -(\underline{\boldsymbol{c}} \times \underset{\approx}{\boldsymbol{A}}^T)^T \tag{116}$$

As a result

$$^{\}}\underset{\approx}{\boldsymbol{A}}^{\{} \;=\; \underset{\approx}{\boldsymbol{1}} \times \overset{\times}{\underline{\boldsymbol{A}}} \;=\; -\underset{\approx}{\boldsymbol{\epsilon}}.\overset{\times}{\underline{\boldsymbol{A}}} \tag{117}$$

Any element $\underset{\approx}{\boldsymbol{R}}$ of the orthogonal group can be represented by the element $\underline{\boldsymbol{\Phi}}$ of the associated Lie group such that

$$\underset{\approx}{\boldsymbol{R}} \;=\; \exp(\underset{\sim}{\boldsymbol{1}} \times \underline{\boldsymbol{\Phi}}) \;=\; \exp(-\underset{\approx}{\boldsymbol{\epsilon}}.\underline{\boldsymbol{\Phi}}) \tag{118}$$

Concerning tensor analysis, our notations are,

nabla operator

$$\boldsymbol{\nabla} \;=\; {}_{,i}\,\underline{\boldsymbol{e}}_i \tag{119}$$

gradient operator

$$grad\ f \;=\; \boldsymbol{\nabla} f \;=\; f_{,i}\,\underline{\boldsymbol{e}}_i \tag{120}$$

$$grad\ \underline{\boldsymbol{u}} \;=\; \underline{\boldsymbol{u}} \otimes \boldsymbol{\nabla} \;=\; u_{i,j}\,\underline{\boldsymbol{e}}_i \otimes \underline{\boldsymbol{e}}_j \tag{121}$$

curl operator

$$curl\ \underline{\boldsymbol{u}} \;=\; \underline{\boldsymbol{u}} \times \boldsymbol{\nabla} \;=\; \epsilon_{ijk}\,u_{j,k}\,\underline{\boldsymbol{e}}_i \tag{122}$$

$$curl\ \underset{\approx}{\boldsymbol{A}} \;=\; \underset{\approx}{\boldsymbol{A}} \times \boldsymbol{\nabla} \;=\; \epsilon_{hjk}\,A_{ij,k}\,\underline{\boldsymbol{e}}_i \otimes \underline{\boldsymbol{e}}_h \tag{123}$$

Note that

$$^{\}}\underline{\boldsymbol{u}} \otimes \boldsymbol{\nabla}^{\{} \;=\; \frac{1}{2}\,\underset{\approx}{\boldsymbol{\epsilon}}.(curl\ \underline{\boldsymbol{u}}) \tag{124}$$

We have made a wide use of theorem

$$\oint_L \underset{\approx}{\boldsymbol{A}}.\underline{\boldsymbol{l}}\ dl \;=\; -\int_S (curl\ \underset{\approx}{\boldsymbol{A}}).\underline{\boldsymbol{n}}\ dS \tag{125}$$

where the open surface S is bounded by the contour L.

2 The micromorphic approach to strain gradient crystal plasticity

2.1 The micromorphic approach

A unifying thermomechanical framework is presented by Forest (2009) that reconciles several classes of gradient elastoviscoplasticity and damage models proposed in the literature during the last 40 years. It is based on the introduction of the micromorphic counterpart ${}^{\chi}\phi$ of a selected state or internal variable ϕ in a standard constitutive model. Following the method of virtual power, the power of internal forces is extended by the contribution of micromorphic power. In addition to the classical balance of momentum equation, a balance of micromorphic momentum is derived that involves generalized stress tensors associated with invariant generalized strain measures based on ${}^{\chi}\phi$ and its first gradient $\boldsymbol{\nabla}{}^{\chi}\phi$. The corresponding additional boundary conditions are also deduced from the procedure. The power of generalized forces is assumed to contribute to the energy balance equation. The free energy density function is then assumed to depend on invariant generalized strain measures involving in particular the relative generalized strain $\phi - {}^{\chi}\phi$ and its gradient $\boldsymbol{\nabla}{}^{\chi}\phi$. The Coleman–Noll procedure is applied to derive the state laws and residual dissipation from the entropy principle.

When applied to the deformation gradient itself, $\phi \equiv \underset{\sim}{\boldsymbol{F}}$, the micromorphic theory of Eringen and Mindlin is recovered Eringen and Suhubi (1964); Mindlin (1964) together with its extension to finite deformation elastoviscoplasticity Sansour (1998a); Forest and Sievert (2003). If the selected variable is the cumulative plastic strain, the theory reduces to the so–called "nonlocal implicit gradient–enhanced elastoplasticity model" provided that simplified linear relationships are adopted between generalized stresses and strains Peerlings et al. (2001); Engelen et al. (2003). The same holds if the micromorphic variable coincides with a damage variable Peerlings et al. (2004).

There are two possible sources of coupling between the macro and micro variables in the proposed approach. If the relative generalized strain associated with $\phi - {}^{\chi}\phi$ explicitly appears in the extended power of internal forces, the associated relative stress acts as a coupling between the balance equation for standard momentum and for generalized momentum, as in Eringen's micromorphic continuum. The relative generalized strain can also be included as an argument of the free energy function which eventually leads to the wanted coupling between standard and generalized stresses. Both formulations have been illustrated recently for the so–called "microstrain" theory Forest and Sievert (2006).

It the internal constraint is introduced that the micromorphic variable

${}^{\chi}\phi$ remains as close as possible to the macroscopic variable ϕ, the micromorphic model reduces to the second gradient or gradient of internal variable approach as defined in Maugin (1990); Maugin and Muschik (1994); Papenfuss and Forest (2006). When the micromorphic variable is the deformation gradient itself, the second gradient theory according to Mindlin and Eshel (1968) is obtained. If the selected variable is the cumulative plastic strain, the constrained micromorphic theory delivers Aifantis strain gradient plasticity model according to Aifantis (1987); Fleck and Hutchinson (2001). When applied to the full plastic strain tensors, the strain gradient plasticity models initially proposed by Forest and Sievert (2003) and Gurtin (2003) are derived.

General procedure for introducing micromorphic variables

We start from an elastoviscoplasticity model formulation within the framework of the classical Cauchy continuum theory and classical continuum thermodynamics according to Germain et al. (1983); Maugin (1999). The material behaviour is characterized by the reference set of state variables

$$STATE0 = \{\underset{\sim}{\boldsymbol{F}}, \quad T, \quad \alpha\} \tag{126}$$

on which the free energy density function ψ may depend. The deformation gradient is denoted by $\underset{\sim}{\boldsymbol{F}}$ whereas α represents the whole set of internal variables of arbitrary tensorial order accounting for nonlinear processes at work inside the material volume element, like isotropic and kinematic hardening variables. The absolute temperature is T.

The proposed systematic method for the enhancement of the previous continuum and constitutive theory to incorporate generalized strain gradient effects proceeds as follows:

1. Select a variable ϕ from the set of state variables, which is supposed to carry the targeted gradient effects:

$$\phi \in \{\underset{\sim}{\boldsymbol{F}}, \quad \alpha, \quad T\} \tag{127}$$

   It can be a tensor variable of arbitrary rank. For the illustration, it is treated as a scalar quantity in this section. The case $\phi = T$ is treated in Forest and Amestoy (2008).
2. Introduce the micromorphic variable ${}^{\chi}\phi$ associated with ϕ. It has the same tensor rank and same physical dimension as ϕ.
3. Extend the virtual power of internal forces to the power done by the micromorphic variable and its first gradient:

$$\mathcal{P}^{(i)}(\underline{\boldsymbol{v}}^{\star}, {}^{\chi}\dot{\phi}^{\star}) = -\int_{\mathcal{D}} p^{(i)}(\underline{\boldsymbol{v}}^{\star}, {}^{\chi}\dot{\phi}^{\star})\, dV \tag{128}$$

$$p^{(i)}(\underline{\boldsymbol{v}}^{\star},{}^{\chi}\dot{\phi}^{\star}) = \underset{\sim}{\boldsymbol{\sigma}} : \boldsymbol{\nabla}\underline{\boldsymbol{v}}^{\star} + a\,{}^{\chi}\dot{\phi}^{\star} + \underline{\boldsymbol{b}}.\boldsymbol{\nabla}{}^{\chi}\dot{\phi}^{\star} \tag{129}$$

where $\mathcal{D}$ is a subdomain of the current configuration Ω of the body. The Cauchy stress is $\underset{\sim}{\boldsymbol{\sigma}}$ and a and $\underline{\boldsymbol{b}}$ are generalized stresses associated with the micromorphic variable and its first gradient.

4. Extend then the power of contact forces as follows:

$$\mathcal{P}^{(c)}(\underline{\boldsymbol{v}}^{\star},{}^{\chi}\dot{\phi}^{\star}) = \int_{\mathcal{D}} p^{(c)}(\underline{\boldsymbol{v}}^{\star},{}^{\chi}\dot{\phi}^{\star})\,dV, \quad p^{(c)}(\underline{\boldsymbol{v}}^{\star},{}^{\chi}\dot{\phi}^{\star}) = \underline{\boldsymbol{t}}.\underline{\boldsymbol{v}}^{\star} + a^{c}\,{}^{\chi}\dot{\phi}^{\star} \tag{130}$$

where $\underline{\boldsymbol{t}}$ is the traction vector.

5. Extend the power of forces acting at a distance by introducing, if necessary, generalized body forces:

$$\mathcal{P}^{(e)}(\underline{\boldsymbol{v}}^{\star},{}^{\chi}\dot{\phi}^{\star}) = \int_{\mathcal{D}} p^{(e)}(\underline{\boldsymbol{v}}^{\star},{}^{\chi}\dot{\phi}^{\star})\,dV \tag{131}$$

$$p^{(e)}(\underline{\boldsymbol{v}}^{\star},{}^{\chi}\dot{\phi}^{\star}) = \rho\underline{\boldsymbol{f}}.\underline{\boldsymbol{v}}^{\star} + a^{e}\,{}^{\chi}\dot{\phi}^{\star} + \underline{\boldsymbol{b}}^{e}.\boldsymbol{\nabla}{}^{\chi}\dot{\phi}^{\star} \tag{132}$$

where $\rho\underline{\boldsymbol{f}}, a^{e}, \underline{\boldsymbol{b}}^{e}$ account for given simple and generalized body forces. Following Germain (1973a), given body couples and double forces working with the gradient of the velocity field, can also be introduced in this theory.

6. Formulate the generalized principle of virtual power with respect to the velocity and micromorphic variable fields, presented here in the static case only:

$$\mathcal{P}^{(i)}(\underline{\boldsymbol{v}}^{\star},{}^{\chi}\dot{\phi}) + \mathcal{P}^{(e)}(\underline{\boldsymbol{v}}^{\star},{}^{\chi}\dot{\phi}^{\star}) + \mathcal{P}^{(c)}(\underline{\boldsymbol{v}}^{\star},{}^{\chi}\dot{\phi}) = 0, \quad \forall\mathcal{D}\subset\Omega, \quad \forall\underline{\boldsymbol{v}}^{\star},{}^{\chi}\dot{\phi} \tag{133}$$

The method of virtual power according to Maugin (1980) is used then to

7. Derive the standard local balance of momentum equation:

$$div\,\underset{\sim}{\boldsymbol{\sigma}} + \rho\underline{\boldsymbol{f}} = 0, \quad \forall\underline{\boldsymbol{x}} \in \Omega \tag{134}$$

and the generalized balance of micromorphic momentum equation:

$$div\,(\underline{\boldsymbol{b}} - \underline{\boldsymbol{b}}^{e}) - a + a^{e} = 0, \quad \forall\underline{\boldsymbol{x}} \in \Omega \tag{135}$$

8. Derive the associated boundary conditions for the simple and generalized tractions:

$$\underline{\boldsymbol{t}} = \underset{\sim}{\boldsymbol{\sigma}}.\underline{\boldsymbol{n}}, \quad \forall\underline{\boldsymbol{x}} \in \partial\mathcal{D} \tag{136}$$

$$a^{c}_{\phi} = (\underline{\boldsymbol{b}} - \underline{\boldsymbol{b}}^{e}).\underline{\boldsymbol{n}}, \quad \forall\underline{\boldsymbol{x}} \in \partial\mathcal{D} \tag{137}$$

9. Enhance the local balance of energy by the generalized micromorphic power already including in the power of internal forces (129):

$$\rho\dot{\epsilon} = p^{(i)} - div\,\underline{\boldsymbol{q}} + \rho r \tag{138}$$

where ϵ is the specific internal energy, $\underline{\boldsymbol{q}}$ the heat flux vector and r denotes external heat sources.

10. Enlarge the state space to include the micromorphic variable and its first gradient:

$$STATE = \{\underset{\sim}{\boldsymbol{F}}, \quad T, \quad \alpha, \quad {}^{\chi}\phi, \quad \boldsymbol{\nabla}^{\chi}\phi\} \tag{139}$$

The free energy density function ψ will in general be a function of the generalized relative strain variable e defined as:

$$e = \phi - {}^{\chi}\phi \tag{140}$$

thus introducing a coupling between macro and micromorphic variables.

11. Formulate the entropy principle in its local form:

$$-\rho(\dot{\psi} + \eta\dot{T}) + p^{(i)} - \frac{\boldsymbol{q}}{T}.\boldsymbol{\nabla}T \geq 0 \tag{141}$$

where it was assumed that the entropy production vector is still equal to the heat vector divided by temperature, as in the classical thermomechanics according to Coleman and Noll (1963). Again, the enhancement of the theory goes through the enriched power density of internal forces (129).

12. Exploit the entropy principle according to classical continuum thermodynamics to derive the state laws. For that purpose, the following constitutive functions are introduced:

$$\psi = \hat{\psi}(\underset{\sim}{\boldsymbol{F}}^e, T, \alpha, {}^{\chi}\phi, \boldsymbol{\nabla}^{\chi}\phi), \underset{\sim}{\boldsymbol{\sigma}} = \hat{\underset{\sim}{\boldsymbol{\sigma}}}(\underset{\sim}{\boldsymbol{F}}^e, T, \alpha, {}^{\chi}\phi, \boldsymbol{\nabla}^{\chi}\phi) \tag{142}$$

$$\eta = \hat{\eta}(\underset{\sim}{\boldsymbol{F}}^e, T, \alpha, {}^{\chi}\phi, \boldsymbol{\nabla}^{\chi}\phi) \tag{143}$$

$$a = \hat{a}(\underset{\sim}{\boldsymbol{F}}^e, T, \alpha, {}^{\chi}\phi, \boldsymbol{\nabla}^{\chi}\phi), \underline{\boldsymbol{b}} = \hat{\underline{\boldsymbol{b}}}(\underset{\sim}{\boldsymbol{F}}^e, T, \alpha, {}^{\chi}\phi, \boldsymbol{\nabla}^{\chi}\phi) \tag{144}$$

$$\tag{145}$$

where $\underset{\sim}{\boldsymbol{F}}^e$ represents the elastic part of total deformation. Its precise definition depends however on the retained decomposition of total deformation into elastic and plastic contribution. The usual multiplicative decomposition is adopted below for the illustration. The state

laws follow:

$$\underset{\sim}{\boldsymbol{\sigma}} = \rho\frac{\partial\hat{\psi}}{\partial\underset{\sim}{\boldsymbol{F}}^e}.\underset{\sim}{\boldsymbol{F}}^{eT} \quad \eta = -\frac{\partial\hat{\psi}}{\partial T} \quad X = \rho\frac{\partial\hat{\psi}}{\partial\alpha} \tag{146}$$

$$a = \frac{\partial\hat{\psi}}{\partial^{\chi}\phi} \tag{147}$$

$$\underline{\boldsymbol{b}} = \frac{\partial\hat{\psi}}{\partial\boldsymbol{\nabla}^{\chi}\phi} \tag{148}$$

and the residual dissipation is

$$D^{res} = W^p - X\dot{\alpha} - \frac{\boldsymbol{q}}{T}.\boldsymbol{\nabla}T \geq 0 \tag{149}$$

where W^p represents the (visco–)plastic power and X the thermodynamic force associated with the internal variable α. The existence of a convex dissipation potential depending on the thermodynamic forces can then be assumed from which the evolution rules for internal variables are derived, that identically fulfill the entropy inequality, as usually done in classical continuum thermomechanics Germain et al. (1983).

In the following, this methodology will be applied to existing theories of plasticity.

At this first stage, there will be no need for considering generalized external body forces so that $a^e = 0, \underline{\boldsymbol{b}}^e = 0$. In the most simple model, assuming isotropic material behavior for brevity, the additional contributions to the free energy are taken as quadratic functions of e and $\boldsymbol{\nabla}^{\chi}\phi$:

$$\psi(\underset{\sim}{\boldsymbol{F}}, T, \alpha, {}^{\chi}\phi, \boldsymbol{\nabla}^{\chi}\phi) = \psi^1(\underset{\sim}{\boldsymbol{F}}, \alpha, T) + \psi^2(e = \phi - {}^{\chi}\phi, \boldsymbol{\nabla}^{\chi}\phi, T), \quad with \tag{150}$$

$$\rho\psi^2 = \frac{1}{2}H_{\chi}(\phi - {}^{\chi}\phi)^2 + \frac{1}{2}A\boldsymbol{\nabla}^{\chi}\phi.\boldsymbol{\nabla}^{\chi}\phi \tag{151}$$

After inserting the state laws (147) and (148)

$$a = \rho\frac{\partial\psi}{\partial^{\chi}\phi} = -H_{\chi}(\phi - {}^{\chi}\phi) \tag{152}$$

$$\underline{\boldsymbol{b}} = \rho\frac{\partial\psi}{\partial\boldsymbol{\nabla}^{\chi}\phi} = A\boldsymbol{\nabla}^{\chi}\phi \tag{153}$$

into the additional balance equation (135),

$$a = div\,\underline{\boldsymbol{b}} \tag{154}$$

the following partial differential equation is obtained:

$$\phi = {}^{\chi}\phi - \frac{A}{H_\chi}\Delta^{\chi}\phi \tag{155}$$

where Δ is the Laplace operator. This type of equation is encountered at several places in the mechanics of generalized continua especially in the linear micromorphic theory Mindlin (1964); Eringen (1999); Forest and Sievert (2003); Dillard et al. (2006) and in the so–called implicit gradient theory of plasticity and damage Peerlings et al. (2001); Engelen et al. (2003); Peerlings et al. (2004). Note however that this equation corresponds to a special quadratic potential and represents the simplest micromorphic extension of the classical theory. It involves a characteristic length scale defined by:

$$l_c^2 = \frac{A}{H_\chi} \tag{156}$$

This length is real for positive values of the ratio A/H_χ. The additional material parameters H_X and A are assumed to be positive in this work. This does not exclude a softening material behaviour that can be induced bu the proper evolution of the internal variables (including $\phi \in \alpha$ itself).

Full micromorphic and microstrain theories

The micromorphic theory proposed in Eringen and Suhubi (1964) and Mindlin (1964) is retrieved by choosing

$$\phi \equiv \underset{\sim}{\boldsymbol{F}} \tag{157}$$

i.e. the selected variable ϕ is the full deformation gradient itself. The associated micromorphic variable is

$${}^{\chi}\phi \equiv \underset{\sim}{\boldsymbol{\chi}} \tag{158}$$

where $\underset{\sim}{\boldsymbol{\chi}}(\underline{\boldsymbol{x}})$ is the generally nonsymmetric and non compatible field of microdeformation introduced by these authors. Following the approach sketched in the previous section, the power of internal forces is extended by the micromorphic power, written here in the small deformation framework for the sake of brevity:

$$p^{(i)} = \underset{\sim}{\boldsymbol{\sigma}} : \boldsymbol{\nabla}\underline{\dot{\boldsymbol{u}}} + \underset{\sim}{\boldsymbol{a}} : \dot{\underset{\sim}{\boldsymbol{\chi}}} + \underline{\underline{\boldsymbol{B}}} \vdots \boldsymbol{\nabla}\dot{\underset{\sim}{\boldsymbol{\chi}}} \tag{159}$$

where $\underline{\boldsymbol{u}}$ is the displacement field. An (infinitesimal) change of observer of rate $\underset{\sim}{\boldsymbol{w}}$ changes the gradient of the velocity field into $\boldsymbol{\nabla}\underline{\dot{\boldsymbol{u}}} + \underset{\sim}{\boldsymbol{w}}$ and the

microdeformation rate into $\dot{\underset{\sim}{\chi}} + \underset{\sim}{w}$. The principle of (infinitesimal) material frame indifference requires the invariance of $p^{(i)}$ with respect to (infinitesimal) Euclidean changes of observers Gurtin (2003). As a result, the sum $\underset{\sim}{\sigma} + \underset{\sim}{a}$ must be a symmetric second–rank tensor. The power density of internal forces can therefore be rewritten in the following form

$$p^{(i)} = \underset{\sim}{\sigma} : \dot{\underset{\sim}{\varepsilon}} + \underset{\sim}{s} : (\boldsymbol{\nabla}\dot{\underline{u}} - \dot{\underset{\sim}{\chi}}) + \underset{\approx}{S} \dot{:} \boldsymbol{\nabla}\dot{\underset{\sim}{\chi}} \tag{160}$$

where $\underset{\sim}{\sigma}$ is symmetric, $\underset{\sim}{s}$ is the generally nonsymmetric relative stress tensor, and $\underset{\approx}{S}$ the higher order stress tensor introduced in the formulation of Eringen (1999). The infinitesimal strain tensor is $\underset{\sim}{\varepsilon}$. The generalized strain rates $\boldsymbol{\nabla}\dot{\underline{u}} - \dot{\underset{\sim}{\chi}}$ and $\boldsymbol{\nabla}\dot{\underset{\sim}{\chi}}$ are invariant with respect to (infinitesimal) changes of observers[1]. The balance equations of momentum and of generalized moment of momentum take the form

$$div\,(\underset{\sim}{\sigma} + \underset{\sim}{s}) + \rho \underline{f} = 0, \quad div\,\underset{\approx}{S} + s = 0 \tag{161}$$

which shows an explicit coupling between both balance equations via the relative stress tensor $\underset{\sim}{s}$. Such a coupling was not explicit in the general formulation of section 2.1 (see equations (134) and (135), but it finally becomes evident through the constitutive coupling in equation (155).

The microstrain theory proposed in Forest and Sievert (2006) is an application of the micromorphic approach when taking

$$\phi \equiv \underset{\sim}{C} = \underset{\sim}{F}^T . \underset{\sim}{F}, \quad {}^{\chi}\phi \equiv {}^{\chi}\underset{\sim}{C} \tag{162}$$

or

$$\phi \equiv \underset{\sim}{\varepsilon}, \quad {}^{\chi}\phi \equiv {}^{\chi}\underset{\sim}{\varepsilon} \tag{163}$$

within the small strain approximation. Because of the symmetry of the microstrain tensor, it is not necessary to introduce a relative stress tensor in the enriched power of internal forces. Instead, the standard form (129) is adopted:

$$p^{(i)} = \underset{\sim}{\sigma} : \dot{\underset{\sim}{\varepsilon}} + \underset{\sim}{a} : {}^{\chi}\dot{\underset{\sim}{\varepsilon}} \tag{164}$$

The coupling between macro and microstrain arises at the constitutive level since the free energy density was proposed in Forest and Sievert (2006) to be a function

$$\psi(\underset{\sim}{\varepsilon}^e, \quad T, \quad \alpha, \quad \underset{\sim}{e} := \underset{\sim}{\varepsilon} - {}^{\chi}\underset{\sim}{\varepsilon}, \quad \underset{\approx}{K} := \boldsymbol{\nabla}{}^{\chi}\underset{\sim}{\varepsilon}) \tag{165}$$

[1] The reasoning holds true at finite deformation as done in Mindlin (1964); Eringen and Suhubi (1964).

The additional arguments can be limited to their non–dissipative parts $\underset{\sim}{\boldsymbol{e}}^e, \underset{\approx}{\boldsymbol{K}}^e$ according to Forest and Sievert (2006). The existence of dissipative micromechanisms is considered in Forest and Sievert (2003). When the following linearized constitutive equations are adopted:

$$\underset{\sim}{\boldsymbol{a}} = H_\chi \underset{\sim}{\boldsymbol{e}}, \quad \underset{\approx}{\boldsymbol{b}} = A \boldsymbol{\nabla}^\chi \underset{\sim}{\boldsymbol{\varepsilon}} \tag{166}$$

the extra balance equation takes the following simple form:

$$^\chi\underset{\sim}{\boldsymbol{\varepsilon}} - l_c^2 \Delta^\chi \underset{\sim}{\boldsymbol{\varepsilon}} = \underset{\sim}{\boldsymbol{\varepsilon}}, \quad with \quad l_c^2 = \frac{A}{H_\chi} \tag{167}$$

as shown in Dillard et al. (2006). This represents an extension of the scalar partial differential (155) to a tensor valued micromorphic variable. The Laplace operator applies here to each individual tensor component, within a Cartesian orthonormal coordinate system.

The full micromorphic continuum can be regarded as the combination of the microstrain and Cosserat continua Forest and Sievert (2006). The Cosserat continuum itself can be interpreted in terms of the proposed methodology. It corresponds to the choice:

$$\phi = \underset{\sim}{\boldsymbol{R}}, \quad ^\chi\phi \equiv ^\chi\underset{\sim}{\boldsymbol{R}} \tag{168}$$

where $\underset{\sim}{\boldsymbol{R}}$ is the material rotation in the polar decomposition of $\underset{\sim}{\boldsymbol{F}}$. The associated quantity $^\chi\underset{\sim}{\boldsymbol{R}}$ is nothing but the micropolar rotation representing the rotation of a triad of directors attributed to each material point. The generalized stress $\underset{\sim}{\boldsymbol{a}}$ in the enriched power of internal forces is then related to the skew–symmetric part of the Cosserat stress tensor. Cosserat models are known to be able to account for some size effects in the softening plastic behavior of granular materials Mühlhaus and Vardoulakis (1987) and in the hardening behaviour of metals Forest et al. (2000).

Microstrain gradient plasticity

The proposed methodology is now applied to the simplest models available for the isothermal elastic–plastic behaviour of materials. Different generalized models are worked out and compared to the existing models in literature. It turns out that several existing strain gradient plasticity models are recovered using the proposed systematic procedure. Some differences are evidenced due to the precise thermodynamical background of the approach which is not always present in the earlier approaches. In particular the

approach can be used to tackle coupled problems, thus provided coupled strain gradient equations not present in the literature. A simple example of this coupling in given to account for a possible dependence of material parameters with temperature. The framework is applicable to plasticity and viscoplasticity.

The reference state space corresponding to a classical elastoplasticity model retained in this subsection is

$$DOF0 = \{\underline{\boldsymbol{u}}\}, \quad STATE0 = \{\underset{\sim}{\boldsymbol{\varepsilon}}^e, \quad p, \quad \alpha\} \tag{169}$$

where $\underset{\sim}{\boldsymbol{\varepsilon}}^e$ is the (infinitesimal) elastic strain tensor, p the cumulated plastic strain variable and α denotes another possible internal variable of any tensorial rank. The selected variable for the micromorphic approach is

$$\phi \equiv p \tag{170}$$

which the micromorphic variable ${}^{\chi}p$ is associated to. The classical power of internal and contact forces are extended in the following way:

$$p^{(i)} = \underset{\sim}{\boldsymbol{\sigma}} : \dot{\underset{\sim}{\boldsymbol{\varepsilon}}} + a\,{}^{\chi}\dot{p} + \underline{\boldsymbol{b}} . \boldsymbol{\nabla}{}^{\chi}p, \quad p^{(c)} = \underline{\boldsymbol{t}} . \dot{\underline{\boldsymbol{u}}} + a^c\,{}^{\chi}\dot{p} \tag{171}$$

in which generalized stresses a and $\underline{\boldsymbol{b}}$ have been introduced. The application of the method of virtual power leads to the following additional local balance equation and boundary conditions in addition to the classical local balance of momentum and traction condition at the outer boundary:

$$div\,\underline{\boldsymbol{b}} - a = 0, \quad \forall \underline{\boldsymbol{x}} \in \Omega, \quad a^c = \underline{\boldsymbol{b}} . \underline{\boldsymbol{n}}\,, \quad \forall \underline{\boldsymbol{x}} \in \partial\Omega \tag{172}$$

Generalized body forces a^e and $\underline{\boldsymbol{b}}^e$ could be introduced in case of necessity in the balance equations. The extended state space on which constitutive functions may depend is

$$STATE = \{\underset{\sim}{\boldsymbol{\varepsilon}}^e, \quad p, \quad \alpha, \quad {}^{\chi}p, \quad \boldsymbol{\nabla}{}^{\chi}p\} \tag{173}$$

The total strain is still split into its elastic and plastic parts:

$$\underset{\sim}{\boldsymbol{\varepsilon}} = \underset{\sim}{\boldsymbol{\varepsilon}}^e + \underset{\sim}{\boldsymbol{\varepsilon}}^p \tag{174}$$

The free energy density function ψ is assumed to be a function of the previous set $STATE$. The Clausius–Duhem inequality takes then the form

$$(\underset{\sim}{\boldsymbol{\sigma}} - \rho\frac{\partial\psi}{\partial\underset{\sim}{\boldsymbol{\varepsilon}}^e}) : \dot{\underset{\sim}{\boldsymbol{\varepsilon}}}^e + (a - \rho\frac{\partial\psi}{\partial{}^{\chi}p}){}^{\chi}\dot{p} + (\underline{\boldsymbol{b}} - \rho\frac{\partial\psi}{\partial\boldsymbol{\nabla}{}^{\chi}p}) . \boldsymbol{\nabla}{}^{\chi}\dot{p} + \underset{\sim}{\boldsymbol{\sigma}} : \dot{\underset{\sim}{\boldsymbol{\varepsilon}}}^p - \rho\frac{\partial\psi}{\partial p}\dot{p} - \rho\frac{\partial\psi}{\partial\alpha}\dot{\alpha} \geq 0 \tag{175}$$

from which the following state laws and residual dissipation are derived:

$$\underset{\sim}{\boldsymbol{\sigma}} = \rho\frac{\partial\psi}{\partial\underset{\sim}{\boldsymbol{\varepsilon}}^e}, \quad a = \rho\frac{\partial\psi}{\partial{}^{\chi}p}, \quad \underline{\boldsymbol{b}} = \rho\frac{\partial\psi}{\partial\boldsymbol{\nabla}^{\chi}p}, \quad R = \rho\frac{\partial\psi}{\partial p}, \quad X = \rho\frac{\partial\psi}{\partial\alpha} \tag{176}$$

$$D^{res} = \underset{\sim}{\boldsymbol{\sigma}} : \dot{\underset{\sim}{\boldsymbol{\varepsilon}}}^p - R\dot{p} - X\dot{\alpha} \geq 0 \tag{177}$$

The plastic behaviour is characterized by the yield function $f(\underset{\sim}{\boldsymbol{\sigma}}, R, X)$. In the micromorphic model, the yield function can still be treated as the dissipation potential providing the flow and evolution rules for internal variables. This corresponds to the hypothesis of maximal dissipation or normality rule:

$$\dot{\underset{\sim}{\boldsymbol{\varepsilon}}}^p = \dot{\lambda}\frac{\partial f}{\partial\underset{\sim}{\boldsymbol{\sigma}}}, \quad \dot{p} = -\dot{\lambda}\frac{\partial f}{\partial R}, \quad \dot{\alpha} = -\dot{\lambda}\frac{\partial f}{\partial X} \tag{178}$$

At this stage, a coupling between the macroscopic and microscopic variables must be introduced, for instance via the relative cumulative plastic strain $p - {}^{\chi}p$. An example of such a possible coupling is given in the next paragraph.

Example

A quadratic form is proposed to model the free energy density function, with respect to elastic strain, cumulative plastic strain, relative plastic strain and micromorphic plastic strain gradient:

$$\rho\psi(\underset{\sim}{\boldsymbol{\varepsilon}}^e, p, {}^{\chi}p, \boldsymbol{\nabla}^{\chi}p) = \frac{1}{2}\underset{\sim}{\boldsymbol{\varepsilon}}^e : \underset{\approx}{\boldsymbol{\Lambda}} : \underset{\sim}{\boldsymbol{\varepsilon}}^e + \frac{1}{2}Hp^2 + \frac{1}{2}H_{\chi}(p - {}^{\chi}p)^2 + \frac{1}{2}\boldsymbol{\nabla}^{\chi}p.\underset{\sim}{\boldsymbol{A}}.\boldsymbol{\nabla}^{\chi}p \tag{179}$$

The corresponding classical model describes an elastoplastic material behaviour with linear elasticity characterized by the tensor of elastic moduli $\underset{\approx}{\boldsymbol{\Lambda}}$ and the linear hardening modulus H. Two additional material parameters are introduced in the micromorphic extension of this classical model, namely the coupling modulus H_{χ} (unit MPa) and the micromorphic "stiffness" $\underset{\sim}{\boldsymbol{A}}$ (unit MPa.m^2). The thermodynamic forces associated with the state variables are given by the relations (176):

$$\underset{\sim}{\boldsymbol{\sigma}} = \underset{\approx}{\boldsymbol{\Lambda}} : \underset{\sim}{\boldsymbol{\varepsilon}}^e, \quad a = -H_{\chi}(p - {}^{\chi}p), \quad \underline{\boldsymbol{b}} = \underset{\sim}{\boldsymbol{A}}.\boldsymbol{\nabla}^{\chi}p, \quad R = (H + H_{\chi})p - H_{\chi}{}^{\chi}p \tag{180}$$

Note that when the relative plastic strain $e = p - {}^{\chi}p$ is close to zero, the linear hardening rule retrieves its classical form and the generalized stress a vanishes. Only the strain gradient effect $\boldsymbol{\nabla}p$ remains in the enriched work of internal forces (171). This is the situation encountered in the strain gradient plasticity models developed in Fleck and Hutchinson (2001). When inserted

in the additional balance equation (172), the previous states laws lead to the following partial differential equation:

$$ {}^{\chi}p - \frac{1}{H_{\chi}} div\,(\underset{\sim}{\boldsymbol{A}}.\boldsymbol{\nabla}{}^{\chi}p) = p \tag{181} $$

Let us specialize this equation to the case of isotropic materials, for which the second order tensor of micromorphic stiffness reduces to

$$ \underset{\sim}{\boldsymbol{A}} = A\underset{\sim}{\mathbf{1}} \tag{182} $$

which involves then a single additional material parameter. The equation (183) then becomes

$$ {}^{\chi}p - \frac{A}{H_{\chi}}\Delta{}^{\chi}p = p \tag{183} $$

which is identical to the second partial differential equation used in the so–called implicit gradient gradient–enhanced elastoplasticity in Engelen et al. (2003). The microstrain ${}^{\chi}p$ is called there the "non local strain measure" $\bar{p}$. Note however that the latter model involves only one additional material parameter, namely $l_c^2 = A/H_{\chi}$ instead of two in the micromorphic approach. It will turn out to be a special case of the micromorphic model for a specific value of the coupling modulus H_{χ}. No thermodynamical framework was proposed for the elastoplasticity model in the original contribution Engelen et al. (2003). Such a framework has been sketched in the reference Peerlings et al. (2004) where a quadratic potential similar to (179) is introduced which involves in particular the same coupling term. In contrast to the micromorphic approach, however, no additional contribution is introduced in the power of internal forces so that the additional partial differential equation is derived as a sufficient condition to identically fulfill the global form of the entropy inequality. In the micromorphic approach, the coupling modulus H_{χ} plays a central role and makes it possible to have a fully consistent thermomechanical basis for the model. When its value is high enough, it acts as a penalty term forcing the micromorphic plastic strain to follow the macroscopic one as close as possible.

The necessity of an additional boundary condition associated with the nonlocal strain measure is recognized in Engelen et al. (2003). The associated Neumann condition is used in the form:

$$ \boldsymbol{\nabla}{}^{\chi}p.\underline{\boldsymbol{n}} = 0 \quad on \quad \partial\Omega \tag{184} $$

It coincides with the more general boundary condition derived in the micromorphic approach:

$$ \underline{\boldsymbol{b}}\,.\underline{\boldsymbol{n}} = a^c \quad on \quad \partial\Omega \tag{185} $$

when $a^c = 0$ and when $\underline{\boldsymbol{b}}$ is linear with respect to $\boldsymbol{\nabla}^{\chi} p$, as it is the case for the quadratic potential (179).

The yield function is now chosen as

$$f(\underset{\sim}{\boldsymbol{\sigma}}, R) = \sigma_{eq} - \sigma_Y - R \tag{186}$$

where σ_{eq} is an equivalent stress measure and σ_Y the initial yield stress. The hardening rule then takes the following form:

$$R = \frac{\partial \psi}{\partial p} = (H + H_\chi) p - H_\chi {}^{\chi}p \tag{187}$$

After substituting the balance (172) into the hardening law, yielding takes place when

$$\sigma_{eq} = \sigma_Y + H^{\chi} p - A(1 + \frac{H}{H_\chi}) \Delta^{\chi} p \tag{188}$$

This expression coincides with the enhanced yield criterion originally proposed in Aifantis (1987) and used for strain localization simulations in Aifantis (1987); Borst et al. (1993) when the micromorphic variable remains as close as possible to the plastic strain: ${}^{\chi}p \simeq p$. In the latter references, the Laplace operator is directly introduced in the yield function as a postulate, whereas its presence is derived here from the combination of the additional balance equation and the linear generalized constitutive equations.

In the reference Engelen et al. (2003), after introducing the partial differential equation (183) in addition to the classical balance and constitutive equations, the authors propose to substitute the classical hardening law $R(p)$ by the same function $R({}^{\chi}p)$ where the argument is replaced by the nonlocal equivalent plastic strain. If such a hardening law is adopted, this model turns out to be a special case of the present microstrain theory for the following specific value of the hardening modulus:

$$H_\chi = -H \tag{189}$$

which follows from the identification $(H + H_\chi) p - H_\chi {}^{\chi}p = H^{\chi} p$ according to equation $(180)_4$. This assumption indeed reduces the number of free additional parameter to one, namely the choice of A related to the intrinsic length of the material. Such a choice, however, is acceptable only for softening materials for which $H < 0$. Otherwise, the additional contribution to the free energy associated with ${}^{\chi}p$ in (179) will act as a destabilizing term in the material behaviour. Furthermore the type of the partial differential equation (183) would be changed. The authors also point out the

limitations of the simplistic method consisting in substituting the microstrain ${}^{\chi}p$ in the classical hardening law instead of p, especially regarding the subsequent evolution inside plastic strain localization bands.

Keeping both H_{χ} and A as free parameters of the theory makes it possible, in principle, to envisage applications to strain localization phenomena in softening materials, as done in Engelen et al. (2003); Dillard et al. (2006) but also to size effects in hardening plasticity, as done in Hutchinson (2000); Forest et al. (2000); Dillard et al. (2006). For a detailed discussion of the pros and the cons of various available strain gradient plasticity models for both types of applications, the reader is referred to Engelen et al. (2006).

The consistency condition and extension to viscoplasticity are described in Forest (2009).

Full microstrain gradient plasticity

The approach is not restricted to scalar micromorphic variables. As in Eringen's micromorphic model where the selected variable is the full deformation gradient itself, it can be applied to the full plastic strain tensor:

$$\phi \equiv \underset{\sim}{\varepsilon}^{p}, \quad {}^{\chi}\phi \equiv {}^{\chi}\underset{\sim}{\varepsilon}^{p} \tag{190}$$

This corresponds to 5 additional degrees of freedom if the micromorphic plastic strain tensor ${}^{\chi}\underset{\sim}{\varepsilon}^{p}$ is treated as a deviatoric tensor like the macroscopic plastic strain tensor. The generalized stresses are symmetric second and third order tensors, respectively:

$$p^{(i)} = \underset{\sim}{\boldsymbol{\sigma}} : \dot{\underset{\sim}{\boldsymbol{\varepsilon}}} + \underset{\sim}{\boldsymbol{a}} : {}^{\chi}\dot{\underset{\sim}{\boldsymbol{\varepsilon}}}^{p} + \underset{\approx}{\boldsymbol{b}} \vdots \boldsymbol{\nabla}^{\chi}\varepsilon^{p} \tag{191}$$

The symmetry condition applies only to the two first indices of b_{ijk}. The power of internal forces is indeed invariant with respect to (infinitesimal) changes of observers, due to the invariance of $\underset{\sim}{\varepsilon}$ and ${}^{\chi}\underset{\sim}{\varepsilon}^{p}$ themselves. The initial and extended sets of state variables are:

$$STATE0 = \{\underset{\sim}{\varepsilon}^{e}, \quad \underset{\sim}{\varepsilon}^{p}\}, \quad STATE = \{\underset{\sim}{\varepsilon}^{e}, \quad \underset{\sim}{\varepsilon}^{p}, \quad {}^{\chi}\underset{\sim}{\varepsilon}^{p}, \quad \boldsymbol{\nabla}^{\chi}\underset{\sim}{\varepsilon}^{p}\} \tag{192}$$

When the micromorphic variable is constrained to remain as close as possible to the macroscopic one, the theories of gradient of plastic strain presented in Forest and Sievert (2003); Gurtin (2003); Abu Al-Rub et al. (2007) are recovered. In these works, generalized stresses are associated with the plastic strain rate tensor in the extended power of internal forces.

As an illustration, we adopt the following quadratic form for the free energy potential:

$$\begin{aligned}\rho\psi(\underset{\sim}{\varepsilon},\underset{\sim}{\varepsilon}^p,{}^{\chi}\underset{\sim}{\varepsilon}^p,\boldsymbol{\nabla}^{\chi}\underset{\sim}{\varepsilon}^p) &= \frac{1}{2}\underset{\sim}{\varepsilon}^e:\underset{\sim}{\boldsymbol{\Lambda}}:\underset{\sim}{\varepsilon}^e+\frac{1}{3}C\underset{\sim}{\varepsilon}^p:\underset{\sim}{\varepsilon}^p \\ &+ \frac{1}{2}(\underset{\sim}{\varepsilon}^p-{}^{\chi}\underset{\sim}{\varepsilon}^p):\underset{\sim}{\boldsymbol{C}}_{\chi}:(\underset{\sim}{\varepsilon}^p-{}^{\chi}\underset{\sim}{\varepsilon}^p) \\ &+ \frac{1}{2}\boldsymbol{\nabla}^{\chi}\underset{\sim}{\varepsilon}^p\vdots\underset{\approx}{\boldsymbol{A}}\vdots\boldsymbol{\nabla}^{\chi}\underset{\sim}{\varepsilon}^p \end{aligned} \tag{193}$$

from which the state laws are derived:

$$\underset{\sim}{\boldsymbol{\sigma}}=\underset{\sim}{\boldsymbol{\Lambda}}:\underset{\sim}{\varepsilon}^e,\quad \underset{\sim}{\boldsymbol{X}}=\frac{2}{3}C\underset{\sim}{\varepsilon}^p+\frac{2}{3}C_{\chi}(\underset{\sim}{\varepsilon}^p-{}^{\chi}\underset{\sim}{\varepsilon}^p) \tag{194}$$

$$\underset{\sim}{\boldsymbol{a}}=-\frac{2}{3}\underset{\sim}{\boldsymbol{C}}_{\chi}:(\underset{\sim}{\varepsilon}^p-{}^{\chi}\underset{\sim}{\varepsilon}^p),\quad \underset{\sim}{\boldsymbol{b}}=\underset{\approx}{\boldsymbol{A}}\vdots\boldsymbol{\nabla}^{\chi}\underset{\sim}{\varepsilon}^p \tag{195}$$

In the simplified situation for which

$$\underset{\sim}{\boldsymbol{C}}_{\chi}=C_{\chi}\underset{\sim}{\mathbf{1}},\quad \underset{\approx}{\boldsymbol{A}}=A\underset{\approx}{\mathbf{1}} \tag{196}$$

where $\underset{\sim}{\mathbf{1}}$ and $\underset{\approx}{\mathbf{1}}$ are the fourth rank and sixth rank identity tensors operating respectively on symmetric second order tensors and symmetric (w.r.t. the two first indices) third rank tensors, the combination of the additional balance equation and state laws leads to the following partial differential equation:

$$\underset{\sim}{\boldsymbol{a}}=div\,\underset{\approx}{\boldsymbol{b}}=A\Delta^{\chi}\underset{\sim}{\varepsilon}^p=-\frac{2}{3}C_{\chi}(\underset{\sim}{\varepsilon}^p-{}^{\chi}\underset{\sim}{\varepsilon}^p)\quad\Longrightarrow\quad {}^{\chi}\underset{\sim}{\varepsilon}^p-\frac{3A}{2C_{\chi}}\Delta^{\chi}\underset{\sim}{\varepsilon}^p=\underset{\sim}{\varepsilon}^p \tag{197}$$

The differential operators act in the following way w.r.t. to a Cartesian frame $(\underline{\boldsymbol{e}}_i)_{i=1,3}$:

$$div\,\underset{\approx}{\boldsymbol{b}}=b_{ijk,k}\underline{\boldsymbol{e}}_i\otimes\underline{\boldsymbol{e}}_j,\quad \Delta^{\chi}\underset{\sim}{\varepsilon}^p=(\Delta^{\chi}\varepsilon^p_{ij})\underline{\boldsymbol{e}}_i\otimes\underline{\boldsymbol{e}}_j \tag{198}$$

The associated boundary conditions on the boundary of the body are given by a set of 6 equations:

$$\underset{\sim}{\boldsymbol{b}}.\underline{\boldsymbol{n}}=\underset{\sim}{\boldsymbol{a}}^c \tag{199}$$

The internal variable $\underset{\sim}{\boldsymbol{\alpha}}=\underset{\sim}{\varepsilon}^p$ is the proper state variable for a plasticity theory incorporating linear kinematic hardening, $\underset{\sim}{\boldsymbol{X}}$ being the back–stress

tensor. The retained isotropic yield function for extended J_2–plasticity is

$$f(\underset{\sim}{\boldsymbol{\sigma}}, \underset{\sim}{\boldsymbol{X}}) = J_2(\underset{\sim}{\boldsymbol{\sigma}} - \underset{\sim}{\boldsymbol{X}}) - \sigma_Y \tag{200}$$

$$= J_2(\underset{\sim}{\boldsymbol{\sigma}} - \frac{2}{3}(C + C_\chi)\underset{\sim}{\boldsymbol{\varepsilon}}^p - \frac{2}{3}C_\chi{}^\chi\underset{\sim}{\boldsymbol{\varepsilon}}^p) - \sigma_Y \tag{201}$$

$$= J_2(\underset{\sim}{\boldsymbol{\sigma}} - \frac{2}{3}C_\chi{}^\chi\underset{\sim}{\boldsymbol{\varepsilon}}^p + A(1 + \frac{C}{C_\chi})\Delta^\chi\underset{\sim}{\boldsymbol{\varepsilon}}^p) - \sigma_Y \tag{202}$$

where $J_2(\underset{\sim}{\boldsymbol{\sigma}}) = \sqrt{3(\underset{\sim}{\boldsymbol{\sigma}}^{dev} : \underset{\sim}{\boldsymbol{\sigma}}^{dev})/2}$ is the von Mises second invariant for symmetric second rank tensors. The normality rule is adopted:

$$\dot{\underset{\sim}{\boldsymbol{\varepsilon}}}^p = \dot{\lambda}\frac{\partial f}{\partial \underset{\sim}{\boldsymbol{\sigma}}} = -\dot{\lambda}\frac{\partial f}{\partial \underset{\sim}{\boldsymbol{X}}} = \dot{p}\underset{\sim}{\boldsymbol{N}} \tag{203}$$

The intrinsic dissipation then takes its classical form:

$$D^{res} = \underset{\sim}{\boldsymbol{\sigma}} : \dot{\underset{\sim}{\boldsymbol{\varepsilon}}}^p - \underset{\sim}{\boldsymbol{X}} : \dot{\underset{\sim}{\boldsymbol{\varepsilon}}}^p = f\dot{p} + \sigma_Y\dot{p} \geq 0 \tag{204}$$

with energy storage associated with kinematic hardening.

The fact that the gradient of the plastic strain tensor (or part of it, in models retaining only the rotational part) mainly impacts on the kinematic hardening of the material has been recognized in Steinmann (1996); Forest et al. (2002); Forest and Sievert (2003); Gurtin (2003). In these references, the divergence of the higher order generalized stress tensor acts as a backs–stress.

Plasticity in single crystals

The proposed micromorphic approach can be applied to crystal plasticity in several ways. For small strain and small rotations, the plastic strain increments and the lattice rotation rate are

$$\dot{\underset{\sim}{\boldsymbol{\varepsilon}}}^p = \sum_{i=1}^{N}\dot{\gamma}^s\,\{\underline{\boldsymbol{m}}^s \otimes \underline{\boldsymbol{n}}^s\}, \quad \underset{\sim}{\boldsymbol{\omega}}^e = \underset{\sim}{\boldsymbol{\omega}} - \underset{\sim}{\boldsymbol{\omega}}^p = \underset{\sim}{\boldsymbol{\omega}} - \sum_{i=1}^{N}\dot{\gamma}^s\,\}\underline{\boldsymbol{m}}^s \otimes \underline{\boldsymbol{n}}^s\{ \tag{205}$$

Definitions of total, plastic and elastic rotation rates are given by (84). Which variable ϕ should be chosen to introduce a micromorphic variable? There are several possibilities depending on the physical nature of the deformation mechanism to be accounted for. If ϕ is the lattice rotation vector given by (84)

$$\phi \equiv \underline{\boldsymbol{\Phi}}^e, \quad {}^\chi\phi \equiv \underline{\boldsymbol{\Phi}} \tag{206}$$

the Cosserat theory proposed in chapter 1 is recovered. The gradient of $\underline{\boldsymbol{\Phi}}^e$ is nothing but the lattice curvature tensor.

One may think also of the following choice:

$$\phi \equiv \gamma^s \tag{207}$$

as proposed in Gurtin (2000); Gurtin and Needleman (2005); Bayley et al. (2006). Such a model is indeed applicable for a single crystal but it seems to have severe limitations when applied to bicrystals or multicrystals for the following reason. The variables γ^s are not uniquely defined in each domain. They are defined only up to a symmetry belonging to the crystal symmetry group of the material. As a result, jump conditions at an interface between two such materials (like two grains) cannot be uniquely defined. Similar difficulties arise in anisotropic damage of composites Germain et al. (2007). An acceptable alternative choice is to consider the full plastic strain $\phi \equiv \underset{\sim}{\boldsymbol{\varepsilon}}^p$ as already illustrated in 2.1.

Internal constraints

The coupling parameter H_χ can be seen as a penalty factor to enforce the internal constraint:

$$\phi \simeq {}^{\chi}\phi \tag{208}$$

Indeed, the generalized stress a was taken proportional to the relative strain $\phi - {}^{\chi}\phi$ so that parameter H_χ acts as a penalty factor in the power of internal forces (129). The constraint (208) can be strictly enforced if H_χ is treated as a Lagrange multiplier in the variational formulation Tian-Hu (2004). Such a model then incorporates the effect of the first gradient $\boldsymbol{\nabla}\phi$ of the selected variable in the constitutive theory.

Second gradient crystal plasticity When $\phi \equiv \underset{\sim}{\boldsymbol{F}}$ is taken as the full deformation gradient, the considered theory is that of the full micromorphic continuum as recognized in 2.1. The internal constraint (208) imposes that the microdeformation coincides with the macrodeformation. As a result, the effect of the gradient of $grad\,\underline{\boldsymbol{u}}$ is introduced in the theory, which corresponds to the second gradient model developed by Mindlin (1965); Mindlin and Eshel (1968); Germain (1973a).

Fleck and Hutchinson have proposed a crystal plasticity theory based on the second grade continuum in Fleck and Hutchinson (1997); Shu and Fleck (1999). This theory is sketched in the appendix 2.2. It incorporates the effect of the dislocation density tensor but also of gradient of slip normal to the slip plane. The latter effect is introduced therefore in addition to the additional hardening associated with the densities of so–called geometrically necessary dislocations. The second gradient and the Cosserat theories of

crystal plasticity are compared in a simple situation of single slip in section 2.2.

Aifantis and Gurtin models When ϕ is related to plastic deformation, this situation corresponds to the strain gradient plasticity models presented in the literature. For instance, if $\phi \equiv p$, the cumulative plastic strain, the following evolution of the stress under plastic loading is deduced from (188), when the internal constraint is enforced ($H \ll H_\chi$):

$$\sigma_{eq} = \sigma_Y + Hp - A\Delta p \tag{209}$$

which is identical to the strain gradient model proposed by Aifantis (1987). It is also closely related to the corresponding deformation theory exposed in Fleck and Hutchinson (2001). There is also a direct connection to the so–called "explicit gradient" theory presented in Engelen et al. (2003). These authors introduce the micromorphic equivalent plastic strain:

$$^{\chi}p = p - c^2\Delta p \tag{210}$$

If this expression is inserted in a hardening law of the form $\sigma_{eq} = \sigma_Y + H\,^{\chi}p$, the partial differential equation (209) is obtained.

The strain gradient plasticity models proposed in Gurtin (2003); Forest and Sievert (2003) result from the choice $\phi \equiv \underset{\sim}{\varepsilon}^p$, i.e. the full plastic strain tensor. In these works, the corresponding generalized balance equation and boundary conditions are clearly stated, based on the method of virtual power.

2.2 Application to simple shear in a two–phase single crystal

In the current endeavour to connect the different scales involved in plasticity of metals from atomistics to continuum plasticity Forest et al. (2001c), there is a strong research stream trying to replace detailed descriptions of the collective behaviour of dislocations by continuum mechanical models. When the size of the investigated microstructure is of the order of magnitude of typically 1 to 10 μm, or below, classical continuum crystal plasticity theory, as settled in Asaro (1983), for instance, ceases to be relevant since it is not able to reproduce the observed size effects. In contrast, nonlocal or generalized–continuum plasticity models incorporating intrinsic length scales account for the size effects, at least in a qualitative manner Fleck and Hutchinson (1997).

The aim of the present section is to directly compare the governing equations and analytical solutions resulting from dislocation-based, Cosserat and strain–gradient models of crystal plasticity. For this purpose, a two-phase

single crystal material oriented for single slip and subjected to shear loading is investigated. A one-dimensional (1D) laminate microstructure consisting of periodically alternating layers of plastically soft and hard phases is considered. The hard phase is supposed to behave only elastically, and the soft channel as an elastic-ideally plastic material. Classical continuum crystal plasticity predicts homogeneous deformation and stress in each phase, possibly with a jump of some quantities at the interface. In contrast, the interest here is focused on the non-homogeneous distribution of plastic slip and lattice rotations in the soft phase arising from the analysis based on dislocation mechanics, as well as on Cosserat and strain gradient continua. Intrinsic length scales which are responsible for size effects in plasticity of such layered microstructures arise naturally in the dislocation analysis. The present simple examples enlighten the importance and physical relevance of the additional boundary or interface conditions usually introduced in generalized plasticity models Shu et al. (2001).

Comparisons between dislocation-based and strain gradient models exist in the literature, at least in two-dimensional cases. Generally, results of 2D discrete dislocation dynamics are compared with nonlocal continuum models. For instance in Bassani et al. (2001), the hardening behavior induced by a periodic distribution of hard precipitates in a crystalline matrix oriented for single slip is analysed for the case of simple shear. For that purpose, dislocation dynamics is resorted to on the discrete level, whereas a nonlocal model is used at the continuum level. Localized or diffuse plastic deformation patterns resulting from the dislocation simulations are compared with the predictions of the nonlocal model. In Shu et al. (2001), shearing of a single crystal layer is studied in detail for both single slip and double slip orientations. Dislocations are not allowed to cross the boundaries of the layer, which leads to non-homogeneous plastic deformation patterns. For both dislocation and continuum models, the analysis is based on numerical simulations, which makes it difficult to interpret clearly the continuum intrinsic length scales present in the model in terms of the corresponding elementary dislocation processes.

The dislocation simulations in Cleveringa et al. (1998); Bassani et al. (2001); Shu et al. (2001) are two-dimensional in the sense that only straight dislocations in a plane perpendicular to them are considered. Formation of dislocation pileups and dipoles are then the most active elementary deformation and hardening mechanisms. However the dislocations which are constrained to glide in the small volumes or narrow channels are generally required to bow-out. Obviously, the bowing of dislocations cannot be taken into account in the 2D dislocation dynamics framework. By contrast, the continuum line-tension dislocation-based model presented in section 2.2 is

able to account for the Orowan bowing which is frequently encountered in the plastic deformation of various dislocation substructures (cells, subgrains, ladders, ...), single-crystal nickel-based superalloys, passivated thin films or microlaminates. The model to be presented here shows that the bowing of dislocations in the narrow channels leads to size effects. For completeness, an analysis of double-ended pileups of straight dislocations that can form in the soft channels under the considered loading conditions are investigated in section 2.2. Pileups are usually regarded as an appropriate illustration of the dislocation accumulation at interfaces or grain boundaries. They classically illustrate the effect of the so–called geometrically necessary dislocations Ashby (1970). As such, they have been the source of inspiration of several strain gradient models. Both line–tension and pileup dislocation-based models will be compared with the response of generalized continuum models. This attempt to directly identify the line-tension dislocation-based model with a Cosserat model has been presented in Sedláček and Forest (2000); Forest and Sedláček (2003); Forest (2008).

The Cosserat elastoplasticity model proposed in section 2.2 mimics the local response of the considered material in various situations, without explicitly introducing dislocation distributions. Analytical solutions under periodicity conditions are found and compared with the above dislocation approach. Especially, it is shown under which circumstances the Cosserat rotation coincides with the lattice rotation. Finally, in section 2.2, the plastic strain gradient models of Shu, Fleck and Hutchinson Fleck and Hutchinson (1997); Shu and Fleck (1999) and of Aifantis Aifantis (1987, 1999) are recalled and applied to the present simple case to compare them with the dislocation and Cosserat models. It will be shown that the interface conditions to be fulfilled in each model play a major role in the modelling of non–homogeneous deformation patterns.

Reference dislocation models

First, the line-tension model presented in Sedláček and Forest (2000); Forest and Sedláček (2003) is briefly reviewed and extended in the following two sections. Then, in section 2.2, an alternative configuration for which an explicit expression of dislocation distribution in the channels under shear is available, viz. that of the double-ended pileup, is briefly presented.

The considered periodic laminate microstructure with direction of the applied stress indicated and the coordinate system used, is sketched in figure 3. Instead of individual dislocations, a continuous field of curved glide dislocations in the soft channel is considered. For simplicity, all quantities are assumed to be independent of y and z. The equilibrium position of a

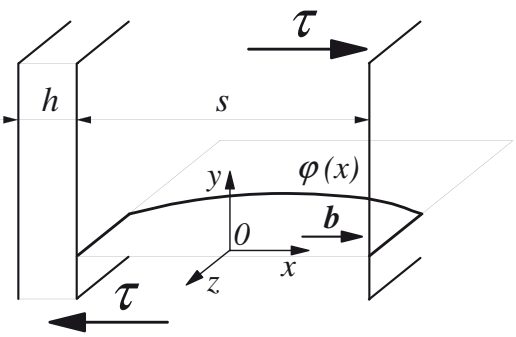

Figure 3. Dislocation bowing in the soft phase. A part of the loop gliding in the xOz plane is shown, with the curved (originally screw) section $\varphi(x)$ and edge segments at the soft / hard phase interface. The resolved shear stress τ and Burgers vector $\boldsymbol{b}$ are indicated. Labels s and h are used to designate the soft and hard phase, respectively.

representative bowing screw dislocation $\varphi(x)$ with Burgers vector magnitude b and constant line tension T in a shear stress field $\tau(x)$ is considered,

$$\tau(x)\, b + T\, \partial_{xx}\, \varphi(x) = 0\,. \tag{211}$$

The second derivative of the dislocation displacement $\varphi(x)$ follows from the linearized dislocation curvature. Strictly speaking, the linearized dislocation model is restricted to anelasticity (bowing of dislocations in the soft phase) since it is unable to describe fully plastic flow i.e. the glide of critically bowed dislocations depositing edge segments at the interfaces. To be able to deal with the plasticity, at least in an approximate way, one can introduce the Orowan stress in the soft channel of width s, $\tau_{Or} \approx 1.5\mu b/s$, as a threshold stress : if the mean shear stress in the channel reaches the value of the Orowan stress, the dislocation shape does not change any more and the bowed-out dislocations glide in the channels, depositing edges at the interfaces. This transition from anelasticity to plasticity, which is introduced here in an ad hoc manner, arises naturally in the framework of the full-curvature model Sedláček and Forest (2000); Sedláček et al. (2003).

Increment of plastic shear caused by the displacement $\varphi(x)$ of the mobile dislocations with density ϱ_m follows from the Orowan relation,

$$\gamma^p(x) = \varrho_m b\, \varphi(x)\,. \tag{212}$$

The non-homogeneous plastic deformation is accommodated by the 'geometrically necessary' content of the bowing dislocations $\varphi(x)$ which is described by the Nye-Kröner dislocation density tensor $\underset{\sim}{\boldsymbol{\alpha}}$. Its only non-vanishing component $\alpha = \alpha_{xz}$ can be directly derived from the plastic shear,

$$\alpha(x) = \partial_x \gamma^p(x)\,. \tag{213}$$

It corresponds formally to continuously distributed 'pileups' of edge dislocations aligned with the z axis of figure 3, which is exactly the edge content of the bowing (originally screw) mobile dislocations with the scalar density ρ_m. By utilizing Hooke's law for elastic shear strain $\varepsilon^{\mathrm{e}} = \varepsilon^{\mathrm{e}}_{xy}$,

$$\tau(x) = 2\mu\varepsilon^{\mathrm{e}}(x)\,, \tag{214}$$

a differential equation for the elastic and plastic shear strains results,

$$2\varepsilon^e(x) + \lambda^2 \partial_{xx}\,\gamma^p(x) = 0\,, \tag{215}$$

with the intrinsic length scale λ given approximately by the average distance between the mobile dislocations,

$$\lambda = \sqrt{\frac{T}{\mu \varrho_m b^2}} \approx \frac{1}{\sqrt{\varrho_m}}\,. \tag{216}$$

We note in passing that the ratio between the channel width and intrinsic length s/λ is crucial for the size effect appearing during plastic deformation of narrow channels, thin films, microlaminates, etc., cf. Sedláček and Forest (2000).

To be able to derive equations for the lattice rotation based on eq. (215), relations for the elastic and plastic strains and rotations which will be extracted from the stress equilibrium and strain compatibility conditions are needed.

A compatible material displacement field $\boldsymbol{u} = (\bar{\gamma}y, u_y(x), 0)^T$ is considered, leading to material displacement gradient, $\boldsymbol{\beta} = grad\,\boldsymbol{u}$, of the form

$$\boldsymbol{\beta} = \begin{bmatrix} 0 & \bar{\gamma} & 0 \\ \partial_x u_y & 0 & 0 \\ 0 & 0 & 0 \end{bmatrix}\,. \tag{217}$$

The non-homogeneous plastic shear (212) causes a generally incompatible plastic distortion

$$\boldsymbol{\beta}^{\mathrm{p}} = \gamma^{\mathrm{p}} \underline{\boldsymbol{m}} \otimes \underline{\boldsymbol{n}} = \begin{bmatrix} 0 & \gamma^{\mathrm{p}} & 0 \\ 0 & 0 & 0 \\ 0 & 0 & 0 \end{bmatrix}\,, \tag{218}$$

The slip direction $\underline{\boldsymbol{m}}$ and the normal to the slip plane $\underline{\boldsymbol{n}}$ coincide with axes x and y, respectively, see figure 3. Finally, the elastic distortion $\boldsymbol{\beta}^{\mathrm{e}} = \boldsymbol{\beta} - \boldsymbol{\beta}^{\mathrm{p}}$ results in the form

$$\boldsymbol{\beta}^{\mathrm{e}} = \begin{bmatrix} 0 & \gamma^{\mathrm{e}} & 0 \\ \partial_x u_y & 0 & 0 \\ 0 & 0 & 0 \end{bmatrix}, \tag{219}$$

where $\gamma^{\mathrm{e}}(x) = \bar{\gamma} - \gamma^{\mathrm{p}}(x)$. The symmetric part of $\boldsymbol{\beta}^{\mathrm{e}}$ determines the elastic strain which enters Hooke's law (214),

$$\varepsilon^{\mathrm{e}}(x) = \frac{\gamma^{\mathrm{e}} + \partial_x u_y}{2}\,. \tag{220}$$

The skew-symmetric part of $\boldsymbol{\beta}^{\mathrm{e}}$ can be represented by the axial vector of lattice rotation $\boldsymbol{\phi}^{\mathrm{e}} = (0, 0, \phi^{\mathrm{e}} = \phi^{\mathrm{e}}_z)^T$,

$$\phi^{\mathrm{e}}(x) = -\frac{\gamma^{\mathrm{e}} - \partial_x u_y}{2}\,. \tag{221}$$

To solve the boundary value problem outlined here, a homogeneous strain and a homogeneous stress approximation are considered successively.

Periodic solution Stress equilibrium ($\operatorname{div}\boldsymbol{\sigma} = 0$) requires that the shear stress is constant and equal to the applied shear stress,

$$\tau(x) = \bar{\tau}\,. \tag{222}$$

With Hooke's law (214) in the form

$$\varepsilon^{\mathrm{e}} = \frac{\bar{\tau}}{2\mu}\,, \tag{223}$$

eq. (215) yields the following equation for the plastic shear strain,

$$\lambda^2\, \partial_{xx}\, \gamma^p(x) = -\frac{\bar{\tau}}{\mu}\,. \tag{224}$$

Due to the fact that the soft phase is elastic - ideally plastic and from the discussion following equation (211), it is clear that $\bar{\tau} \leq \tau_{\mathrm{Or}}$. To obtain a unique solution to the problem at $\bar{\tau} = \tau_{\mathrm{Or}}$ (plastic regime), one has to fix the mean material strain by requiring that e.g. for the mean applied material shear strain

$$\frac{\bar{\gamma}}{2} \;=\; \frac{1}{s+h}\left(\bar{\varepsilon}_{\mathrm{h}} h + \int_{\langle s\rangle} \varepsilon_{\mathrm{s}}(x)\, dx\right). \tag{225}$$

From equations (217), (220), (223) and (225), the amount of plastic deformation can be found,

$$\int_{\langle s \rangle} \gamma^{\mathrm{p}}(x)\, dx = \left(\bar{\gamma} - \frac{\bar{\tau}}{\mu} \right) (s + h)\,. \tag{226}$$

The lattice rotation can be obtained from eqs. (220), (221) and (223) as

$$\phi^{\mathrm{e}}(x) = \frac{\bar{\tau}}{2\mu} - \bar{\gamma} + \gamma^{\mathrm{p}}(x)\,. \tag{227}$$

As a consequence of (227), $\partial_x \gamma^{\mathrm{p}} = \partial_x \phi^{\mathrm{e}}$, and the governing equation for the lattice rotation in the soft phase $\phi^{\mathrm{e}}_{\mathrm{s}}$ becomes,

$$\lambda^2\, \partial_{xx}\, \phi^{\mathrm{e}}_{\mathrm{s}}(x) = -\frac{\bar{\tau}}{\mu}\,. \tag{228}$$

Accordingly, the lattice rotation and plastic slip (equation (224)) displays a parabolic profile,

$$\phi^{\mathrm{e}}_{\mathrm{s}}(x) = ax^2 + bx + c\,, \tag{229}$$

with $a = -\bar{\tau}/(2\lambda^2\mu)$. Note that, in the iso-stress framework, the exact solution of the full-curvature problem is well known: it is a circular arc. Nevertheless, we have linearized the curvature in equation (211), to be consistent with the rest of the paper. From symmetry reasons (periodicity),

$$\partial_x \phi^{\mathrm{e}}(0) = 0\,, \tag{230}$$

which implies $b = 0$. In the anelastic regime ($\bar{\tau} < \tau_{Or}$), the requirement for continuity of lattice rotation,

$$\phi^{\mathrm{e}}_{\mathrm{s}}(\pm\frac{s}{2}) = \phi^{\mathrm{e}}_{\mathrm{h}}\,, \quad \bar{\tau} < \tau_{Or}\,, \tag{231}$$

determines the constant c. Lattice rotation in the hard phase results from eq. (227),

$$\phi^{\mathrm{e}}_{h} = \frac{\bar{\tau}}{2\mu} - \bar{\gamma}\,. \tag{232}$$

Accordingly, the solution takes the form

$$\phi^{\mathrm{e}}_{\mathrm{s}}(x) = \left(\frac{\bar{\tau}}{2\mu} - \bar{\gamma} \right) - \frac{\bar{\tau}}{2\mu} \left(\frac{x^2}{\lambda^2} - \frac{s^2}{4\lambda^2} \right)\,, \quad \bar{\tau} < \tau_{Or}\,. \tag{233}$$

In the plastic regime ($\bar{\tau} = \tau_{Or}$), there is a discontinuity of the lattice rotation $\Delta\phi^{\mathrm{e}}$ caused by the discontinuity of the plastic strain $\Delta\gamma^{p}$ which is

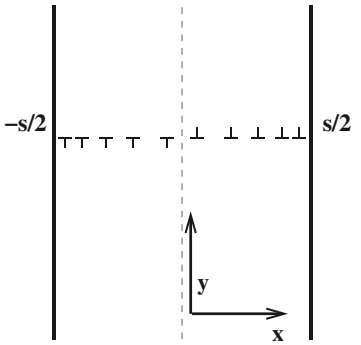

Figure 4. Double–ended dislocation pile–up in the soft phase under simple shear.

accommodated by the edge dislocations deposited at the interfaces. The solution is

$$\phi_{\rm s}^{\rm e}(x) = \left(\frac{\bar{\tau}}{2\mu} - \bar{\gamma}\right) - \frac{\bar{\tau}}{2\mu}\left(\frac{x^2}{\lambda^2} - \frac{s^2}{4\lambda^2}\right) + \Delta\phi^{\rm e}\,, \quad \bar{\tau} = \tau_{Or}\,. \tag{234}$$

The magnitude of the discontinuity $\Delta\phi^{\rm e}$ is determined from the equations (226) and (227),

$$\Delta\phi^{\rm e} = \frac{s+h}{s}\left(\bar{\gamma} - \frac{\bar{\tau}}{\mu}\right) - \frac{\bar{\tau}}{12\mu}\frac{s^2}{\lambda^2}\,. \tag{235}$$

We will return to the meaning of the step in lattice rotation later in the text.

Even though the stress equilibrium and strain compatibility are fulfilled exactly in the 1D iso-stress framework, the model is not realistic enough, for it cannot account for the internal stresses (i.e. kinematic hardening) which would arise in 2D or 3D structures. In the 1D model, the internal stresses are fully relaxed by the lattice rotations.

Pileup model This subsection presents a different model of dislocation structure that can form under the same applied loading conditions and that leads to a one-dimensional distribution of plastic slip in the macroscopic limit, that is dislocation pileups. This model is often advocated for the motivation of nonlocal theories and is recalled here, although its ingredients are different from the models in section 2.2 based on line tension effects.

A configuration for which an explicit expression of dislocation distribution in the channels under shear is available, is that of the double–ended pileup Hirth and Lothe (1982); Tanaka and Mura (1981), caused by the simple shearing of a single Frank–Read source at the centre of the channel of width s (figure 4). For simplicity, we take $h \simeq 0$ so that any image force due to the presence of the hard phase h acting on dislocations in the channel can be neglected. The approach based on the continuum theory of dislocations is briefly recalled here, in the case of pileups of edge dislocations with Burgers vector of magnitude b. The equilibrium of dislocations under the applied stress $\bar{\tau}$ can be written :

$$\bar{\tau} + \tau_d + \tau_c = 0\,, \tag{236}$$

where τ_d is the stress at x due to all present dislocations and τ_c the (assumed constant) threshold for the onset of dislocation motion. If $n(x)$ denotes the number of dislocations per unit length, the dislocation stress takes the form :

$$\tau_d(x) = A \int_{-s/2}^{s/2} \frac{n(x')}{x - x'} dx' \quad with \quad A = \frac{\mu b}{2\pi(1-\nu)}\,. \tag{237}$$

A solution $n(x)$ of the integral equation (236) exists under the condition of unbounded density at two tips of the pileup, viz. $x = \pm s/2$ in figure 4 :

$$n(x) = \frac{\bar{\tau} - \tau_c}{\pi A} \frac{x}{\sqrt{\left(\frac{s}{2}\right)^2 - x^2}}\,. \tag{238}$$

The total number of dislocations in each pileup is

$$N = \int_0^{s/2} n(x) dx = \frac{\bar{\tau} - \tau_c}{\pi A} \frac{s}{2}\,. \tag{239}$$

The displacement of material above the slip plane with respect to that below is given by

$$u_x(x, y) = bH(y) \int_x^{s/2} n(x') dx'\,, \tag{240}$$

where H is the Heaviside function and the pileups are assumed to lie at $y = 0$ in the volume considered here. Differentiating the previous equation with respect to y yields :

$$\partial_y u_x(x, y) = b\delta(y) \int_x^{s/2} n(x') dx'\,. \tag{241}$$

with δ the Dirac distribution. The corresponding amount of plastic slip is defined by

$$\gamma^{\mathrm{p}}(x) = \frac{1}{l}\int_{-l/2}^{l/2} \partial_y u_x(x,y)dy = \frac{b}{l}\int_x^{s/2} n(x)dx \tag{242}$$

$$= \frac{b}{l}\frac{\bar{\tau}-\tau_c}{\pi A}\sqrt{\left(\frac{s}{2}\right)^2 - x^2}\,, \quad for \quad -s/2 \le x \le s/2 \tag{243}$$

It is assumed that the pileups are periodically distributed along direction y perpendicular to slip plane with period l. The length l is assumed to be large enough for the interaction between parallel pileups to be neglected. As a result, the distribution of plastic slip in the channel is the arc of an ellipse. It vanishes at the tips of the pileups and takes its maximal value Nb/l at the centre. This distribution is therefore different from the parabolic profile found in section 2.2. The mean value of the plastic slip is

$$\bar{\gamma}^{\mathrm{p}} = \frac{2}{s}\int_0^{s/2} \gamma(x)dx = \frac{b}{l}\frac{\bar{\tau}-\tau_c}{2\pi A}\frac{s}{2}\,. \tag{244}$$

It can be shown that the dislocation stress τ_d introduced in equation (236) does not depend on x, as required by the equilibrium condition

$$\tau_d = -(\bar{\tau}-\tau_c) = -\frac{2\mu l}{\pi(1-\nu)s}\bar{\gamma}^{\mathrm{p}}\,. \tag{245}$$

This proves that the double–ended dislocation pileup produces a hardening component of linear kinematic type :

$$X = -\tau_d = C\bar{\gamma}^{\mathrm{p}} \quad with \quad C = \frac{2\mu l}{\pi(1-\nu)s}\,. \tag{246}$$

We note that that the pileup model is formulated at a different level of approximation than the line-tension models of subsection 2.2. Especially, a periodic distribution of pileups is assumed along the y direction. This enables the presence of the dislocation stress τ_d in the 1D model. Furthermore, each pileup is completely embedded in an elastic matrix, so that the stress cannot relax. If the pileups were distributed continuously along the y direction, as the bowed dislocations in the previous sections are, the stress would then relax exactly as in section 2.2 and the local internal stresses and thus the macroscopic hardening would disappear.

Application of the Cosserat model

The two-phase material now is a heterogeneous Cosserat continuum. In the first paragraph, both phases will be assumed to have a linearized behaviour,

with different moduli. In the two following ones, the soft phase exhibits elastoplastic behaviour. We look here for solutions fulfilling all compatibility and equilibrium requirements with the only constraint that all fields must be periodic along x with period $s + h$ (see figure 3).

Linear approximation Both phases are Cosserat linear materials with constants μ_h, μ_{ch}, β_h and μ_s, μ_{cs}, β_s (see section 1.2 for the definition of isotropic Cosserat elasticity). The moduli of phase s can be also treated as secant elastoplastic moduli and the elastic and plastic parts will not be distinguished. Phase h must be thought of as almost classical, which means that β_h is small, but the solution is given here in the general case.

A mean shear deformation $\overline{\gamma}$ is applied along the direction x. We look again for a displacement field of the form :

$$u_x = \overline{\gamma} y, \quad u_y(x), \quad u_z = 0\,. \tag{247}$$

The deformation of a Cosserat material is described also by the micro–rotation axial vector field :

$$\phi_x = \phi_y = 0, \quad \phi_z = \phi(x)\,. \tag{248}$$

Thus, the Cosserat deformation and curvature tensors take the form :

$$\boldsymbol{e} = \begin{bmatrix} 0 & \overline{\gamma} + \phi & 0 \\ \partial_x u_y - \phi & 0 & 0 \\ 0 & 0 & 0 \end{bmatrix}, \quad \boldsymbol{\kappa} = \begin{bmatrix} 0 & 0 & 0 \\ 0 & 0 & 0 \\ \partial_x \phi & 0 & 0 \end{bmatrix}. \tag{249}$$

The associated non–vanishing components of the force and couple–stress tensors are :

$$\sigma_{xy} = \mu(\overline{\gamma} + \phi + e_{yx}) + \mu_c(\overline{\gamma} + \phi - e_{yx})\,, \tag{250}$$

$$\sigma_{yx} = \mu(\overline{\gamma} + \phi + e_{yx}) - \mu_c(\overline{\gamma} + \phi - e_{yx})\,, \tag{251}$$

$$\mu_{zx} = 2\beta \partial_x \phi\,. \tag{252}$$

The balance equations give

$$\partial_x \sigma_{yx} = 0, \quad \partial_x \mu_{zx} - (\sigma_{xy} - \sigma_{yx}) = 0\,, \tag{253}$$

Taking the elasticity relations into account, these equations become :

$$\mu(\partial_x \phi + \partial_x e_{yx}) - \mu_c(\partial_x \phi - \partial_x e_{yx}) = 0\,, \tag{254}$$

$$\beta \partial_{xx} \phi - \mu_c(\overline{\gamma} + \phi - e_{yx}) = 0\,. \tag{255}$$

Equation (254) can be rearranged to give

$$\partial_x e_{yx} = -\frac{\mu - \mu_c}{\mu + \mu_c}\,\partial_x \phi\,. \tag{256}$$

The equation for ϕ follows then from (255) :

$$\beta \partial_{xxx}\phi - \frac{2\mu\mu_c}{\mu + \mu_c}\,\partial_x \phi = 0\,. \tag{257}$$

We define for each phase :

$$\omega_s^2 = \frac{2\mu_s\mu_{cs}}{\beta_s(\mu_s + \mu_{cs})}, \quad \omega_h^2 = \frac{2\mu_h\mu_{ch}}{\beta_h(\mu_h + \mu_{ch})}\,, \tag{258}$$

Each ω is the inverse of a length. The solution of (257) takes the form :

$$\phi_s = a_s \cosh(\omega_s x) + d_s, \quad for \quad -s/2 < x < s/2\,, \tag{259}$$

$$\phi_h^+ = a_h \cosh(\omega_h(x - \frac{s+h}{2})) + d_h, \quad for \quad s/2 < x < (s+h)/2\,, \tag{260}$$

$$\phi_h^- = a_h \cosh(\omega_h(x + \frac{s+h}{2})) + d_h, \quad for \quad -(s+h)/2 < x < -s/2\,. \tag{261}$$

To reduce the number of integration constants in equations (259) to (261), the periodicity of ϕ has been used, together with the following symmetry conditions :

$$\partial_x\phi(0) = \partial_x\phi(-\frac{s+h}{2}) = \partial_x\phi(\frac{s+h}{2}) = 0\,. \tag{262}$$

Then, e_{yx} can now be determined from (256) as follows :

$$\begin{aligned} e_{yx}^{s} &= -\frac{\mu_s - \mu_{cs}}{\mu_s + \mu_{cs}}\phi_s + e_s\,, \\ e_{yx}^{h+} &= -\frac{\mu_h - \mu_{ch}}{\mu_h + \mu_{ch}}\phi_h^+ + e_h\,, \qquad (263) \\ e_{yx}^{h-} &= -\frac{\mu_h - \mu_{ch}}{\mu_h + \mu_{ch}}\phi_h^- + e_h\,. \qquad (264) \end{aligned}$$

where e_h and e_s are integration constants. Furthermore, equation (255) implies that :

$$e_{yx} = -\frac{\beta}{\mu_c}\partial_{xx}\phi + \overline{\gamma} + \phi\,, \tag{265}$$

$$e_{yx}(0) = -\frac{\beta_s}{\mu_{cs}}a_s\omega_s^2 + \overline{\gamma} + a_s + d_s = -\frac{\mu_s - \mu_{cs}}{\mu_s + \mu_{cs}}(a_s + d_s) + e_s\,, \tag{266}$$

$$e_{yx}(\frac{s+h}{2}) = -\frac{\beta_h}{\mu_{ch}}a_h\omega_h^2 + \overline{\gamma} + a_h + d_h = -\frac{\mu_h - \mu_{ch}}{\mu_h + \mu_{ch}}(a_h + d_h) + e_h\,, \tag{267}$$

from which the values of e_s and e_h are deduced :

$$e_s = \overline{\gamma} + d_s \frac{2\mu_s}{\mu_s + \mu_{cs}}\,, \quad e_h = \overline{\gamma} + d_h \frac{2\mu_h}{\mu_h + \mu_{ch}}\,. \tag{268}$$

For the determination of the four integration constants a_s, d_s, a_h, d_h, certain conditions at the interface must be enforced. In the Cosserat theory, the degrees of freedom u_i and ϕ_i are continuous if one excludes cracks and kinks. Therefore, the corresponding traction and couple–stress vectors must also be transmitted at the interface. Alternative conditions would be to prescribe specific values or jumps at the interface for displacement and micro–rotation at the interface, as done for instance in Shu and Fleck (1999). We note that in the dislocation-based model, the value of the step in lattice rotation given by eq. (235), follows from the condition of mean prescribed glide $\bar{\gamma}$. Here, this condition is automatically satisfied by the periodicity requirement to be enforced by equation (273). Thus, continuity requirements are imposed in this work in the absence of a more specific interface model. The interface conditions require :

- continuity of ϕ at $s/2$:

$$a_s \cosh(\omega_s \frac{s}{2}) + d_s = a_h \cosh(\omega_h \frac{h}{2}) + d_h\,. \tag{269}$$

- continuity of μ_{zx} at $s/2$:

$$\beta_s a_s \omega_s \sinh(\omega_s \frac{s}{2}) = -\beta_h a_h \omega_h \sinh(\omega_h \frac{h}{2})\,. \tag{270}$$

- continuity of σ_{yx} at $s/2$. Rearranging equation (251) as follows :

$$\sigma_{yx} = (\mu + \mu_c) e_{yx} + (\mu - \mu_c)(\overline{\gamma} + \phi) = 2\mu(\overline{\gamma} + d) \tag{271}$$

  one obtains the third equation :

$$\mu_s(\overline{\gamma} + d_s) = \mu_h(\overline{\gamma} + d_h)\,. \tag{272}$$

- periodicity of u_y implies

$$< e_{yx} > = < \partial_x u_y - \phi > = < -\phi >\,,$$

  where the brackets denote averaging over x from $-(s+h)/2$ to $(s+h)/2$. One finds :

$$< \phi + e_{yx} > = < \frac{2\mu_c}{\mu + \mu_c}\phi + e > = < \frac{2\mu_c}{\mu + \mu_c}\phi + \overline{\gamma} + \frac{2\mu}{\mu + \mu_c} d >\,,$$

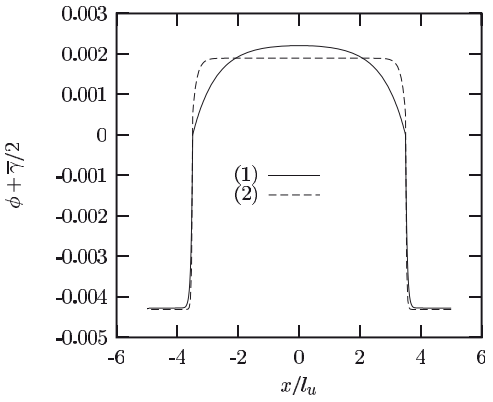

Figure 5. Distribution of microrotation of a two-phase linear elastic Cosserat material undergoing simple glide, using two different sets of parameters : (1) $\mu_h = 10\mu_s = 26923$MPa, $\mu_{ch} = 20\mu_{cs} = 100000$MPa, $\beta_h = \beta_s/30. = 100$MPa.$l_u^2$; and (2) $\beta_h = \beta_s/100 = 1$MPa.$l_u^2$; l_u is the chosen length unit (mm, μm...) and $s + h = 10l_u$, $\bar{\gamma} = 0.01$.

which gives the fourth equation

$$\frac{4\mu_{cs}}{\mu_s + \mu_{cs}} \frac{a_s}{\omega_s} \sinh(\omega_s \frac{s}{2}) \quad + \quad \frac{4\mu_{ch}}{\mu_h + \mu_{ch}} \frac{a_h}{\omega_h} \sinh(\omega_h \frac{h}{2}) + \quad \overline{\gamma}(s+h) + 2d_s s + 2d_2 h = 0\,. \quad (273)$$

The four equations (269), (270), (272) and (273) represent a linear system of equations for the unknowns a_s, a_h, d_s and d_h. For conciseness, the final expressions are not given explicitly. Instead, the profiles of ϕ are plotted in figure 5 for two different sets of material parameters. It can be seen that, for an appropriate choice of the material parameters ($\mu_h > \mu_s$, $\mu_{ch} > \mu_{cs}$, $\beta_s > \beta_h$), ϕ_h is almost constant and ϕ_s displays a cosh profile with a characteristic length $1/\omega_s$. This profile mimics the distribution found in subsection 2.2 and suggests that ϕ can be interpreted as a lattice rotation, providing that ω_s is taken to be of the order of the magnitude of λ.

In the limiting case when $\beta \longrightarrow 0$, it can be shown that stresses and strains are constant in each phase, as expected for the solution of this simple glide problem for the classical Cauchy continuum. This can also be inferred from figure 5.

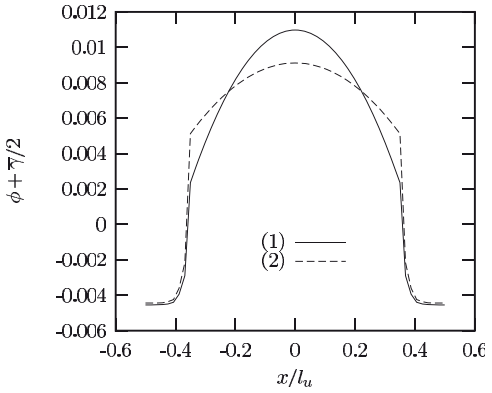

Figure 6. Distribution of microrotation of a two-phase elastoplastic Cosserat material undergoing simple glide, using two different sets of parameters : (1) $\mu_h = \mu_s = 26923$MPa, $\mu_{ch} = 5\mu_{cs} = 500000$MPa, $\beta_h = \beta_s/10. = 10\text{MPa}.l_u^2$, $\tau_c = 10$ MPa; and (2) $\beta_h = \beta_s/30 = 1\text{MPa}.l_u^2$; $s + h = l_u$, $\overline{\gamma} = 0.01$.

It can be checked also that $< \sigma_{yx} - \sigma_{xy} >= 0$, so that the macroscopic stress is of course symmetric. This point indicates that we are implicitly considering the problem of the homogenization of heterogeneous Cosserat media. This general problem is tackled in Forest et al. (1999, 2001b). The definition of the effective stress is

$$\overline{\sigma}_{ij} =< \sigma_{ij} > \ .$$

If neither mean curvature nor relative rotation is prescribed to the unit cell, the effective stress is symmetric.

Elastoplastic case Deformation in the soft phase is now decomposed into its elastic and plastic parts and the Schmid law is used as the yield criterion. The threshold shear stress τ_c is taken as constant (thus no hardening is considered). In contrast, we still do not distinguish between elastic and plastic curvature and keep a linearized relation between couple–stresses and total curvature. In this case, he total deformation in the cell is split into elastic and plastic parts :

$$\underset{\sim}{\boldsymbol{e}} = \underset{\sim}{\boldsymbol{e}}^e + \underset{\sim}{\boldsymbol{e}}^p \, . \tag{274}$$

Only single slip is considered. The normal $\boldsymbol{\nu}$ to the slip plane is supposed to be parallel to the y-direction (figure 3) and the slip direction $\boldsymbol{s}$ is parallel

to x :

$$\boldsymbol{e}^p = \gamma^p \underline{\boldsymbol{m}} \otimes \underline{\boldsymbol{n}} = \begin{bmatrix} 0 & \gamma^p & 0 \\ 0 & 0 & 0 \\ 0 & 0 & 0 \end{bmatrix}, \quad \boldsymbol{e}^e = \begin{bmatrix} 0 & e^e_{xy} & 0 \\ e^e_{yx} & 0 & 0 \\ 0 & 0 & 0 \end{bmatrix},$$

so that $e^e_{yx} = e_{yx}$. The non-vanishing force–stress components are :

$$\sigma_{xy} = \mu_s(e^e_{xy} + e_{yx}) + \mu_{cs}(e^e_{xy} - e_{yx}), \tag{275}$$

$$\sigma_{yx} = \mu_s(e_{yx} + e^e_{xy}) + \mu_{cs}(e_{yx} - e^e_{xy}). \tag{276}$$

The driving force to activate plastic slip is taken as the projection τ of the symmetric part of the force–stress tensor on the normal to the slip plane, and in the slip direction. Kröner (1956) suggests to take the full non–symmetric force stress in the computation of the resolved shear stress. This is not done here since the main Cosserat effects shown in this work do not come from the asymmetry of stress but rather from the presence of lattice curvature and the associated couple–stresses. Additional effects associated with the asymmetric character of the stress tensor have not yet been studied. Comments on the role of the skew–symmetric part of the force–stress tensor are given in subsection 2.2. The yield criterion therefore gives :

$$\tau = (\sigma_{xy} + \sigma_{yx})/2 = \tau_c = \mu_s(e^e_{xy} + e_{yx}). \tag{277}$$

From the first balance equation, viz. $\partial_x \sigma_{yx} = 0$, and (277), it can be seen that e_{yx} and e^e_{xy} are constant. The second balance equation reads :

$$\beta_s \partial_{xx}\phi - \mu_{cs}(e^e_{xy} - e_{yx}) = 0, \tag{278}$$

which gives

$$\partial_{xxx}\phi = 0. \tag{279}$$

Thus, ϕ displays a parabolic profile in the cell. The wall of width h in figure 3 is taken as an elastic Cosserat solid. The profile is the same as in section 2.2 :

$$\phi_s = a_s x_1^2 + d_s, \quad for \quad -s/2 < x < s/2, \tag{280}$$

$$\phi_h = a_h \cosh(\omega_h(x - \frac{s+h}{2})) + d_h \quad for \quad s/2 < x < (s+h)/2 \tag{281}$$

where ω_h is still given by (258). To determine the integration constants, the following conditions must be accounted for :

- continuity of ϕ at $x = s/2$:

$$a_s \frac{s^2}{4} + d_s = a_h \cosh(\omega_h \frac{h}{2}) + d_h. \tag{282}$$

- continuity of μ_{zx}

$$\beta_s a_s s = -\beta_h a_h \omega_h \sinh(\omega_h \frac{h}{2}) \,. \tag{283}$$

- continuity of σ_{yx}; e_{yx}, e^e_{xy} and σ_{yx} are determined in each phase :

$$e_{yx} + e^e_{xy} = \frac{\tau_c}{\mu_s}, \quad e^e_{xy} - e_{yx} = \frac{2\beta_s}{\mu_{cs}} a_s \,,$$

$$\sigma^s_{yx} = \tau_c - 2\beta_s a_s, \quad \sigma^h_{yx} = 2\mu_h(\overline{\gamma} + d_h) \,,$$

so that

$$2\mu_h(\overline{\gamma} + d_h) = \tau_c - 2\beta_s a_s \,. \tag{284}$$

- periodicity of u_y; we use again the property

$$< e_{yx} > = < \partial_x u_y - \phi > = < -\phi > \,,$$

$$e^s_{yx} = \frac{\tau_c}{2\mu_s} - \frac{\beta_s}{\mu_{cs}} a_s, \quad e^h_{yx} = -\frac{\mu_h - \mu_{ch}}{\mu_h + \mu_{ch}} \phi_h + \overline{\gamma} + d_h \frac{2\mu_h}{\mu_h + \mu_{ch}} \,, \tag{285}$$

$$e^s_{yx} + \phi_s = \frac{\tau_c}{2\mu_s} - \frac{\beta_s}{\mu_{cs}} a_s + a_1 x_1^2 + d_1 \,,$$

$$e^h_{yx} + \phi_h = \frac{2\mu_{ch}}{\mu_h + \mu_{ch}} \phi_h + \overline{\gamma} + \frac{2\mu_h}{\mu_h + \mu_{ch}} d_h \tag{286}$$

$$= \frac{2\mu_{ch}}{\mu_h + \mu_{ch}} a_h \cosh(\omega_h (x - \frac{s+h}{2})) + \overline{\gamma} + 2d_h \,, \tag{287}$$

from which the last equation for the determination of the integration constants is deduced :

$$(\frac{\tau_c}{2\mu_s} - \frac{\beta_s}{\mu_{cs}} a_s + d_s) s + \frac{a_s s^3}{12} + 2d_h h + \overline{\gamma} h + \frac{4\mu_{ch}}{\mu + \mu_{ch}} \frac{a_h}{\omega_h} \sinh(\omega_h \frac{h}{2}) = 0 \,. \tag{288}$$

The linear system (282), (283), (284), and (288) can be solved for the four unknowns (a_s, d_s, a_h, b_h), as in the previous section.

Once the micro–rotation $\phi(x)$ is known, the amount of plastic slip can be found from :

$$\gamma^p = \overline{\gamma} + \phi - \frac{\tau_c}{2\mu_s} - \frac{\beta_s a_s}{\mu_{cs}} \,. \tag{289}$$

The resulting parabolic distribution of Cosserat micro–rotation and plastic strain are given in figure 6 for two different sets of parameters. Note that for the classical limiting case when β_s tends to zero (and μ_c to infinity, see next section), the classical relation (227) is retrieved.

Limiting case for constrained Cosserat single crystal plasticity At this point, a precise discussion of the links between the Cosserat micro–rotation ϕ and the lattice rotation ϕ^{e} must be given. The previous analysis of two different situations has shown the similarity between the profiles of ϕ and ϕ^e, as deduced from the combination of classical continuum mechanics and equilibrium of a dislocation line. In the continuum framework of classical crystal plasticity, in which dislocations are not considered individually, a clear definition of lattice rotation exists. For instance, in the specific case of the shear test, it is given by equation (221). Such continuum description of lattice rotation will now be compared with the Cosserat micro–rotation computed in section (2.2). By definition, the lattice rotation is related to the skew–symmetric part of the elastic distortion :

$$\boldsymbol{e}^e = \begin{bmatrix} 0 & \overline{\gamma} - \gamma^p + \phi & 0 \\ \partial_x u_y - \phi & 0 & 0 \\ 0 & 0 & 0 \end{bmatrix}, \tag{290}$$

the corresponding axial vector being $(0, \quad 0, \quad \dfrac{\overline{\gamma} - \gamma^p - \partial_x u_y}{2} + \phi)^T$.
If the skew–symmetric part of the Cosserat elastic deformation tensor vanishes, the following relation is found :

$$\phi = -\frac{\overline{\gamma} - \gamma^p - \partial_x u_y}{2} \tag{291}$$

which is exactly that given by equation(221). Thus, the Cosserat micro–rotation is found to coincide exactly with the standard definition of lattice rotation when the Cosserat elastic deformation is symmetric. It is recalled that the skew–symmetric part of the stress and elastic deformation are linked by the elastic modulus μ_c (see equations (275) and (276)). Thus the value of μ_c controls the difference between the Cosserat micro–rotation and lattice rotation. The physical meaning of ϕ in the case of crystal plasticity is therefore clear only when it is close or equal to the lattice rotation. This is the case when μ_c is large compared to the other moduli. The condition $\mu_c \to \infty$ enforces indeed the symmetry condition for the elastic deformation. The resulting finite skew–symmetric part of the stress can be regarded as reaction stresses (similarly to pressure in classical incompressible materials). This is a kind of constrained Cosserat continuum for which the Cosserat micro–rotation follows strictly lattice rotation, which is different from the well–known couple–stress medium, for which the Cosserat rotation is forced to follow the material rotation, namely pure rotation component of the overall deformation gradient Koiter (1963).

Consider the analysis of section 2.2 in the case when μ_c goes to infinity. The equations are indeed simplified and a clearer connection between material and geometric constants can be derived. The characteristic length in the hard phase becomes :

$$\frac{1}{\omega_h} = \sqrt{\frac{\beta_h}{2\mu_h}}\,. \tag{292}$$

In the previous system of four equations (282),(283), (284) and (288), the fourth one now becomes :

$$(\frac{\tau_c}{2\mu_s} + d_s)s + \frac{a_s s^3}{12} + (2d_h + \gamma)h - \frac{2\beta_s}{\mu_h} a_s s = 0\,. \tag{293}$$

The solution can then be given in a rather concise form, at least for a_s which characterizes the parabolic profile of the lattice rotation distribution :

$$a_s = -6\frac{\overline{\gamma}(s+h) - \frac{\tau_c}{2\mu_h}(s + 2h + s\frac{\mu_h}{\mu_s})}{s^3 + \frac{\beta_s}{\mu_h}(18s + 12h + 3s^2\omega_h cotanh(\omega_h \frac{h}{2}))}\,. \tag{294}$$

It can be seen that, contrary to the result of the analysis in the purely linear case of subsection 2.2, both material and geometric parameters contribute to the shape of the distribution ϕ in the elastoplastic channel. It can also be noted that when $\beta_h \to 0$, i.e. $\omega_h \to \infty$, the coefficient a_s vanishes and the classical homogeneous distribution of rotation and plastic slip is retrieved. Interestingly, when a non–zero and constant value of β_h is assumed and when $\beta_s \to 0$, the coefficient a_s does not vanish but rather reaches the limit :

$$a_s = -6(\overline{\gamma} - \frac{\tau_c}{\mu})\frac{s+h}{s^3} \tag{295}$$

where $\mu_h = \mu_s = \mu$ has been assumed for simplicity. The fact that the classical homogeneous solution is not found in this case can be interpreted as follows. Letting β_s vanish in the moment of momentum balance equation (278) makes this second partial differential equation disappear, so that in principle we are left with the usual force–stress balance equation and a classical solution could be expected. However, if equation (278) is multiplied by $1/\beta_s$ and differentiated again, we are left with (279) that can be assumed to hold in the limit for $\beta_s \to 0$. It amounts then to finding a parabolic distribution of ϕ fulfilling the classical equation (227) and continuity conditions at the interface. Indeed for very low values of β_s finite element simulations provide this limit solution. Identifying the present result (295) and the corresponding solution of the dislocation model (216), the link between the

Cosserat model and the intrinsic length scale is

$$\frac{1}{\lambda^2} = 24(\frac{\overline{\gamma}\mu}{\tau_c} - 1)\frac{s+h}{s} \simeq \varrho_m \tag{296}$$

which provides a reasonable but very approximate estimate of the density of mobile dislocation. The complete solution with all available material constants is of course more elaborate and incorporates the length scale associated with a non–vanishing β_s. In the latter case, the complete identification of the Cosserat model with the corresponding dislocation model can be done using (294) in order to calibrate β_s, as a function of ϱ_m.

Comparison with strain gradient plasticity models

Alternative nonlocal continuum theories are available to model size effects in crystal plasticity, usually called strain gradient plasticity models. In this section, the response predicted by two of them is investigated in the simple case of shearing of laminate microstructures. In particular, the shape of the non–homogeneous plastic slip profiles are compared to the previous Cosserat results.

Second gradient formulation Based on the continuum framework introduced by Mindlin and Germain Mindlin and Eshel (1968); Germain (1973a), a strain gradient plasticity constitutive framework has been developed by Shu, Fleck and Hutchinson Fleck and Hutchinson (1997); Shu and Fleck (1999). Two main models have been proposed by the authors. The first one deals with isotropic plasticity, the second one with crystal plasticity. The main constitutive and balance equations are recalled in section 2.2 in a simplified case of single slip. Moreover the originally viscoplastic framework is translated into a purely elastoplastic one, for which analytical solutions can be found in the shear test considered in this work.

As in section 2.2, the displacement field in a periodic two–phase laminate microstructure subjected to mean shear deformation $\bar{\gamma}$ is considered. The solution must fulfill balance and constitutive equations in each phase and interface conditions. First, a solution is obtained assuming a linear approximation for the constitutive behaviour without distinction between elastic and plastic parts. The second solution is valid for the nonlinear elastoplastic regime.

Using the same coordinate frame as in section 2.2, the solution still takes the form $u_x = (\bar{\gamma}y, u_y(x), 0)^T$. The non–vanishing components of the strain gradient tensor $\boldsymbol{\eta}$, as defined in Appendix 2.2, are

$$\eta_{xyx} = \eta_{yxx} = \frac{1}{2}\partial_{xx}u_y\,. \tag{297}$$

Elastoplastic case

Adopting the additive decomposition (1) of total strain and strain gradient into elastic and plastic parts, the elastic laws become

$$\sigma_{xy} = 2\mu\varepsilon^e_{xy} = \mu(\bar{\gamma} + u_{y,x} - \gamma^p)\,, \tag{298}$$

$$m_{yxx} = 2l_e^2\mu(\eta_{yxx} - \eta^p_{yxx}) = l_e^2\mu(\partial_{xx}u_y - \gamma^S)\,, \tag{299}$$

where γ^S is the slip gradient variable (see Appendix 2.2). The yield condition is a generalized Schmid law involving resolved shear stress and hyperstress :

$$\sigma_{eq} = |\tau| + |m|/l_p = \sigma_{xy} + m_{yxx}/l_p = \tau_c\,. \tag{300}$$

It must be noted that a second characteristic length l_p enters the yield criterion. The yield condition combined with the balance equation

$$\partial_x\sigma_{xy} - \partial_{xx}m_{yxx} = 0\,. \tag{301}$$

can then be shown to lead to the following partial differential equations

$$\partial_{xx}u_y - l_p^2\partial_{xxxx}u_y = 0, \quad \partial_x\gamma^p - l_p^2\partial_{xxx}\gamma^p = 0\,. \tag{302}$$

Since the definition of lattice rotation (227) still holds, one is led to the following partial differential equation for ϕ :

$$\partial_x\phi - l_p^2\partial_{xxx}\phi = 0\,, \tag{303}$$

which again gives a *cosh*−profile but associated with the characteristic length l_p. This result is different from the parabolic profile found in the same analysis with the Cosserat model. The reason is however clear : it stems from the modified yield condition (300). A consequence of this choice is that shear stress σ_{xy} does not remain constant in space, contrary to all investigated cases in the previous sections. It introduces hardening associated with strain gradient.

The strain gradient model can however be slightly modified to be closer to the simple Cosserat constitutive equations used in section 2.2. We let l_p go to infinity and do not distinguish elastic and plastic parts in $\boldsymbol{\eta}$:

$$\sigma_{eq} = \tau = \sigma_{xy} = \tau_c, \quad m_{yxx} = 2\mu l_e^2\eta_{yxx}\,. \tag{304}$$

l_e is in fact here the characteristic length of the elastoplastic secant moduli in the second elasticity law, since $\boldsymbol{\eta}$ has not been partitioned. The balance equation (301) now yields :

$$\partial_{xxxx}u_y = 0, \quad \partial_{xxx}\gamma^p = 0, \quad \partial_{xxx}\phi = 0\,, \tag{305}$$

and a parabolic profile is retrieved.

Crystal plasticity with gradient of internal variable One of the earliest proposals to introduce higher–order gradients in the relevant constitutive variables is Aifantis' model that belongs to a class of generalized continua different from the theories used in the previous sections. The models presented and illustrated in Aifantis (1987, 1999) do not introduce additional rotational degrees of freedom like the Cosserat theory, nor higher order derivatives of the displacement field. Instead, the constitutive behaviour of the material is assumed to depend on an internal variable γ^p and its gradient $grad\,\gamma^p$. The free energy is a function of temperature, elastic strain, plastic slip and its gradient. The classical expression of work of internal forces is in fact complemented by terms related to the internal variable and its gradient Forest et al. (2002) :

$$p^{int} = \sigma_{ij}\dot{\varepsilon}_{ij} + \alpha\dot{\gamma}^p + B_i\partial_i\dot{\gamma}^p\,, \tag{306}$$

where α and B_i are the thermodynamical forces associated with the internal variable and its gradient. The principle of virtual work can be used to derive the balance equations :

$$div\,\boldsymbol{\sigma} = 0, \quad \alpha = div\,\boldsymbol{B}\,. \tag{307}$$

The classical balance equation is conserved, whereas the second one can be regarded as a definition of the introduced generalized force α. The degrees of freedom and associated reaction forces are therefore the pairs $(u_i, t_i = \sigma_{ij}n_j)$ and $(\gamma^p, B = B_i n_i)$. The dissipation rate takes the form

$$D = \sigma_{ij}\dot{\varepsilon}^p_{ij} + (div\,B)\dot{\gamma}^p = (\tau + div\,B)\dot{\gamma}^p\,. \tag{308}$$

The latter expression leads one to propose a yield condition of the form :

$$\sigma_{eq} = \tau + div\,B = \tau_c\,. \tag{309}$$

In Aifantis model, $\boldsymbol{B}$ is assumed to be simply proportional to $grad\,\gamma^p$ (quadratic potential) :

$$B_i = c\partial_i\gamma^p\,, \tag{310}$$

where c is a constitutive parameter. The yield condition (309) then becomes :

$$\tau = \tau_c - c\Delta\gamma^p\,, \tag{311}$$

which is the well–known gradient–enhanced yield criterion, with Δ being the Laplace operator. This theemodynamics of Aifantis model has also been investigated by Bardella (2007); Gurtin and Anand (2009); Forest and Aifantis (2010).

This theory is now applied to the simple situation investigated in the present article. The yield condition reduces to the simple form :

$$\tau = \sigma_{xy} = \tau_c - c\,\partial_{xx}\gamma^p\,. \tag{312}$$

The equilibrium equation requires constant shear stress so that we must have :

$$\partial_{xxx}\gamma^p = 0\,. \tag{313}$$

The elasticity relation (298) implies again $\partial_{xx}u_y = \partial_x\gamma^p$ so that lattice rotation ϕ must fulfill the same partial differential equation :

$$\phi = \frac{\partial_x u_y + \gamma^p - \bar{\gamma}}{2}, \quad \partial_{xxx}\phi = 0\,. \tag{314}$$

This model therefore gives the same answer for the lattice rotation and plastic slip distribution as the Cosserat model of section 2.2, namely a parabolic one. The interface conditions are dictated by the chosen degrees of freedom and associated forces :

- displacement u_y and traction vector $\sigma_{xy}n_x$ are continuous across the interface;
- plastic slip γ^p and force $B = (c\,grad\,\gamma^p).n = c\partial_x\gamma^p$ are continuous across the interface.

In contrast to the Cosserat theory, plastic slip is assumed to be continuous, whereas lattice rotation need not necessarily to be continuous (this comes from the fact that $\partial_x u_y$ is not necessarily continuous in contrast to the strain gradient theory).

If linear hardening is introduced in the yield condition (309), it can be shown that a *cosh* distribution is obtained. However, this situation cannot be compared to that of section 2.2 and 2.2 since there no hardening was taken into account.

Direct comparison between the dislocation and generalized continuum frameworks

A direct comparison between the dislocation models and the continuum frameworks is difficult insofar as the dislocation models considered in this work are very specific whereas the continuum models can be used in very general situations. The line tension model considers a representative bowing screw dislocation which is a convenient and idealized situation. As for the pile–up model, it deals with periodic arrays of edge dislocations. However, a parallel between the line tension dislocation model and the Cosserat, second gradient and Aifantis models can be drawn. All models share the

main variables plastic slip γ^p and lattice rotation ϕ^e, even though the two gradient models more explicitly introduce the gradient of plastic slip. The classical divergence equation for the stress tensor is valid for all theories. The generalized continuum involve an additional (or a higher order) balance equation which reflects in a continuum way the dislocation line tension equilibrium equation. A one–to–one identification is however not possible since the continuum theories do not explicitly introduce densities of line defects. The consequence is that the governing partial differential equations in the case of shearing of the elastoplastic laminate microstructure have almost the same structure. The gradient theories are somewhat different, in the sense that they predict that the shear stress τ does not remain equal to the critical resolved shear stress τ_c. In the strain gradient theory, the shear stress τ is equal to $\tau_c - m_{yxx}/l_p$ and to $\tau_c - c\partial_{xx}\gamma^p$ in Aifantis model. This strain–gradient induced hardening behaviour is not introduced nor predicted in the idealized line tension dislocation and Cosserat models. The strain gradient theory can be simplified to get rid of this hardening component, as shown at the end of section 2.2. The similarity of the governing p.d.e. makes it possible to identify some parameters of the generalized continuum models with the dislocation based quantities, especially the involved characteristic lengths.

As a consequence of the choice of the primary variables, the interface conditions are different for all generalized continuum models. In the line tension model, at least in the plastic regime, plastic slip and lattice rotation are not necessarily continuous, which corresponds to a density of edge dislocations deposited at the interface. In contrast, the Cosserat theory assumes the continuity of lattice rotation whereas plastic slip is continuous in the gradient of internal variable theory. The second gradient model introduces the continuity of the normal gradient of displacement, the physical meaning of which is more difficult to assess. These differences in interface conditions make the previous identification of characteristic lengths at the level of the governing equations insufficient. That is why, we must also compare the final solution, namely the predicted distribution of slip and lattice rotation in the considered simple glide test. As shown in section 2.2, the lattice distributions predicted by the Cosserat and line tension models can be identified. The phenomenological moduli are then related to dislocation material parameters but also to the geometry of the microstructure, especially the layer thicknesses s and h.

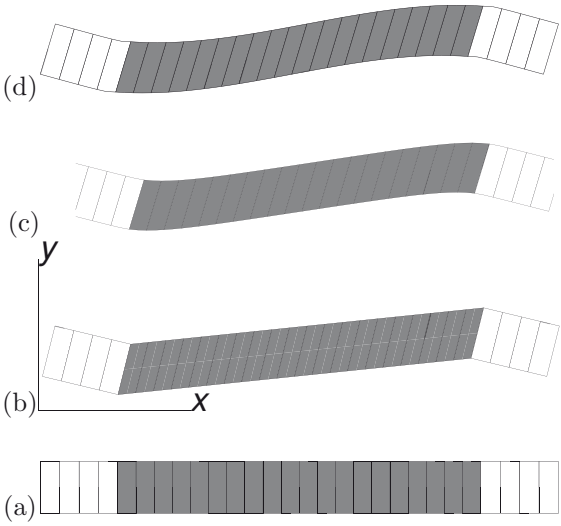

Figure 7. Deformed states of a two–phase material element under simple shear : (a) initial state; (b) solution according to classical crystal plasticity; (c) Cosserat elasticity (see subsection 2.2); (d) Cosserat elastoplasticity (see subsection 2.2). The solutions have been computed using the finite element method and each phase is divided into elements : hard phase in white, soft phase in grey; the mean deformation is the same in (b,c,d).

Non–homogeneous plastic deformation in channels

In the simple situation investigated in this work, several available nonlocal models of crystal plasticity - ranging from Cosserat, second grade to gradient of internal variable theories - predict development of a non–homogeneous distribution of plastic slip and lattice rotation in the soft channels of the laminate microstructure under shear. Each of the nonlocal models has its own advantages and drawbacks. The Cosserat model naturally comes out of almost thirty years old theoretical reflexions on crystal plasticity Mandel (1973) but the physical meaning of the skew–symmetric part of the stress still remains unclear. In the strain gradient model recalled in Appendix 2.2, the constitutive links between slip gradient variables γ^S and the gradient of slip $grad\,\gamma^p$ remains phenomenological. This model gives also the opportunity of incorporating effects that are not associated with geometrically necessary dislocations (in particular the gradient of slip in the direction normal to the slip plane, the physical interpretation of which remains to be

explained). Regarding Aifantis' model, the Laplace term in yield condition (311) can in some cases be derived from the physics of dislocations (see for instance Estrin et al. (1998) in the case of double slip).

Anyway, the use of Cosserat, strain gradient or Aifantis models invariably leads to parabolic or *cosh*- distributions of plastic slip and lattice rotation, depending on specific constitutive assumptions. Each profile is characterized by a length that is directly related to the constitutive length(s) introduced in each model. This intrinsic length enters the elastic or the plastic part of the constitutive equations, or both. Figure 7 summarizes and illustrates the different deformed states of a sample of such two–phase material, according to the classical and Cosserat models.

The parabolic or *cosh*- distributions of plastic slip and lattice rotation result also from the line–tension dislocation–based model that incorporates the bowing of screw dislocations in narrow channels into a simple one–dimensional continuum–mechanics description. Loosely speaking, the anelastic regime for which dislocations move over short distances can be associated with a *cosh*- distribution, whereas the fully plastic regime corresponds to a parabolic profile.

Thus it appears that the plastic slip and lattice rotation distribution obtained within the proposed Cosserat framework accurately mimics the results of the dislocation–based line–tension models. On the generalized–continuum level, simple linear and/or perfectly plastic constitutive equations that are usual in phenomenological modelling can be used. The balance of moment of momentum equation $(253)_2$, that does not exist in the classical continuum framework, turns out to be the continuum counterpart of the equilibrium condition (211) for a representative dislocation bowing in the channel.

Even a direct identification of the dislocation and Cosserat models is possible. In particular, the wavelength λ of the dislocation model (216) enables one to compute the corresponding value of the Cosserat parameter β_s from (292) :

$$\beta_s \simeq \frac{2\mu}{\varrho_m} \tag{315}$$

Since it depends on the density of mobile dislocations which may vary during deformation, β_s should not be seen as a constant material parameter. In the case of the parabolic profile, not only the constant β_s, but also explicitly the channel width s are the determinant parameters (see equation (295)). The identification for the iso–strain model has been proposed in Sedláček and Forest (2000). The present work focuses on the detailed solution of the iso–stress periodic problem. Other models like strain gradient and Aifantis' model have been shown to reproduce the line–tension effects as well.

Interestingly, the mentioned nonlocal theories were not originally designed for the modelling of line tension effects but rather hardening effects due to so–called geometrically necessary dislocations as in the pileup model. Admittedly, several nonlocal models have shown their ability to account for particle or grain size effects that can be related to the presence of dislocation pileups (see Forest et al. (2000); Acharya and Beaudoin (2000) for the simulation of Hall–Petch effects in polycrystals). However one should not hastily associate strain gradient plasticity and dislocation pileup effects. In fact, the distribution of plastic slip in dislocation pileups in the soft phase is not correctly described by any of the mentioned nonlocal models. Double–ended pileups are dislocation structures that can also form in the laminate microstructure under the prescribed loading conditions, for instance because of periodically distributed Frank–Read sources, or as the result of passage of many bowed screw dislocations. It could be argued that the pileup model includes internal stresses and associated hardening, which has not been taken into account in the Cosserat model. However, the strain gradient model used in section 2.2 incorporates hardening associated with hyperstresses and still provides a *cosh*- distribution. A Cosserat model including classical linear hardening would lead in fact also to a *cosh*- distribution. It shows that the main ingredients of the current nonlocal crystal plasticity models are not really best–suited for the description of dislocation pileup effects in crystals, but rather of dislocation line tension effects. This is surprising since the size effects arising from dislocation bowing did not belong explicitly to the initial main motivations that have led to the development of the nonlocal theories. Conversely, this fact can be regarded as an important property of the nonlocal models since the line tension effects have proved to dominate the mechanical response of many engineering materials. The case of single-crystal nickel-based superalloys is of special interest, since they display a periodic microstructure of hard precipitates and soft channels. A description of precipitate size effects in single crystal superalloys based on the Cosserat theory can be found in Forest et al. (2000). An alternative model including gradients of internal variables has also been applied to this single crystal material Busso et al. (2000). Size effects associated with the channel width are predicted by the models. For example, it can be checked that the solution of the elastoplastic Cosserat model tends towards the classical one when the relative size s/h goes to infinity (coefficient a_s of the parabolic profile then vanishes according to equation (294)).

The presented results are applicable to cyclic loading conditions. Further effort must now be concentrated on dislocation interaction and hardening, which remains challenging since the line tension model becomes difficult

to handle explicitly in the three–dimensional case Sedláček et al. (2003). Dislocation dynamics and finite element simulations are then useful tools to go towards more realistic multi–slip situations, as initiated in Shu and Fleck (1999); Shu et al. (2001). The situation of double slip has been shown to be dramatically different from the single slip case in Shu et al. (2001), from the dislocation dynamics point of view.

Role of interface conditions

In the present study, nonlocal mechanical models incorporating additional higher order boundary or interface conditions have been considered. It appears clearly in Shu et al. (2001) that models that keep the classical structure of the boundary value problem unchanged, like Acharya and Bassani (2000); Busso et al. (2000), predict homogeneous glide as the classical continuum mechanics does for the shearing of a crystalline layer. Non–homogeneous distributions can be obtained with a nonlocal model by applying higher order boundary conditions at the boundary of the sheared layer. The higher order boundary conditions concern the additional degrees of freedom of higher order derivatives, introduced in the model, and their associated forces. Similarly, in the two–phase microstructure considered in this work, the enriched interface conditions are responsible for the development of a non–homogeneous plastic slip pattern in the soft phase. Since neither special constitutive properties nor direct boundary conditions have been applied to the interface, both phases must be treated as generalized continua, and not only the soft one. If one considers in the Cosserat model of section 2.2, the limit case for which $\mu_{ch} = \infty$ and $\beta_h = 0$, constant values for ϕ are obtained in each phase with a jump. It means that, in order to get a non–constant distribution, the wall cannot be regarded as purely classical : it must be able to carry the surface couples produced in phase s at the boundary. This can be achieved by setting a relatively low value of β_h and a 100 time bigger β_s. In that case, the distribution in the hard phase is then almost flat with a steep rise close to the boundary, that mimics a jump of the considered variable. The same holds for the two other nonlocal models handled in section 2.2. An alternative method could be to consider the hard phase as a classical material and to set directly boundary conditions at the interface (see for instance Shu and Fleck (1999) for the interface between two crystallites). This has not been done here because the conditions to be prescribed are not necessarily known a priori. Instead, in the Cosserat theory, lattice rotation, the additional degree of freedom, is continuous at the interface and so does the traction vector and the couple–stress vector. Similarly in the second gradient theory, the normal gradient of the displace-

ment and the associated force must be continuous at the interface. So does plastic slip and associated force in Aifantis' model. These conditions are therefore slightly different for each theory, even if the governing partial differential equation may be the same in the bulk. It is however difficult to assess which continuity requirement is the most realistic from the physical point of view. The main point is that these continuity constraints are the origin of the non–uniform lattice rotation field in the soft phase.

More general grain boundary behavior could include discontinuities of lattice rotation, plastic strain, or even grain boundary sliding and opening for damage Acharya (2007); Gurtin and Anand (2008).

Description of internal stresses and hardening

The attention has been focused on the continuum description of plastic slip and lattice rotation distribution, but the question of hardening is also an important point from the macroscopic point of view. The pileup model of subsection 2.2 leads to the existence of linear hardening due to internal stresses, described by equation (246). This kinematic hardening component can be seen as a sort of nonlocal hardening law since it depends on the mean value of plastic slip and not on the local value of γ. It has the classical form used in phenomenological constitutive equations for single crystal under cyclic loading Méric et al. (1991), although nonlinear kinematic hardening is usually observed experimentally. It appears also that this hardening term does not depend on lattice curvature or dislocation density tensor and therefore has no direct relation to the density of geometrically necessary dislocations (see also Mughrabi (2001)). A size effect is expected from the dependence of the hardening modulus C on the channel width s, see equation (246).

Such a hardening term should be introduced in the continuum model of section 2.2 to account for arising internal stresses. It can be easily done by replacing τ_c in (277) by a term of the form $\tau_c + C\bar{\gamma}$. The form of the solution is not affected by this term which does not depend on position x. It is clear however that the continuum Cosserat model does not account for the exact distribution of plastic strain in a double–ended pileup (parabolic profile instead of an elliptic one). The introduction of the linear hardening component then keeps a phenomenological character.

In Shu et al. (2001), the local hardening modulus entering the constitutive equations of the second grade model has been identified numerically using the mean response of the discrete dislocation dynamics model. The hardening modulus links the equivalent stress and plastic strain rates $\dot{\sigma}_{eq}$ and $\dot{q}$ (see section 2.2). However the plastic multiplier q is a measure of

cumulated plastic strain and strain gradient without distinction, because of the use of a single coupled yield criterion (300) in the spirit of Borst (1991) :

$$\dot{q} = |\dot{\gamma}^p| + l_p|\dot{\gamma}^S| \,. \tag{316}$$

The pileup model indicates that hardening originates from mean plastic slip and not from local slip gradient. Accordingly, a distinction between both contributions should be preferable in the continuum model. Such a distinction exists in the full Cosserat model used in Forest et al. (2000) by considering two different plastic multipliers, one for plastic slip, the other one for lattice curvature. This means also that the single yield criterion (300) is replaced by two yield conditions : one involves resolved shear stresses, the second one involves resolved couple–stresses. Coupling between both comes then from the hardening laws. It must be noticed that this hardening law for the two–phase material must be of kinematic type for application to cyclic plasticity.

In many generalized crystal plasticity models, the higher order stresses generate kinematic hardening, generallly linear. Different classes of such models are compared in Forest (2008); Cordero et al. (2010).

Appendix: Second grade continuum

The strain and its gradient are decomposed into their elastic and plastic parts :

$$\varepsilon_{ij} = \varepsilon^e_{ij} + \varepsilon^p_{ij}, \quad \eta_{ijk} = \partial_{x_k}\varepsilon_{ij} = \eta^e_{ijk} + \eta^p_{ijk} \,. \tag{1}$$

The associated stresses are the classical Cauchy stress σ_{ij} and the hyperstress tensor m_{ijk}. The following simplified form of the elastic relations has been chosen in Shu and Fleck (1999) :

$$\sigma_{ij} = C_{ijkl}\varepsilon^e_{kl}, \quad m_{ijk} = l_e^2 C_{ijpq}\eta^e_{pqk} \,, \tag{2}$$

where the usual four–rank elasticity tensor is denoted by C_{ijkl} and l^e is a characteristic length associated with the higher order elasticity law. For the structure to be in equilibrium, the stress tensors must fulfill the following balance equation :

$$\partial_{x_j}\sigma_{ij} - \partial_{x_j x_k} m_{ijk} = 0 \,, \tag{3}$$

where volume simple and double forces have been excluded. Note that equilibrium is governed by a single higher order partial differential equation whereas two balance equations must be fulfilled for the Cosserat continuum. For this continuum, a boundary value problem is well–posed provided that boundary conditions are prescribed to one element in each pair (u_i, t_i) and (Du_i, r_i). The unknown displacement is denoted by u_i and Du_i is the normal gradient of u_i defined by

$$Du_i = (\partial_{x_j} u_i) n_j \tag{4}$$

for a unit vector $\boldsymbol{n}$ normal to a surface. The corresponding tangent gradient operator is

$$D_j(.) = \partial_{x_j}(.) - D(.)n_j \tag{5}$$

The traction vector $\boldsymbol{t}$ and double traction vector $\boldsymbol{r}$ on a surface element of normal $\boldsymbol{n}$ are respectively defined by

$$t_i = (\sigma_{ij} - \partial_{x_k} m_{ijk})n_j + (D_l n_l) m_{ijk} n_j n_k - D_j(m_{ijk} n_k) \tag{6}$$

$$r_i = m_{ijk} n_j n_k \,. \tag{7}$$

In the case of single slip in a system $(\underline{\boldsymbol{m}}, \underline{\boldsymbol{\nu}})$ (slip direction $\boldsymbol{s}$ and slip plane normal $\boldsymbol{\nu}$), the plastic strain and strain gradient are related to the amount of slip γ^p and the slip gradient variable γ^S by :

$$\dot{\varepsilon}^p_{ij} = \dot{\gamma}^p \, s_{(i}\nu_{j)}, \quad \dot{\eta}^p_{ijk} = \dot{\gamma}^S \, s_{(i}\nu_{j)} s_k \,, \tag{8}$$

where the parentheses around indices stand for symmetrization. Note that in the general theory proposed in Shu and Fleck (1999), additional slip gradient variables γ^T, γ^M are introduced, that we do not include in the simple case investigated here. It must be noted also that in this theory, the slip gradient variable γ^S does not necessarily coincide with the gradient of slip γ^p.

The plastic yield criterion is a generalized Schmid law involving resolved shear stresses and hyperstresses :

$$\sigma_{eq} = |\tau| + |m|/l_p, \quad with \quad \tau = \sigma_{ij} s_i \nu_j, \quad and \quad m = m_{ijk} s_i \nu_j s_k \,. \tag{9}$$

Plastic deformation can then occur when σ_{eq} reaches the threshold τ_c. The authors in Shu and Fleck (1999) propose a viscoplastic formulation of the constitutive framework. In contrast, an elastoplastic formulation is used here, for the simple case of single slip. Associative plastic flow is assumed. Thus, the normality rule is given as :

$$\dot{\gamma}^p = \dot{q} \partial_\tau \sigma_{eq} = \dot{q} \, sign \, \tau \,, \tag{10}$$

$$\dot{\gamma}^S = \dot{q} \partial_m \sigma_{eq} = \frac{\dot{q}}{l^p} sign \, m \,, \tag{11}$$

where $\dot{q}$ denotes the plastic multiplier in both equations.

Two characteristic lengths appear in the theory, namely l^e in equations (2) and l^p in equation (9).

3 Continuum modelling of size effects in the mechanics of single and polycrystals

3.1 Plasticity at the crack tip in single crystals

The stress–strain field at the crack tip in a single crystal can be simulated using dislocation dynamics and continuum crystal plasticity Van der Giessen et al. (2001). The problem of the crack in an infinite medium has been addressed very often during the development of the mechanics of generalized continua in the 60s and 70s. Solutions are available for the elastic couple stress medium and fully non local elasticity. In the case of crystal plasticity, numerical solutions with the Cosserat continuum have been compared to Rice's solution for the classical continuum in Forest et al. (2001a). The classical solution, derived for an elastoplastic single crystal without hardening, predicts the existence of sectors with constant stress separated by localization bands. The physical nature of the bands depends on crystal structure and orientation. Intense slip bands, kink bands and multislip bands can coexist. The use of the Cosserat continuum leads to the weakening and even elimination of kink bands at the crack tip when additional hardening associated to lattice curvature is introduced. The figure 8 shows the profiles of equivalent plastic slip along half a circle close to the crack tip for three different values of extra–hardening modulus H assuming a simple extra–hardening model linear in the variable θ (see equation (106)). For the considered crystal orientation, kink bands lie at 55° and 125° from the horizontal axis, whereas the vertical band is a pure slip band. The intensity of the kink bands decreases for increasing H values. Note that asymptotic analyses of the crack tip field are possible within classical crystal plasticity that exclude kink banding Drugan (2001) but they are difficult to implement numerically. Recent experimental investigations on nickel–base superalloys at room temperature confirm in fact the existence of kink bands at the crack tip under monotonous loading (cf. figure 9 and reference Flouriot et al. (2003)). Extra–hardening parameter H can be identified from the found intensity of the kink bands.

The use of physically more realistic models at the crack tip than classical crystal plasticity is an important issue for the prediction of subsequent crack growth, especially in fatigue Deshpande et al. (2001).

3.2 Strain heterogeneities in polycrystals

The continuum crystal plasticity framework can be used to evaluate the development of plastic strain heterogeneities in thin or bulk polycrystals. We report first computations based on classical continuum crystal plasticity,

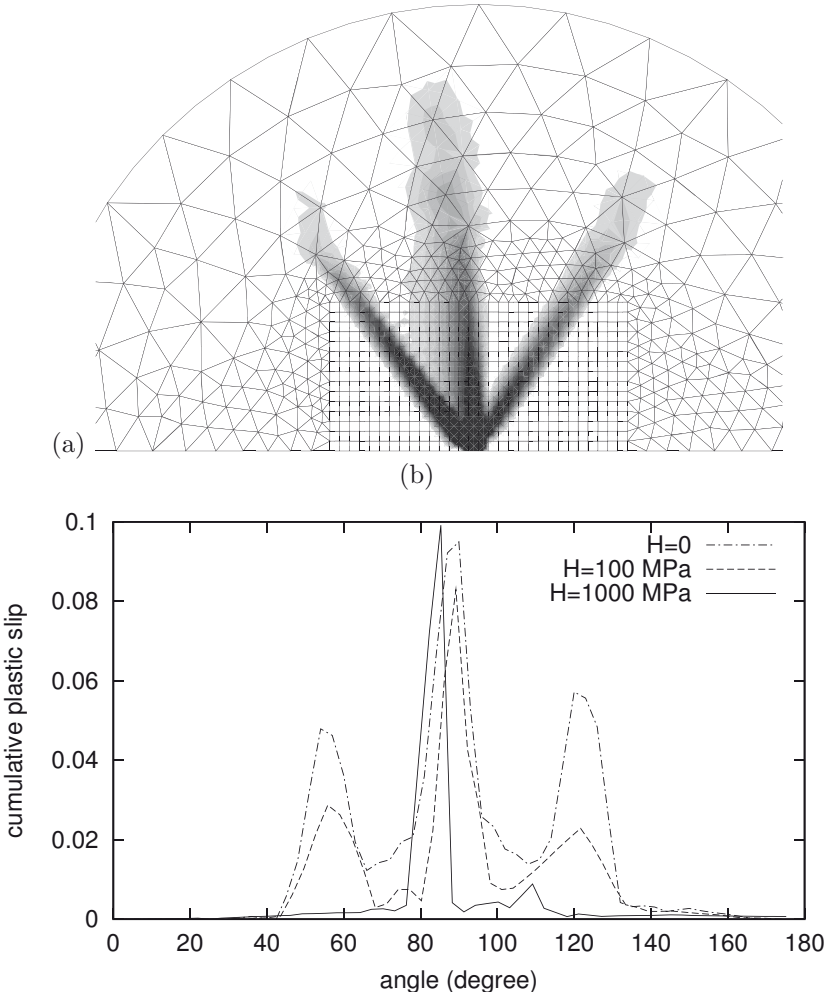

Figure 8. Equivalent plastic strain at a crack tip in an elastic ideally–plastic Cosserat single crystal under mode I loading conditions (F.C.C. crystal, the vertical and horizontal directions are respectively [011] and [100]). The results are obtained from finite element computations of cracked Cosserat single crystals. The equivalent plastic strain is localized in 3 bands (a). The amount of plastic slip is plotted along half a circle close to the crack tip for three different values of the extra–hardening parameter H (b).

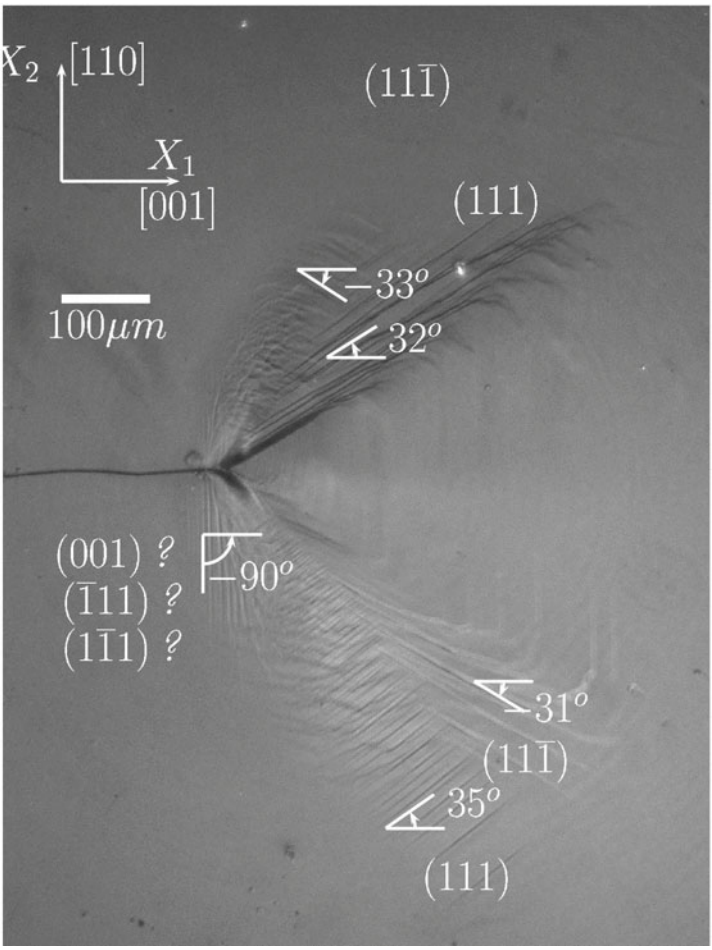

Figure 9. Slip lines at the crack tip of a nickel–base superalloy single crystal in a CT specimen. The crack plane is (110) and the crack propagation direction is [001]. Two kink bands are clearly visible on each side of the crack tip (after Flouriot et al. (2003)).

theory recalled in section 1.1. The presented simulations and the results obtained in Barbe et al. (2001a,b); Cailletaud et al. (2003); Parisot et al. (2004); Šiška et al. (2007) can integrate only relative grain size effects and size–independent strain incompatibilities. The application of the Cosserat model to polycrystals is postponed to section 3.3.

Multicrystalline specimens and coatings Metallic multicrystals have been investigated both experimentally and numerically in several situations in the past ten years: copper bicrystals Méric et al. (1994), copper, nickel, aluminum or iron muticrystals Teodosiu et al. (1993); Eberl et al. (1998); Ziegenbein et al. (1998); Delaire et al. (2000). The specimens may be strained in situ in a SEM. An EBSD analysis provides the lattice rotation field and the use of grids on the surface enables one to derive some components of the strain fields. In all mentioned contributions, the experimental results have been compared with success with realistic 3D computations using crystal plasticity.

The interest of computing samples containing a small number of large grains lies in the fact that the whole framework can be checked experimentally by comparing local and global predictions to strain or stress field measurements. In the case of coatings for instance, the computations are also of industrial interest since they can be used to optimise the microstructure, like grain size for instance.

The case of zinc coatings on steel sheets has been presented in Parisot et al. (2004) and the case of copper thin films in Šiška et al. (2007). The finite element computation of the tension or expansion of a coating on its substrate reveals the following features of the coating behaviour:

- the multiaxial stress state of each grain depending on its orientation;
- activated slip systems in the core of the grains, at the grain boundaries and at the interface coating/substrate;
- the gradient of strain that can develop from the interface to the free surface; this gradient can be shown to increase when the ratio between in–plane grain size and coating thickness decreases;
- forces acting at grain boundaries and at the interface, that can lead to intergranular fracture or interface decohesion;
- the coating roughness induced by local plasticity.

Computation of polycrystalline aggregates The type of geometrical aggregates shown in figure 10 can be used to investigate the intragranular fields, and to contribute to a better knowledge of the state of stress and strain in a current point of a polycrystal, and in more critical areas like the vicinity of the surface or at the grain boundaries. To be significant,

the calculation must involve a reasonable number of grains *and* a reasonable number of elements in each grain. According to the literature related to texture effect, one thousand of grains seems to be a good number for representing a given material. The following examples are restricted to 200 grains, in order to have more than 1000 integration points in each grain ($10 \times 10 \times 10$, in 3D). Averaged values can then be considered on the mesh, in order to compare the FE model to the results given by more simple models like self–consistent approaches, on the level of each grain, and for the global mechanical response. The elements used are 20–node bricks with 27 integration points per element.

Boundary conditions and representativity of the volume element Three types of boundary conditions will be considered on a cube containing 200 grains Kanit et al. (2003) :

- Homogeneous strain based boundary conditions: the three components of the displacement at each node of the outer surface are prescribed according to the equations :

$$\underline{\boldsymbol{u}} = \underset{\sim}{\boldsymbol{E}}.\underline{\boldsymbol{x}} \tag{12}$$

  where $\underset{\sim}{\boldsymbol{E}}$ is a given constant strain tensor and $\underline{\boldsymbol{x}}$ the position of the point. We apply in this work a strain $\underset{\sim}{\boldsymbol{E}}$ corresponding to average uniaxial tension. The values of the component are taken from a simulation with a homogenized polycrystal model;
- Mixed boundary conditions for which only the displacement normal to the surface is prescribed according to the previous equation; lateral free surfaces may be considered for the case of simple tension for instance.
- Homogeneous stress based boundary conditions for which the traction vector is prescribed at each point of the boundary.

In this section, the local and global behaviour of the polycrystal is investigated. No special property is attributed to the grain boundaries. In particular, grain boundary sliding or damage are not considered.

The representativity of the considered polycrystalline volume element is a central issue. The number of grains must be large enough for the volume to be sufficiently representative. On the other hand, the number of elements inside each grain must be large enough for a sufficiently accurate description of the local intragranular strain field. That is why the presented computations belong to the largest computations of polycrystals available in literature and require parallel computing. With the number of processors used, the compromise is a volume containing 200 grains. The representativity of the volume element depends on the contrast of phase properties,

on the type of boundary conditions and on the wanted accuracy of the estimation of the effective property Kanit et al. (2003). It can be assessed by applying strain based and stress based boundary conditions on the same volume Huet (1990). The difference between the apparent properties found for both conditions is due to the lack of representativity of the sample. For large volumes, the choice of the boundary conditions should not matter any more. The tensile curves obtained for both conditions on the considered sample of 200 grains differ by about 6%. The tensile curves can be found in Barbe et al. (2001b). The interest of periodic boundary conditions compared to homogeneous ones is illustrated in Kanit et al. (2003).

Intragranular fields Figure 10 shows the finite element mesh, and the strain and stress field in the polycrystal in overall simple tension. The material is IN600 Barbe et al. (2001b), the cube is submitted to a 1.5% overall tension, and the orientations of the grains are randomly distributed, in order to simulate an initially isotropic material. The slip activity is mainly due to the gradients of stress at the grain boundaries and not related to a kind of propagation of slip across boundaries. The development of deformation bands is observed independently of the grain morphology. In contrast the stress level is generally higher close to grain boundaries.

Free surface effect Contradictory results can be read in the literature concerning the effect of a free surface on local plastic behaviour Mughrabi (1992). After extensive TEM studies, some authors Pangborn et al. (1981) observe a hardened surface, due to the increase of dislocation density, but other works Fourie (1967); Mughrabi (1970) display an inverse effect, with lower dislocation densities and larger cell sizes. On the other hand, attempts have been made to approach the surface effect from a mechanical point of view, using a crystallographic inclusion in a homogeneous semi–infinite medium, considered as elastoviscoplastic Pilvin (1998) or in full polycrystals Barbe et al. (2001b). In these simulations the presence of a free surface seems to lead to lower stress levels, the perturbed area corresponding to about 3 grains. In the simulation of polycrystalline aggregates in tension with one free lateral surface, the first order surface effect is *scatter*. Relaxing the boundary condition can produce a drop of the local stress, but in some other location, a very low stress level obtained with homogeneous strain conditions can increase when freeing the surface. Averaged quantities can be considered, by plotting the average value of a critical variable in a slice at a given distance of the free surface. In that case, the observed effect is small (less than 10%). In general at a free surface of the cube, the number of active slip systems is significantly smaller (more than 15% less than in

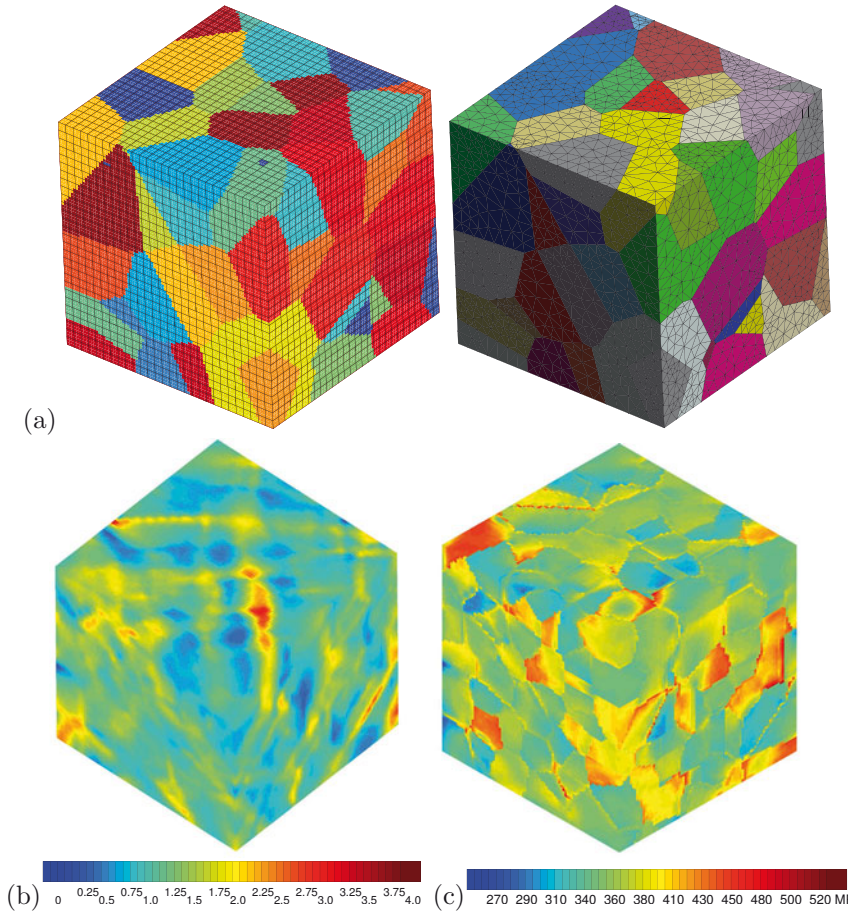

Figure 10. Two meshing strategies for polycrystalline volume elements (a). Contour (b) of the total strain in the tensile direction, (c) of von Mises equivalent stress, for a FCC polycrystal subjected to a mean tensile strain of 1.5%.

the core of the specimen), then the sum of the plastic slip is also smaller.

A systematic study of the 3D morphology of grains on the strain field at a free surface can be found in Zeghadi et al. (2007b,a).

Grain boundary effect Like the surface, the presence of a grain boundary will first induce a large scatter, in terms of stress and strain. However, the averaged stress over one or several grains as a function of the distance to the closest grain boundary is rather constant Barbe et al. (2003). The main results obtained by this statistical analysis are the following. The number of active slip systems and the sum of the plastic slips increase near the grain boundary. The von Mises strain is larger in the center of the grain.

The situation is quite different in the case of an aggregate of h.c.p. crystals like zinc. For this class of symmetry, elasticity and plastic slip are strongly anisotropic. In the zinc alloy studied in Parisot et al. (2004), the activated slip system families are mainly basal slip and pyramidal Π_2, the latter having an initial critical resolved shear stress ten times larger than the former. The consequence is that pyramidal slip takes place principally near the grain boundaries whereas basal slip spreads over the entire grain.

3.3 Grain size effects in polycrystals

Generalized homogenization method for polycrystals The polycrystal can also be regarded as a heterogeneous Cosserat material since it is an aggregate of Cosserat single crystal grains. As a result, some homogenization procedures must be designed to study the resulting properties of the polycrystal. The classical homogenization methods well–established for heterogeneous Cauchy media, as described in details in Sanchez-Palencia and Zaoui (1987); Suquet (1997); Jeulin and Ostoja-Starzewski (2001), must be extended to heterogeneous higher order continua. This task has been undertaken for heterogeneous Cosserat media in Forest et al. (1999, 2001b) and for micromorphic continua in Forest (2002). The theory is presented at small deformation for the sake of brevity.

Hill-Mandel approach The aim is to replace a heterogeneous material by a homogeneous substitute medium (HSM) which can be said to be equivalent in a sense to be made precise. Following Hill-Mandel's approach of the mechanics of heterogeneous materials, a condition of macro-homogeneity is required stipulating that the (isothermal for simplicity) free energy of the HSM at point $\underline{\boldsymbol{x}}$ can be identified to the mean value of the free energy over a representative volume element V under the same overall loading conditions at $\underline{\boldsymbol{x}}$. In the case of heterogeneous Cosserat materials for which the local

fields are the relative strain, curvature and force and couple stress tensors $\underset{\sim}{\boldsymbol{e}}, \underset{\sim}{\boldsymbol{\kappa}}, \underset{\sim}{\boldsymbol{\sigma}}$ and $\underset{\sim}{\boldsymbol{\mu}}$ inside V, this condition can be generalized in the following forms. If the overall substitute medium (to be used for structural calculations for instance) is treated as a Cauchy continuum, the condition reads :

$$< \underset{\sim}{\boldsymbol{\sigma}} : \underset{\sim}{\boldsymbol{e}} + \underset{\sim}{\boldsymbol{\mu}} : \underset{\sim}{\boldsymbol{\kappa}} >= \underset{\sim}{\boldsymbol{\Sigma}} : \underset{\sim}{\boldsymbol{E}} \tag{13}$$

where $\underset{\sim}{\boldsymbol{E}}$ and $\underset{\sim}{\boldsymbol{\Sigma}}$ are the effective (symmetric) deformation and stress tensors. If the HSM is regarded as a Cosserat continuum itself, it becomes

$$< \underset{\sim}{\boldsymbol{\sigma}} : \underset{\sim}{\boldsymbol{e}} + \underset{\sim}{\boldsymbol{\mu}} : \underset{\sim}{\boldsymbol{\kappa}} >= \underset{\sim}{\boldsymbol{\Sigma}} : \underset{\sim}{\boldsymbol{E}} + \underset{\sim}{\boldsymbol{M}} : \underset{\sim}{\boldsymbol{K}} \tag{14}$$

where $\underset{\sim}{\boldsymbol{K}}$ and $\underset{\sim}{\boldsymbol{M}}$ are effective curvature and couple stress tensors, $\underset{\sim}{\boldsymbol{E}}$ and $\underset{\sim}{\boldsymbol{\Sigma}}$ being not necessarily symmetric any more. The procedure (14) is of course more general and contains (13) as a special case to which it reduces if the effective characteristic length is very small.

The determination of the effective properties then goes through the resolution of a boundary value problem on V. Boundary conditions on ∂V must then be chosen that automatically fulfill conditions (13) or (14). For instance the following homogeneous conditions at the boundary can be considered:

$$\underline{\boldsymbol{u}} = \underset{\sim}{\boldsymbol{E}}.\underline{\boldsymbol{x}} \quad and \quad \underline{\boldsymbol{\Phi}} = \underset{\sim}{\boldsymbol{K}}.\underline{\boldsymbol{x}}, \quad \forall \underline{\boldsymbol{x}} \in \partial V \tag{15}$$

where $\underset{\sim}{\boldsymbol{E}}$ and $\underset{\sim}{\boldsymbol{K}}$ are given and constant. It follows that

$$\underset{\sim}{\boldsymbol{E}} =< \underline{\boldsymbol{u}} \otimes \boldsymbol{\nabla} > \quad and \quad \underset{\sim}{\boldsymbol{K}} =< \underset{\sim}{\boldsymbol{\kappa}} > \tag{16}$$

Condition (14) then is automatically satisfied for the following definition of the effective stress tensors

$$\underset{\sim}{\boldsymbol{\Sigma}} =< \underset{\sim}{\boldsymbol{\sigma}} > \quad and \quad \underset{\sim}{\boldsymbol{M}} =< \underset{\sim}{\boldsymbol{\mu}} + \Big(\underset{\sim}{\boldsymbol{\epsilon}} : \underset{\sim}{\boldsymbol{\sigma}}\Big) \otimes \underline{\boldsymbol{x}} >=< \mu_{ij} + \epsilon_{imn}\sigma_{mn}x_j > \ \underline{\boldsymbol{e}}_i \otimes \underline{\boldsymbol{e}}_j \tag{17}$$

Asymptotic methods In the case of periodic microstructures, a unit cell V can be defined and asymptotic methods are well-adapted for deriving the form of the effective balance and constitutive equations Sanchez-Palencia (1974). The key-point is the choice of the small parameter ε introduced in the multiscale asymptotic developments. Two different schemes have been proposed in Forest et al. (2001b) for periodic heterogeneous Cosserat media. Three characteristic lengths must be distinguished : the size l of the unit cell V, a typical characteristic length l_c of the constituents of the heterogeneous Cosserat material, and a typical wave length L_ω associated with the applied loading conditions. In classical homogenization theory, one

usually speaks of slowly varying mean fields when $l \ll L_\omega$ and, in this case, the small parameter is $\varepsilon = l/L_\omega$. In the present situation, one may first consider a limiting process $H^I$with $\varepsilon \longrightarrow 0$, for which the Cosserat length scale l_c varies in the same way as l, so that the small parameter can also be written $\varepsilon = l_c/L_\omega$. In this case, the effective medium can be shown to be a Cauchy continuum. According to a second limiting process H^{II}, l_c is kept constant, which corresponds to $\varepsilon = l/l_c$. The main fields are now treated as functions of the two variables $\underline{\boldsymbol{x}}$ and $\underline{\boldsymbol{y}} = \underline{\boldsymbol{x}}/\varepsilon$. The local fields can be expanded in power series of ε,

$$\underline{\boldsymbol{u}}^{\,\varepsilon}(\underline{\boldsymbol{x}}) = \underline{\boldsymbol{u}}^{\,0}(\underline{\boldsymbol{x}}, \underline{\boldsymbol{y}}) + \varepsilon\, \underline{\boldsymbol{u}}^{\,1}(\underline{\boldsymbol{x}}, \underline{\boldsymbol{y}}) + \varepsilon^2\, \underline{\boldsymbol{u}}^{\,2}(\underline{\boldsymbol{x}}, \underline{\boldsymbol{y}}) + ... \tag{18}$$

$$\underline{\boldsymbol{\Phi}}^{\,\varepsilon}(\underline{\boldsymbol{x}}) = \underline{\boldsymbol{\Phi}}^{\,0}(\underline{\boldsymbol{x}}, \underline{\boldsymbol{y}}) + \varepsilon\, \underline{\boldsymbol{\Phi}}^{\,1}(\underline{\boldsymbol{x}}, \underline{\boldsymbol{y}}) + \varepsilon^2\, \underline{\boldsymbol{\Phi}}^{\,2}(\underline{\boldsymbol{x}}, \underline{\boldsymbol{y}}) + ... \tag{19}$$

where the $\underline{\boldsymbol{u}}^{\,i}$ and $\underline{\boldsymbol{\Phi}}^{\,i}$ are assumed to have the same order of magnitude and are periodic in $\underline{\boldsymbol{y}}$. Similar expansions exist for the force and couple stresses:

$$\underset{\sim}{\boldsymbol{\sigma}}^{\varepsilon}(\underline{\boldsymbol{x}}) = \underset{\sim}{\boldsymbol{\sigma}}^{0}(\underline{\boldsymbol{x}}, y) + \varepsilon\, \sigma^1(\underline{\boldsymbol{x}}, \underline{\boldsymbol{y}}) + \varepsilon^2\, \underset{\sim}{\boldsymbol{\sigma}}^{2}(\underline{\boldsymbol{x}}, \underline{\boldsymbol{y}}) + ... \tag{20}$$

$$\underset{\sim}{\boldsymbol{\mu}}^{\varepsilon}(\underline{\boldsymbol{x}}) = \underset{\sim}{\boldsymbol{\mu}}^{0}(\underline{\boldsymbol{x}}, y) + \varepsilon\, \mu^1(\underline{\boldsymbol{x}}, \underline{\boldsymbol{y}}) + \varepsilon^2\, \underset{\sim}{\boldsymbol{\mu}}^{2}(\underline{\boldsymbol{x}}, \underline{\boldsymbol{y}}) + ... \tag{21}$$

The form of the constitutive equations is different for each homogenization procedure and in the case of linear elasticity, they read:

$$H^I : \quad \underset{\sim}{\boldsymbol{\sigma}}^{\varepsilon} = \underset{\sim}{\boldsymbol{D}}(\underline{\boldsymbol{y}}) : \underset{\sim}{\boldsymbol{e}}^{\varepsilon}(\underline{\boldsymbol{x}}) \quad \textit{and} \quad \underset{\sim}{\boldsymbol{\mu}}^{\varepsilon} = \varepsilon^2 \underset{\sim}{\boldsymbol{C}}(\underline{\boldsymbol{y}}) : \underset{\sim}{\boldsymbol{\kappa}}^{\varepsilon}(\underline{\boldsymbol{x}}) \tag{22}$$

$$H^{II} : \quad \underset{\sim}{\boldsymbol{\sigma}}^{\varepsilon} = \underset{\sim}{\boldsymbol{D}}(\underline{\boldsymbol{y}}) : \underset{\sim}{\boldsymbol{e}}^{\varepsilon}(\underline{\boldsymbol{x}}) \quad \textit{and} \quad \underset{\sim}{\boldsymbol{\mu}}^{\varepsilon} = \underset{\sim}{\boldsymbol{C}}(\underline{\boldsymbol{y}}) : \underset{\sim}{\boldsymbol{\kappa}}^{\varepsilon}(\underline{\boldsymbol{x}}) \tag{23}$$

After noting that $\boldsymbol{\nabla} = \boldsymbol{\nabla}_x + 1/\varepsilon \boldsymbol{\nabla}_y$ (with obvious notations), we compute the gradient of the kinematic variables and the divergence of the stresses in order to introduce them in the balance and constitutive equations. Ordering the terms according to ε leads to a set of equations from which a series of auxiliary boundary value problems to be solved on the unit cell can be defined (see Boutin (1996) for the classical case). The first auxiliary problem for the procedure H^{II} consists in determining vector fields $\underline{\boldsymbol{v}}$ and $\underline{\boldsymbol{\psi}}$ such that :

$$\underline{\boldsymbol{u}} = \underset{\sim}{\boldsymbol{E}}.\underline{\boldsymbol{y}} + \underline{\boldsymbol{v}} \quad \textit{with} \quad \underline{\boldsymbol{\Phi}} = \underset{\sim}{\boldsymbol{K}}.\underline{\boldsymbol{y}} + \underline{\boldsymbol{\psi}}, \quad \forall \underline{\boldsymbol{y}} \in V \tag{24}$$

$$\underset{\sim}{\boldsymbol{\sigma}} = \underset{\sim}{\boldsymbol{D}} : (\underline{\boldsymbol{u}} \otimes \boldsymbol{\nabla}_y) \quad \textit{and} \quad \underset{\sim}{\boldsymbol{\mu}} = \underset{\sim}{\boldsymbol{C}} : (\underline{\boldsymbol{\Phi}} \otimes \boldsymbol{\nabla}_y) \tag{25}$$

$$\underset{\sim}{\boldsymbol{\sigma}}.\boldsymbol{\nabla}_y = 0 \quad \textit{and} \quad \underset{\sim}{\boldsymbol{\mu}}.\boldsymbol{\nabla}_y = 0 \tag{26}$$

where $\underline{\boldsymbol{v}}$ and $\underline{\boldsymbol{\psi}}$ take the same values on opposite sides of the cell and the traction and surface couple vectors $\underset{\sim}{\boldsymbol{\sigma}}.\underline{\boldsymbol{n}}$ and $\underset{\sim}{\boldsymbol{\mu}}.\underline{\boldsymbol{n}}$ are anti-periodic. The

solution of this problem gives in fact the terms $\underline{\boldsymbol{u}}_1, \underline{\boldsymbol{\Phi}}_1, \underset{\sim}{\boldsymbol{\sigma}}^0$ and $\underset{\sim}{\boldsymbol{\mu}}^0$. This leads to the following expression of the mean work of internal forces :

$$< \underset{\sim}{\boldsymbol{\sigma}} : \underset{\sim}{\boldsymbol{e}} + \underset{\sim}{\boldsymbol{\mu}} : \underset{\sim}{\boldsymbol{\kappa}} >=< \underset{\sim}{\boldsymbol{\sigma}} >:< \underline{\boldsymbol{u}} \otimes \boldsymbol{\nabla} > + < \underset{\sim}{\boldsymbol{\mu}} >:< \underset{\sim}{\boldsymbol{\kappa}} > \tag{27}$$

which defines the effective deformation, curvature, force and couple stress tensors. The effective medium then is a Cosserat continuum.

Retained approach for non linear multiphase materials The polycrystal is a heterogeneous material with a disordered distribution of phases, each phase being a crystal orientation, and Hill-Mandel approach has proved to be efficient for deriving effective properties in such cases Sanchez-Palencia and Zaoui (1987). This requires however computations on a large representative volume element V containing many grains. Such aggregates have already been computed in classical crystal plasticity in section 3.2. But for Cosserat materials, the number of degrees of freedom and internal variables increases dramatically in the three-dimensional case so that we will work here on smaller samples of grains. In the latter case, periodic boundary conditions will induce less pronounced boundary effects than the Dirichlet conditions (15) (see Kanit et al. (2003)). That is why a mixed approach between Hill-Mandel and periodic ones is retained here, combining the periodic scheme H^{II} and unaltered local constitutive equations and thus different from (25). It has been shown numerically in Forest et al. (2001b), at least in the case of linear elasticity, that the approach H^{II} works well even if $l_c \sim l$, which will be the case in section 4 to 6.

Accordingly, the following initial boundary value problem P is considered on a single unit cell V :

$$\begin{gathered} \underline{\boldsymbol{u}} = \underset{\sim}{\boldsymbol{E}}.\underline{\boldsymbol{x}} + \underline{\boldsymbol{v}}, \quad \underline{\boldsymbol{\Phi}} = \underset{\sim}{\boldsymbol{K}}.\underline{\boldsymbol{x}} + \underline{\boldsymbol{\psi}}, \\ \textit{constitutive} \quad \textit{equations}, \\ \underset{\sim}{\boldsymbol{\sigma}}.\boldsymbol{\nabla} = 0, \quad \underset{\sim}{\boldsymbol{\mu}}.\boldsymbol{\nabla} - \underline{\underline{\boldsymbol{\epsilon}}} : \underset{\sim}{\boldsymbol{\sigma}} = 0 \end{gathered} \tag{28}$$

where $\underline{\boldsymbol{v}}$ (resp. $\underline{\boldsymbol{\psi}}$) takes the same value on opposite sides of the cell. The traction and surface couple vectors of two homologous points on opposite sides of V are opposite. This problem is solved on a single cell V and no attempt is made to extrapolate the solution in a regular solution on the entire body, although it may be possible in particular for symmetric $\underset{\sim}{\boldsymbol{E}}$ or $\underset{\sim}{\boldsymbol{\Sigma}}$ and vanishing $\underset{\sim}{\boldsymbol{K}}$.

Scale dependent behaviour of polycrystals Continuum crystal plasticity models can be enhanced to account for size effects in single or multiphase metal polycrystals. Strain gradient, gradient of internal variable

and Cosserat models are available to introduce additional hardening primarily associated with densities of so–called geometrically necessary dislocations Kubin and Mortensen (2003). Direct simulations of polycrystalline aggregates including a detailed description of non–homogeneous deformation inside individual grains can then be used to predict grain size effects classically observed in metal polycrystals Acharya and Beaudoin (2000); Forest et al. (2000). The advantage of such models is that the grain size D is not explicitly introduced in the constitutive equations, so that the size effect scaling is the result of complex in–grain stress–strain fields and interactions between grains. As a result, once identified, the same model can be used for other size effects associated with the interaction with other phases (lamellar structures, two–phase materials).

The aim of the next sections is the identification of the material parameters of a Cosserat crystal plasticity model to account for grain size effects in an IF ferritic steel. Tensile curves for grains sizes ranging from 120 μm to 5 μm can be found in Bouaziz et al. (2001) and show strong effects for smaller grains. This hardening is not only due to grain size effects but also to solid solution hardening since it is impossible to produce IF steels with such small grains with exactly the same composition as for larger grains. The solid solution hardening part can be isolated and estimated by suited experiments so that the present work can concentrate on the remaining part of hardening due solely to grain size changes. Scaling laws in $D^{-0.7}$ were found experimentally. Precise modelling of IF steels based on crystal plasticity at a fixed grain size can be found in the referenced Paquin (2001); Hoc et al. (2001).

The Cosserat crystal plasticity model is specialized in section 3.3 to the case of small strain and rotation. The main capabilities of the model are illustrated by two–dimensional finite element simulations showing the development of lattice rotation and curvature inside grains for different grain sizes. The actual identification of the model for IF steels requires the 3D simulations of section 3.3. Some of the presented results were published in Zeghadi et al. (2005). Simulations based on strain gradient plasticity models also exist for polycrystals in miniaturized samples Bayley et al. (2007); Bargmann et al. (2010). The obtained lattice orientation fields can be compared to experimental results like EBSD field measurements St-Pierre et al. (2008).

Cosserat crystal plasticity model at small strain and rotation Cosserat continuum mechanics introduces, at each material point, not only a displacement vector $\underline{\boldsymbol{u}}$ but also an independent rotation field, represented by the axial vector ϕ_i. The Cosserat deformation and curvature tensors are

respectively:

$$e_{ij} = u_{i,j} + \epsilon_{ijk}\Phi_k \qquad \kappa_{ij} = \Phi_{i,j} \tag{29}$$

In the static case,the force and couple stress tensors associated with the previous deformation measures, must fulfill two balance equations Nowacki (1986):

$$\sigma_{ij,j} + f_i = 0, \qquad \mu_{ij,j} - \epsilon_{ijk}\sigma_{jk} = 0 \tag{30}$$

The isotropic elasticity law involves the 2 Lamé constants and 4 additional moduli:

$$\sigma_{ij} = \lambda\delta_{ij}e^e_{kk} + 2\mu e^e_{(ij)} + 2\mu_c e^e_{\{ij\}}, \qquad \mu_{ij} = \alpha\delta_{ij}\kappa^e_{kk} + 2\beta\kappa^e_{(ij)} + 2\gamma\kappa^e_{\{ij\}} \tag{31}$$

where (ij) and $\{ij\}$ respectively denote the symmetric and skew-symmetric parts of the tensor. The Cosserat directors can be identified with lattice directions when the elastic strain tensor e^e_{ij} is almost symmetric. That is why the constant parameter μ_c is used as a penalty factor in the crystal plasticity Cosserat model. An intrinsic length $l_e = \sqrt{\beta/\mu}$ can be defined. Plastic deformation is due to the activation of plastic slip γ^s on slip system s:

$$\dot{e}_{ij} = \dot{e}^e_{ij} + \dot{e}^p_{ij}, \quad \dot{e}^p = \sum_{s=1}^{N} \dot{\gamma}^s P^s_{ij}, \quad P^s_{ij} = m^s_i n^s_j \tag{32}$$

where m^s_i and n^s_i respectively are the slip direction and normal to the slip plane. For IF steels, the 24 slip systems $\{110\} < 111 >$ and $\{112\} < 111 >$ are retained Paquin (2001); Hoc et al. (2001). Similarly, lattice curvature is accommodated by elastic and plastic parts:

$$\dot{\kappa}_{ij} = \dot{\kappa}^e_{ij} + \dot{\kappa}^p_{ij}, \qquad \dot{\kappa}^p_{ij} = \sum_{s=1}^{n} \left(\frac{\dot{\theta}^s_{\perp}}{l_p} Q^s_{ij\perp} \right), \quad Q^s_{ij\perp} = \epsilon_{ikl} n^s_k m^s_l m^s_k \tag{33}$$

where ϵ_{ijk} is the permutation symbol. Plastic lattice bending only is accounted for in the present work, based on Nye's formula. It is represented for each slip system by the angle θ^s divided by a second characteristic length l_p. Viscoplastic flow rules are adopted for both plastic slip and curvature:

$$\dot{\gamma}^s = \langle \frac{\mid \tau^s \mid - r^s}{k} \rangle^n \; sign\,(\tau^s), \quad \dot{\theta}^s = \langle \frac{\mid \nu^s \mid \; - \; l_p \; r^s_{c0}}{l_p \; k^s_c} \rangle^{n_c} \; sign\;(\nu^s) \tag{34}$$

where $\tau^s = \sigma_{ij}P^s_{ij}$ and $\nu^s = \mu_{ij}Q^s_{ij\perp}$ respectively are the resolved shear stress and the resolved couple stress. The brackets $\langle\rangle$ denote the positive

E	ν	k	n	r_0	q	b_1
(MPa)		$(MPa.s^{1/n})$		(MPa)	(MPa)	
208000.	0.3	3.	10.	29.	39.	16.

β	r_{c0}	H'	l_p	k_c	n_c	b_2
$(MPa.mm^2)$	(MPa)	(MPa)	(mm)	$(MPa.s^{1/n_c})$		
0.001	0.000001	10.	1.	0.01	1.	5.

Table 1. (a) Classical parameters used in the computations (b) Specific Cosserat parameters used in the computations

part. A simple nonlinear evolution law is adopted for the critical resolved shear stress r^s:

$$r^s = r_0 + Q\sum_{r=1}^{n} h^{sr}(1 - \exp(-bv^r)) + r^{\perp}, \qquad v^s = \mid \dot{\gamma}^s \mid \tag{35}$$

with an interaction matrix h^{rs} which represents a simplified version of the model used in Hoc et al. (2001).

Influence of Cosserat elasticity and curvature hardening The Cosserat bending modulus β was introduced by Kröner in dislocated crystals Kröner (1963) and related to the density of geometrically necessary dislocations and therefore to θ^s/l_p. In the simple case of single slip in periodic layered microstructures analysed in Forest and Sedláček (2003), it has been related to line tension effects associated with the collective bowing of dislocations in narrow channels. As a result, this parameter (and the corresponding intrinsic length l_e) influences the spreading of lattice curvature inside grains. To show that, finite element simulations of the shearing of a 2D aggregate containing nine ferritic grains were performed for two different values of the bending modulus, under plane strain conditions. Non–homogeneous deformation and lattice rotation are due to plastic strain incompatibilities between grains having different (random) orientations. Lattice curvature primarily develops close to grain boundaries. Higher values of β promote a larger spreading of lattice curvature for the same mean prescribed strain value. This feature will play an important role in the following simulations of grain size effects.

In equation (35), an additional hardening term $r_{\perp}$ associated with lattice

curvature is introduced. The following evolution rule is proposed

$$r_\perp = Q_\perp (\sum_{s=1}^{n} (1 - \exp(-b_\perp \theta^s)))^{\frac{1}{2}} \tag{36}$$

Similar additional hardening terms are summarized and commented in Kubin and Mortensen (2003) and involve the square root of a combination of the density of statistically stored dislocations and density of geometrically dislocations. Such rules are relevant for f.c.c. crystals but they are questionable in b.c.c. crystals. The function (36) of plastic lattice curvature angles is of purely phenomenological nature. It has two advantageous features: a vertical tangent at zero plastic curvature and saturation for higher curvature levels. This allows strong effects at incipient plasticity, as recommended by Ashby Ashby (1970). The effect of extra–hardening is illustrated in the 2D case on figure 12 for two different grain sizes. The geometry of the grains is the same for both computations but the absolute sizes of the aggregates differ, which correspond to grain sizes of 120 and 5 μm respectively. At the very beginning of intragranular plastic flow (0.075% overall shear strain), plastic strain and lattice rotation maps are quite similar for both grain sizes. As a consequence, plastic curvature fields strongly differ (figures 12(a)(b) and (c)). Lattice curvature being much larger in the small grains, the curvature hardening rule (36) induces higher stress levels for small grain sizes, as shown on figures 12(d). This will strongly affect subsequent plastic flow in the grains. This mechanism is the main ingredient in the following simulations of grain size effects in ferritic polycrystals.

3D finite element analyses of ferritic steels 2D simulations were used in the previous section to illustrate the different capabilities of the Cosserat crystal plasticity model. 3D simulations are necessary to actually reproduce the experimental results on grain size effects in ferritic steels. A mean tensile strain up to 10% is prescribed to a small aggregate containing 10 grains. Geometrical and kinematic periodicity conditions are chosen because a periodic homogenization scheme is available for Cosserat continua, and also because smaller representative volumes can be considered Forest et al. (2000). The considered volume element is shown in figure 13.

The identification of the material parameters of the Cosserat models for the considered material proceeds as follows. The initial critical resolved shear stress r_0, the hardening parameters Q, b (equation (35)), are deduced from the tensile curve of IF steel with D =120 μm (large grain polycrystal behaviour). The interaction matrix h^{rs} is taken from the references Paquin (2001); Hoc et al. (2001). The Cosserat parameters $\beta, Q_\perp, b_\perp$ (equation

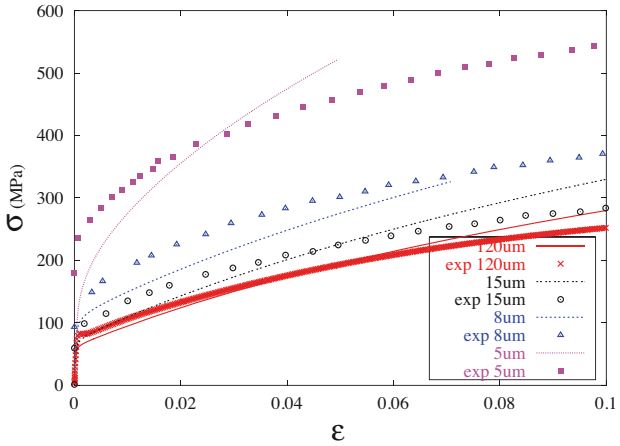

Figure 11. Mean axial stress–mean axial strain curves predicted by the finite element analysis compared with experimental results

.

(36)) are identified from the dependence of the tensile curve on grain size. For all simulations at different grains sizes, the material parameters, the morphology of the grains and the boundary conditions are the same. The finite element meshes take the actual size of the grains into account. The inverse approach requires large amounts of time since each simulation on one aggregate is time consuming. The best parameters found are given in table 3.3. Reference computations have also been performed with classical polycrystalline model. The Cosserat parameters are such that its response is close to the classical one for grain sizes larger than D =120 μm. The results after identification are shown in figure 11 which gives the average values of axial stress and strain. As expected, the finite element response is significantly harder for the smallest grain size. In both cases, the same grains are activated and the maximal stress is localised near the grains boundaries. The predicted grain size scaling at 0.2% plastic strain can be checked. Grain size effects saturate for grain larger than 120 μm (classical case) and for grains smaller than 1μm with the present parameters.

The effect of grain size on the local fields in 3D is illustrated in figure 13. As expected, plastic strain is higher in larger grains for the same mean total strain. Lattice curvature is higher in small grains and is observed mainly close to grain boundaries where most strain incompatibilities arise.

An enhanced continuum crystal plasticity model was used to simulate grain size effects in a ferritic steel using the finite element method and pe-

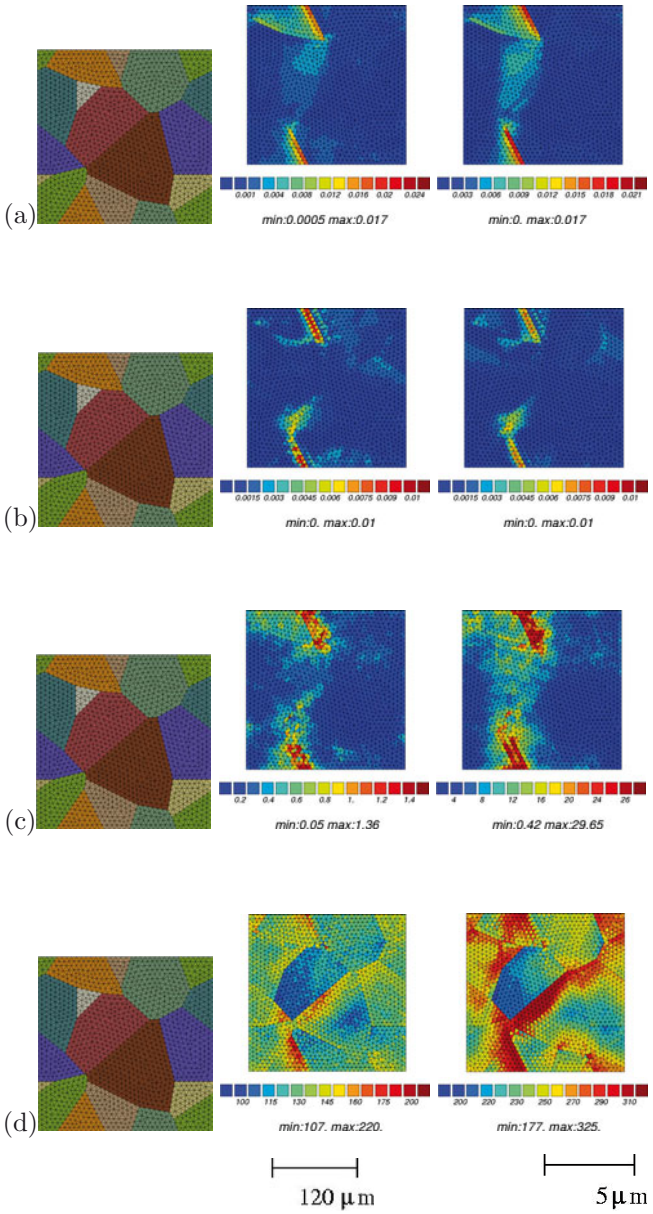

Figure 12. Two–dimensional simulation of microplasticity in a polycrystalline volume element with two grain sizes and periodicity conditions: (a) equivalent plastic strain, (b) norm of the lattice rotation vector (in rad.), (c) norm of lattice curvature, (d) von Mises stress. The mean total strain is 0.00075 in both computations.

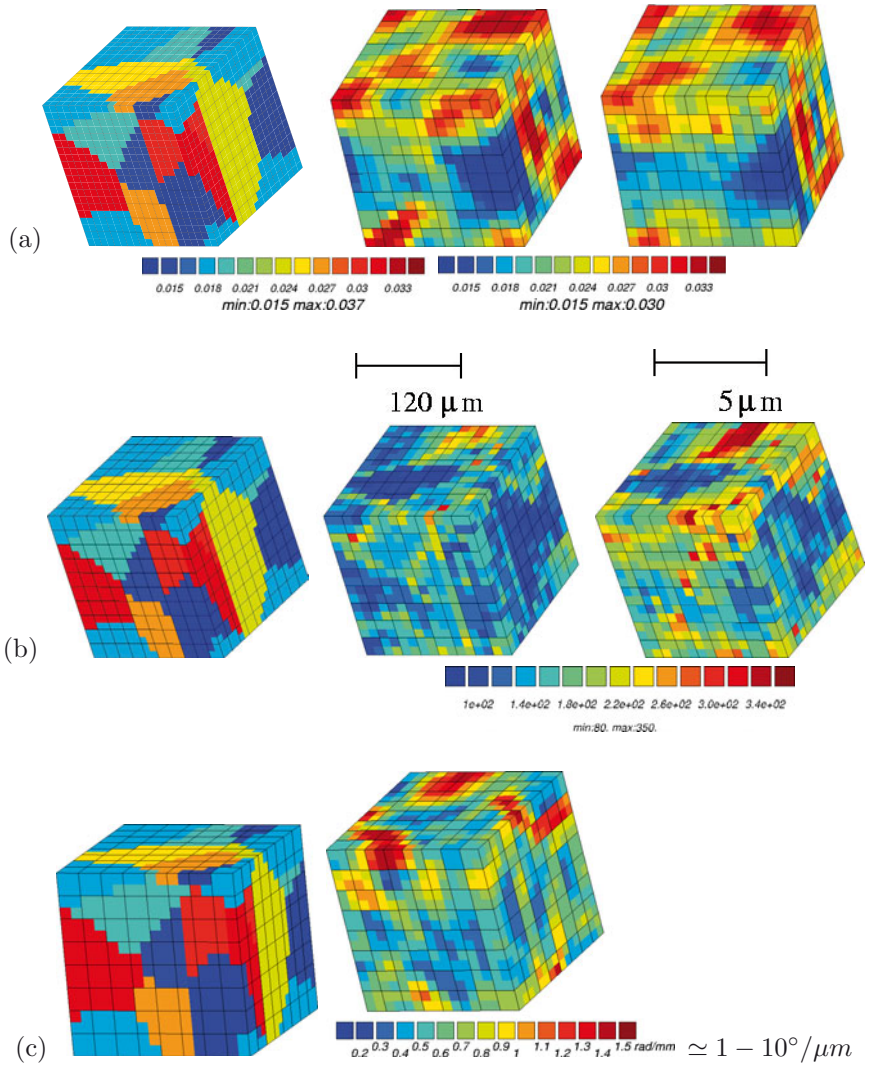

Figure 13. Computation of a periodic volume element of a ferritic steel for two grain sizes at the same mean strain level 0.01: (a) field of equivalent plastic strain, (b) field of equivalent stress, (c) field of equivalent plastic curvature for the smaller grains.

riodic polycrystalline aggregates. In the simulation, the size effect is due to an increase of plastic curvature for small grains associated with additional curvature hardening. A second significant component is the increase of the volume fraction of curved lattice within the grains for decreasing grain size. This also contributes to higher macroscopic stress levels. However, the present simulations still significantly underestimate the grain size effect observed experimentally. This may be due to too coarse meshes, to insufficient lattice curvature spreading at small grains, or to deeper metallurgical physical reasons that remain to be sorted out.

Alternative crystal plasticity models accounting for the overall grain size effects are based on mean field homogenization approaches Pipard et al. (2009).

Bibliography

K. Abu Al-Rub, G.Z. Voyiadjis, and D.J. Bammann. A thermodynamic based higher-order gradient theory for size dependent plasticity. *Int. J. Solids Structures*, 44:2888–2923, 2007.

A. Acharya. Jump condition for GND evolution as a constraint on slip transmission at grain boundaries. *Philosophical Magazine*, 87:1349–1359, 2007.

A. Acharya. New inroads in an old subject: Plasticity, from around the atomic to the macroscopic scale. *Journal of the Mechanics and Physics of Solids*, 58:766–778, 2010.

A. Acharya and J.L. Bassani. Lattice incompatibility and a gradient theory of crystal plasticity. *Journal of the Mechanics and Physics of Solids*, 48: 1565–1595, 2000.

A. Acharya and A.J. Beaudoin. Grain size effects in viscoplastic polycrystals at moderate strains. *Journal of the Mechanics and Physics of Solids*, 48: 2213–2230, 2000.

E.C. Aifantis. The physics of plastic deformation. *International Journal of Plasticity*, 3:211–248, 1987.

E.C. Aifantis. Gradient deformation models at nano, micro and macro scales. *J. of Engineering Materials and Technology*, 121:189–202, 1999.

R.J. Asaro. Crystal plasticity. *J. Appl. Mech.*, 50:921–934, 1983.

R.J. Asaro and J.R. Rice. Strain localization in ductile single crystals. *J. Mech. Phys. Solids*, 25:309–338, 1977.

M.F. Ashby. The deformation of plastically non–homogeneous materials. *Philosophical Magazine*, 21:399–424, 1970.

M.F. Ashby. The deformation of plastically non-homogeneous alloys. In A. Kelly and R.B. Nicholson, editors, *Strengthening Methods in Crystals*, pages 137–192. Applied Science Publishers, London, 1971.

F. Barbe, L. Decker, D. Jeulin, and G. Cailletaud. Intergranular and intragranular behavior of polycrystalline aggregates. Part 1: FE model. *International Journal of Plasticity*, 17:513–536, 2001a.

F. Barbe, S. Forest, and G. Cailletaud. Intergranular and intragranular behavior of polycrystalline aggregates. Part 2: Results. *International Journal of Plasticity*, 17:537–563, 2001b.

F. Barbe, S. Forest, S. Quilici, and G. Cailletaud. Numerical study of crystalline plasticity : measurements of the heterogeneities due to grain boundaries under small strains. *La Revue de Métallurgie*, 101:815–823, 2003.

L. Bardella. Some remarks on the strain gradient crystal plasticity modelling, with particular reference to the material length scales involved. *International Journal of Plasticity*, 23:296–322, 2007.

S. Bargmann, M. Ekh, K. Runesson, and B. Svendsen. Modeling of polycrystals with gradient crystal plasticity: A comparison of strategies. *Philosophical Magazine*, 90(10):1263–1288, 2010.

J.L. Bassani, A. Needleman, and E. Van der Giessen. Plastic flow in a composite : a comparison of nonlocal continuum and discrete dislocation predictions. *Int. J. Solids Structures*, 38:833–853, 2001.

C.J. Bayley, W.A.M. Brekelmans, and M.G.D. Geers. A comparison of dislocation induced back stress formulations in strain gradient crystal plasticity. *International Journal of Solids and Structures*, 43:7268–7286, 2006.

C.J. Bayley, W.A.M. Brekelmans, and M.G.D. Geers. A three–dimensional dislocation field crystal plasticity approach applied to miniaturized structures. *Philosophical Magazine*, 87:1361–1378, 2007.

A. Bertram. *Elasticity and Plasticity of Large Deformations*. Springer, 2005.

D. Besdo. Ein Beitrag zur nichtlinearen Theorie des Cosserat-Kontinuums. *Acta Mechanica*, 20:105–131, 1974.

J. Besson, G. Cailletaud, J.-L. Chaboche, and S. Forest. *Mécanique non linéaire des matériaux*. ISBN 2-7462-0268-9, EAN13 9782746202689, 445 p., Hermès, France, 2001.

B.A. Bilby, R. Bullough, L.R.T. Gardner, and E. Smith. Continuous distributions of dislocations iv: Single glide and plane strain. *Proc. Roy. Soc. London*, A236:538–557, 1957.

R. de Borst. Simulation of strain localization: a reappraisal of the Cosserat continuum. *Engng Computations*, 8:317–332, 1991.

R. de Borst, L.J. Sluys, H.B. Mühlhaus, and J. Pamin. Fundamental issues in finite element analyses of localization of deformation. *Engineering Computations*, 10:99–121, 1993.

O. Bouaziz, T. Iung, M. Kandel, and C. Lecomte. Physical modelling of microstructure and mechanical properties of dual–phase steel. *Journal de Physique IV*, 11:Pr4–223–229, 2001.

C. Boutin. Microstructural effects in elastic composites. *Int. J. Solids Structures*, 33:1023–1051, 1996.

E.P. Busso, F.T. Meissonnier, and N.P. O'Dowd. Gradient–dependent deformation of two–phase single crystals. *Journal of the Mechanics and Physics of Solids*, 48:2333–2361, 2000.

G. Cailletaud. A micromechanical approach to inelastic behaviour of metals. *Int. J. Plasticity*, 8:55–73, 1992.

G. Cailletaud, S. Forest, D. Jeulin, F. Feyel, I. Galliet, V. Mounoury, and S. Quilici. Some elements of microstructural mechanics. *Computational Materials Science*, 27:351–374, 2003.

J.D. Clayton, D.L. McDowell, and D.J. Bammann. Modeling dislocations and disclinations with finite micropolar elastoplasticity. *International Journal of Plasticity*, 22:210–256, 2006.

H. Cleveringa, E. Van der Giessen, and A. Needleman. Discrete dislocation simulations and size dependent hardening in single slip. *Journal de Physique IV*, 8:Pr4–83–92, 1998.

B.D. Coleman and W. Noll. The thermodynamics of elastic materials with heat conduction and viscosity. *Arch. Rational Mech. and Anal.*, 13:167–178, 1963.

N.M. Cordero, A. Gaubert, S. Forest, E. Busso, F. Gallerneau, and S. Kruch. Size effects in generalised continuum crystal plasticity for two–phase laminates. *Journal of the Mechanics and Physics of Solids*, 58:1963–1994, 2010.

E. Cosserat and F. Cosserat. *Théorie des corps déformables.* Hermann, Paris, 1909.

F. Delaire, J.L. Raphanel, and C. Rey. Plastic heterogeneities of a copper multicrystal deformed in uniaxial tension: experimental study and finite element simulations. *Acta mater.*, 48:1075–1087, 2000.

V.S. Deshpande, A. Needleman, and E. Van Der Giessen. A discrete dislocation analysis of near threshold fatigue crack growth. *Acta materialia*, 49:3189–3203, 2001.

T. Dillard, S. Forest, and P. Ienny. Micromorphic continuum modelling of the deformation and fracture behaviour of nickel foams. *European Journal of Mechanics A/Solids*, 25:526–549, 2006.

P.H. Dluzewski. Finite deformation of polar media in angular coordinates. *Arch. Mech.*, 43:783–793, 1991.

P.H. Dluzewski. Finite elastic-plastic deformations of oriented media. In A. Benallal and D. Marquis, editors, *MECAMAT'92, Int. Seminar on Multiaxial Plasticity.* Cachan, 1992.

W.J. Drugan. Asymptotic solutions for tensile crack tip fields without kink–type shear bands in elastic ideally–plastic single crystals. *Journal of the Mechanics and Physics of Solids*, 49:2155–2176, 2001.

M.K. Duszek-Perzyna and P. Perzyna. Adiabatic shear band localization in elastic-plastic single crystals. *Int. J. Solids Structures*, 30(1):61–89, 1993.

F. Eberl, F. Feyel, S. Quilici, and G. Cailletaud. Approches numériques de la plasticité cristalline. *J. Phys. IV France*, 8:Pr4–15–25, 1998.

M. Eisenberg. On the relation between continuum plasticity and dislocation theories. *Int. J. Engng. Sci.*, 8:261–271, 1970.

R.A.B. Engelen, M.G.D. Geers, and F.P.T. Baaijens. Nonlocal implicit gradient-enhanced elasto-plasticity for the modelling of softening behaviour. *International Journal of Plasticity*, 19:403–433, 2003.

R.A.B. Engelen, N.A. Fleck, R.H.J. Peerlings, and M.G.D. Geers. An evaluation of higher–order plasticity theories for predicting size effects and localisation. *International Journal of Solids and Structures*, 43:1857–1877, 2006.

A.C. Eringen. *Polar and non local fields theories, in Continuum Physics*, volume IV. Academic Press, 1976.

A.C. Eringen. *Microcontinuum field theories.* Springer, New York, 1999.

A.C. Eringen and W.D. Claus. A micromorphic approach to dislocation theory and its relation to several existing theories. In J.A. Simmons, R. de Wit, and R. Bullough, editors, *Fundamental Aspects of Dislocation Theory*, pages 1023–1062. Nat. Bur. Stand. (US) Spec. Publ. 317, II, 1970.

A.C. Eringen and E.S. Suhubi. Nonlinear theory of simple microelastic solids. *Int. J. Engng Sci.*, 2:189–203, 389–404, 1964.

Y. Estrin, B. Sluys, Y. Bréchet, and A. Molinari. A dislocation based gradient plasticity model. *Journal de Physique IV*, 8:Pr8–135–141, 1998.

M. Fivel and S. Forest. *Plasticité cristalline et transition d'échelle : cas du monocristal.* Techniques de l'Ingénieur, M4016, 23 pages, 2004.

M.C. Fivel, C.F. Robertson, G.R. Canova, and L. Boulanger. Three-dimensional modeling of indent-induced plastic zone at a mesoscale. *Acta materialia*, 46:6183–6194, 1998.

N.A. Fleck and J.W. Hutchinson. A reformulation of strain gradient plasticity. *Journal of the Mechanics and Physics of Solids*, 49:2245–2271, 2001.

N.A. Fleck and J.W. Hutchinson. Strain gradient plasticity. *Adv. Appl. Mech.*, 33:295–361, 1997.

S. Flouriot, S. Forest, G. Cailletaud, A. Köster, L. Rémy, B. Burgardt, V. Gros, S. Mosset, and J. Delautre. Strain localization at the crack tip

in single crystal CT specimens under monotonous loading : 3D finite element analyses and application to nickel–base superalloys. *International Journal of Fracture*, 124:43–77, 2003.

S. Forest. Modeling slip, kink and shear banding in classical and generalized single crystal plasticity. *Acta Materialia*, 46(9):3265–3281, 1998.

S. Forest. The micromorphic approach for gradient elasticity, viscoplasticity and damage. *ASCE Journal of Engineering Mechanics*, 135:117–131, 2009.

S. Forest. Some links between cosserat, strain gradient crystal plasticity and the statistical theory of dislocations. *Philosophical Magazine*, 88: 3549–3563, 2008.

S. Forest. Homogenization methods and the mechanics of generalized continua–Part 2. *Theoretical and Applied Mechanics*, 28–29:113–143, 2002.

S. Forest and E. C. Aifantis. Some links between recent gradient thermo-elasto-plasticity theories and the thermomechanics of generalized continua. *International Journal of Solids and Structures*, 47:3367–3376, 2010.

S. Forest and M. Amestoy. Hypertemperature in thermoelastic solids. *Comptes Rendus Mécanique*, 336:347–353, 2008.

S. Forest and G. Cailletaud. Strain localization in single crystals: Effect of boundaries and interfaces. *European Journal of Mechanics A/Solids*, 14 (5):747–771, 1995.

S. Forest and R. Sedláček. Plastic slip distribution in two–phase laminate microstructures: Dislocation–based vs. generalized–continuum approaches. *Philosophical Magazine A*, 83:245–276, 2003.

S. Forest and R. Sievert. Elastoviscoplastic constitutive frameworks for generalized continua. *Acta Mechanica*, 160:71–111, 2003.

S. Forest and R. Sievert. Nonlinear microstrain theories. *International Journal of Solids and Structures*, 43:7224–7245, 2006.

S. Forest, G. Cailletaud, and R. Sievert. A Cosserat theory for elastoviscoplastic single crystals at finite deformation. *Archives of Mechanics*, 49 (4):705–736, 1997.

S. Forest, R. Dendievel, and G.R. Canova. Estimating the overall properties of heterogeneous Cosserat materials. *Modelling Simul. Mater. Sci. Eng.*, 7:829–840, 1999.

S. Forest, F. Barbe, and G. Cailletaud. Cosserat modelling of size effects in the mechanical behaviour of polycrystals and multiphase materials. *International Journal of Solids and Structures*, 37:7105–7126, 2000.

S. Forest, P. Boubidi, and R. Sievert. Strain localization patterns at a crack tip in generalized single crystal plasticity. *Scripta Materialia*, 44: 953–958, 2001a.

S. Forest, F. Pradel, and K. Sab. Asymptotic analysis of heterogeneous Cosserat media. *International Journal of Solids and Structures*, 38:4585–4608, 2001b.

S. Forest, E. van der Giessen, and L. Kubin, Editors. *Scale transitions from atomistics to continuum plasticity.* J. Phys. IV, France, Vol. 11, Pr5, Les Editions de Physique, 2001c.

S. Forest, R. Sievert, and E.C. Aifantis. Strain gradient crystal plasticity : Thermomechanical formulations and applications. *Journal of the Mechanical Behavior of Materials*, 13:219–232, 2002.

J.T. Fourie. The flow stress gradient between the surface and centre of deformed copper single crystals. *Philosophical Magasine*, 15:735–756, 1967.

J. Friedel. *Dislocations.* Pergamon, 1964.

N. Germain, J. Besson, and F. Feyel. Simulation of laminate composites degradation using mesoscopic non–local damage model and non–local layered shell element. *Modelling and Simulation in Materials Science and Engineering*, 15:S425–S434, 2007.

P. Germain. La méthode des puissances virtuelles en mécanique des milieux continus, première partie : théorie du second gradient. *J. de Mécanique*, 12:235–274, 1973a.

P. Germain. The method of virtual power in continuum mechanics. part 2 : Microstructure. *SIAM J. Appl. Math.*, 25:556–575, 1973b.

P. Germain, Q.S. Nguyen, and P. Suquet. Continuum thermodynamics. *J. of Applied Mechanics*, 50:1010–1020, 1983.

P. Gumbsch and R. Pippan. *Multiscale Modelling of Plasticity and Fracture by means of Dislocation Mechanics.* CISM Lecture Notes, Udine, 2005.

M.E. Gurtin. On the plasticity of single crystals: free energy, microforces, plastic-strain gradients. *Journal of the Mechanics and Physics of Solids*, 48:989–1036, 2000.

M.E. Gurtin. On a framework for small–deformation viscoplasticity: free energy, microforces, strain gradients. *International Journal of Plasticity*, 19:47–90, 2003.

M.E. Gurtin and L. Anand. Nanocrystalline grain boundaries that slip and separate: A gradient theory that accounts for grain-boundary stress and conditions at a triple-junction. *Journal of the Mechanics and Physics of Solids*, 56:184–199, 2008.

M.E. Gurtin and L. Anand. Thermodynamics applied to gradient theories involving the accumulated plastic strain: The theories of Aifantis and Fleck & Hutchinson and their generalization. *Journal of the Mechanics and Physics of Solids*, 57:405–421, 2009.

M.E. Gurtin and A. Needleman. Boundary conditions in small–deformation, single–crystal plasticity that account for the burgers vector. *Journal of the Mechanics and Physics of Solids*, 53:1–31, 2005.

H.T. Hahn and W. Jaunzemis. A dislocation theory of plasticity. *Int. J. Engng. Sci.*, 11:1065–1078, 1973.

F. Hehl and E. Kröner. Zum Materialgesetz eines elastischen Mediums mit Momentenspannungen. *Z. Naturforschg.*, 20a:336–350, 1958.

J.P. Hirth and J. Lothe. *Theory of Dislocations*. Wiley Intersciences, 1982.

T. Hoc, C. Rey, and J.L. Raphanel. Experimental and numerical analysis of localization during sequential test for an IF-Ti steel. *Acta Mater.*, 49: 1835–1846, 2001.

C. Huet. Application of variational concepts to size effects in elastic heterogeneous bodies. *J. Mech. Phys. Solids*, 38:813–841, 1990.

J.W. Hutchinson. Plasticity at the micron scale. *Int. J. Solids Structures*, 37:225–238, 2000.

B. Jaoul. *Etude de la plasticité et application aux métaux*. Dunod, Paris, 1965.

D. Jeulin and M. Ostoja-Starzewski. *Mechanics of Random and Multiscale Microstructures*. CISM Courses and Lectures No. 430, Udine, Springer Verlag, 2001.

C.B. Kafadar and A.C. Eringen. Micropolar media: I the classical theory. *Int. J. Engng Sci.*, 9:271–305, 1971.

T. Kanit, S. Forest, I. Galliet, V. Mounoury, and D. Jeulin. Determination of the size of the representative volume element for random composites : statistical and numerical approach. *International Journal of Solids and Structures*, 40:3647–3679, 2003.

S. Kessel. Lineare Elastizitätstheorie des anisotropen Cosserat-Kontinuums. *Abhandlungen der Braunschweig. Wiss. Ges.*, 16, 1964.

S. Kessel. Spannungsfelder einer Schraubenversetzung und einer Stufenversetzung im Cosseratschen Kontinuum. *ZAMM*, 50:547–553, 1970.

W.T. Koiter. Couple-stresses in the theory of elasticity. i and ii. *Proc. K. Ned. Akad. Wet.*, B67:17–44, 1963.

E. Kröner. Die Versetzung als elementare Eigenspannungsquelle. *Z. Naturforschg.*, 11:969–985, 1956.

E. Kröner. *Kontinuumstheorie der Versetzungen und Eigenspannungen*. Ergebnisse der angewandten Mathematik, Vol. 5, Springer-Verlag, 1958.

E. Kröner. On the physical reality of torque stresses in continuum mechanics. *Int. J. Engng. Sci.*, 1:261–278, 1963.

E. Kröner. Initial studies of a plasticity theory based upon statistical mechanics. In M.F. Kanninen, W.F. Adler, A.R. Rosenfield, and R.I. Jaffee, editors, *Inelastic Behaviour of Solids*, pages 137–147. McGraw-Hill, 1969.

E. Kröner. *Statistical Continuum Mechanics*. CISM Courses and Lectures No. 92, Udine, Springer Verlag, Wien, 1971.

Kröner, E. *Mechanics of generalized continua, Proc. of the IUTAM-Symposium on the generalized Cosserat continuum and the continuum theory of dislocations with applications, Freudenstadt, Stuttgart*. Springer Verlag, 1967.

L. Kubin and A. Mortensen. Geometrically necessary dislocations and strain–gradient plasticity. *Scripta materialia*, 48:119–125, 2003.

D. Lachner, H. Lippmann, and L.S. Tóth. On Cosserat plasticity and plastic spin for isotropic materials. *Archives of Mechanics*, 46:531–539, 1994.

R.W. Lardner. Dislocation dynamics and the theory of the plasticity of single crystals. *ZAMP*, 20:514–529, 1969.

H. Lippmann. Eine Cosserat-Theorie des plastischen Fließens. *Acta Mechanica*, 8:255–284, 1969.

J. Mandel. Une généralisation de la théorie de la plasticité de W.T. Koiter. *Int. J. Solids Structures*, 1:273–295, 1965.

J. Mandel. *Plasticité classique et viscoplasticité*. CISM Courses and Lectures No. 97, Udine, Springer Verlag, Berlin, 1971.

J. Mandel. Equations constitutives et directeurs dans les milieux plastiques et viscoplastiques. *Int. J. Solids Structures*, 9:725–740, 1973.

G.A. Maugin. *The Thermomechanics of plasticity and fracture*. Cambridge University Press, 1992.

G.A. Maugin. The method of virtual power in continuum mechanics : Application to coupled fields. *Acta Mechanica*, 35:1–70, 1980.

G.A. Maugin. Internal variables and dissipative structures. *J. Non–Equilib. Thermodyn.*, 15:173–192, 1990.

G.A. Maugin. *Thermomechanics of nonlinear irreversible behaviors*. World Scientific, 1999.

G.A. Maugin and W. Muschik. Thermodynamics with internal variables, Part I. general concepts. *J. Non-Equilib. Thermodyn.*, 19:217–249, 1994.

J.R. Mayeur, D.L. McDowell, and D.J. Bammann. Dislocation–based micropolar single crystal plasticity: Comparison if multi– and single cristerion theories. *Journal of the Mechanics and Physics of Solids*, 59:398–422, 2011.

F.A. McClintock, P.A. André, K.R. Schwerdt, and R.E. Stoeckly. Interface couples in crystals. *Nature*, 4636:652–653, 1958.

L. Méric and G. Cailletaud. Single crystal modeling for structural calculations. Part 2: Finite element implementation. *J. of Engng. Mat. Technol.*, 113:171–182, 1991.

L. Méric, P. Poubanne, and G. Cailletaud. Single crystal modeling for structural calculations. Part 1: Model presentation. *J. Engng. Mat. Technol.*, 113:162–170, 1991.

L. Méric, G. Cailletaud, and M. Gaspérini. F.E. calculations of copper bicrystal specimens submitted to tension–compression tests. *Acta metall. mater.*, 42:921–935, 1994.

R.D. Mindlin. Micro–structure in linear elasticity. *Arch. Rat. Mech. Anal.*, 16:51–78, 1964.

R.D. Mindlin. Second gradient of strain and surface–tension in linear elasticity. *Int. J. Solids Structures*, 1:417–438, 1965.

R.D. Mindlin and N.N. Eshel. On first strain gradient theories in linear elasticity. *Int. J. Solids Structures*, 4:109–124, 1968.

H. Mughrabi. On the role of stress gradients and long-range internal stresses in the composite model of crystal plasticity. *Mater. Sci. Eng. A*, 317: 171–180, 2001.

H. Mughrabi. Investigations of plastically deformed copper single crystals in the stress-applied state. *Physica Status Solidi*, 39:317–327, 1970.

H. Mughrabi. Introduction to the viewpoint set on : Surface effect in cyclic deformation and fatigue. *Scripta Metallurgica and Materiala*, 26:1499–1504, 1992.

H.B. Mühlhaus and I. Vardoulakis. The thickness of shear bands in granular materials. *Géotechnique*, 37:271–283, 1987.

Mura, T. On dynamic problems of continuous distribution of dislocations. *Int. J. Engng. Sci.*, 1:371–381, 1963.

Mura, T. Continuous distribution of dislocations and the mathematical theory of plasticity. *Phys. stat. sol.*, 10:447–453, 1965.

W. Nowacki. *Theory of asymmetric elasticity.* Pergamon, 1986.

J.F. Nye. Some geometrical relations in dislocated crystals. *Acta Metall.*, 1:153–162, 1953.

R.N. Pangborn, S. Weissmann, and I.R. Kramer. Dislocations distribution and prediction of fatigue damage. *Metallurgical Transaction*, 12A:109–120, 1981.

C. Papenfuss and S. Forest. Thermodynamical frameworks for higher grade material theories with internal variables or additional degrees of freedom. *Journal of Non-Equilibrium Thermodynamics*, 31:319–353, 2006.

A. Paquin. Micromechanical modeling of the elastic-viscoplastic behavior of polycrystalline steels. *International Journal of Plasticity*, 17:1267–1302, 2001.

R. Parisot, S. Forest, A. Pineau, F. Grillon, X. Démonet, and J.-M. Mataigne. Deformation and Damage Mechanisms of Zinc Coatings on Galvanized Steel Sheets, Part I : Deformation Modes. *Metallurgical and Materials Transactions*, 35A:797–811, 2004.

R.H.J. Peerlings, M.G.D. Geers, R. de Borst, and W.A.M. Brekelmans. A critical comparison of nonlocal and gradient–enhanced softening continua. *Int. J. Solids Structures*, 38:7723–7746, 2001.

R.H.J. Peerlings, T.J. Massart, and M.G.D. Geers. A thermodynamically motivated implicit gradient damage framework and its application to brick masonry cracking. *Comput. Methods Appl. Mech. Engrg.*, 193: 3403–3417, 2004.

H. Petryk. Material instability and strain-rate discontinuities in incrementally nonlinear continua. *J. Mech. Phys. Solids*, 40:1227–1250, 1992.

P. Pilvin. Une approche simplifiée pour schématiser l'effet de surface sur le comportement mécanique d'un polycristal. *J. Phys. IV France*, 4: Pr4–33–38, 1998.

J. M. Pipard, N. Nicaise, S. Berbenni, O. Bouaziz, and M. Berveiller. A new mean field micromechanical approach to capture grain size effects. *Computational Materials Science*, 45(3):604–610, 2009.

J.R. Rice. Inelastic constitutive relations for solids: An internal variable theory and its application to metal plasticity. *J. Mech. Phys. Solids*, 19: 433–455, 1971.

E. Sanchez-Palencia. Comportement local et macroscopique d'un type de milieux physiques hétérogènes. *International Journal of Engineering Science*, 12:331–351, 1974.

E. Sanchez-Palencia and A. Zaoui. *Homogenization techniques for composite media*. Lecture Notes in Physics No. 272, Springer, Berlin, 1987.

C. Sansour. A unified concept of elastic–viscoplastic Cosserat and micromorphic continua. *Journal de Physique IV*, 8:Pr8–341–348, 1998a.

C. Sansour. A theory of the elastic–viscoplastic cosserat continuum. *Archives of Mechanics*, 50:577–597, 1998b.

A. Sawczuk. On yielding of Cosserat continua. *Archives of Mechanics*, 19: 3–19, 1967.

R. Sedláček and S. Forest. Non-local plasticity at microscale : A dislocation-based model and a Cosserat model. *physica status solidi (b)*, 221:583–596, 2000.

R. Sedláček, J. Kratochvil, and E. Werner. The importance of being curved: bowing dislocations in a continuum description. *Philosophical Magazine*, 83:3735–3752, 2003.

J.Y. Shu and N.A. Fleck. Strain gradient crystal plasticity : size–dependent deformation of bicrystals. *Journal of the Mechanics and Physics of Solids*, 47:297–324, 1999.

J.Y. Shu, N.A. Fleck, E. Van der Giessen, and A. Needleman. Boundary layers in constrained plastic flow : comparison of non local and discrete dislocation plasticity. *Journal of the Mechanics and Physics of Solids*, 49:1361–1395, 2001.

R. Sievert. *Eine Systematik für elastisch-plastische Stoffgleichungen*. Schriftenreihe Physikalische Ingenieurwissenschaft, Band 23, Techn. Univ. Berlin, 1992.

F. Šiška, S. Forest, P. Gumbsch, and D. Weygand. Finite element simulations of the cyclic elastoplastic behavior of copper thin films. *Modeling and Simulation in Materials Science and Engineering*, 15:S217–S238, 2007.

F. Šiška, D. Weygand, S. Forest, and P. Gumbsch. Comparison of mechanical behaviour of thin film simulated by discrete dislocation dynamics and continuum crystal plasticity. *Computational Materials Science*, 45: 793–799, 2009.

V.P. Smyshlyaev and N.A. Fleck. The role of strain gradients in the grain size effect for polycrystals. *Journal of the Mechanics and Physics of Solids*, 44:465–495, 1996.

L. St-Pierre, E. Héripré, M. Dexet, J. Crépin, G. Bertolino, and N. Bilger. 3D simulations of microstructure and comparison with experimental microstructure coming from oim analysis. *International Journal of Plasticity*, 24:1516–1532, 2008.

P. Steinmann. A micropolar theory of finite deformation and finite rotation multiplicative elastoplasticity. *Int. J. Solids Structures*, 31:1063–1084, 1994.

P. Steinmann. Views on multiplicative elastoplasticity and the continuum theory of dislocations. *International Journal of Engineering Science*, 34: 1717–1735, 1996.

R. Stojanović. *Recent developments in the theory of polar continua.* CISM Courses and Lectures No. 27, Udine, Springer Verlag, Berlin, 1970.

P. Suquet. *Continuum micromechanics.* CISM Courses and Lectures No. 377, Udine, Springer Verlag, Berlin, 1997.

K. Tanaka and T. Mura. A dislocation model for fatigue crack initiation. *Journal of Applied Mechanics*, 48:97–103, 1981.

V. Taupin, S. Berbenni, C. Fressengeas, and O. Bouaziz. On particle size effects: An internal length mean field approach using field dislocation mechanics. *Acta Materialia*, 58:5532–5544, 2010.

C. Teodosiu. A dynamic theory of dislocations and its applications to the theory of the elastic-plastic continuum. In J.A. Simmons, R. de Wit, and R. Bullough, editors, *Fundamental Aspects of Dislocation Theory*, pages 837–876. Nat. Bur. Stand. (US) Spec. Publ. 317, II, 1970.

C. Teodosiu. *Large plastic deformation of crystalline aggregates.* CISM Courses and Lectures No. 376, Udine, Springer Verlag, Berlin, 1997.

C. Teodosiu and F. Sidoroff. A theory of finite elastoviscoplasticity of single crystals. *Int. J. of Engng Science*, 14:165–176, 1976.

C. Teodosiu, J. Raphanel, and L. Tabourot. Finite element simulation of the large elastoplastic deformation of multi-crystals. In C. Teodosiu and F. Sidoroff, editors, *Large Plastic Deformations MECAMAT'91*, pages 153–158. Balkema, Rotterdam, 1993.

H. Tian-Hu. Lagrange multiplier method of the general variational principles of finite deformation theory of couple stress and its application in the strain gradient plasticity. *International Journal of Engineering Science*, 42:1949–1969, 2004.

E. Van der Giessen, V.S. Deshpande, H.H.M Cleveringa, and A. Needleman. Discrete dislocation plasticity and crack tip fields in single crystals. *J. Mech. Phys. Solids*, 49:2133–2153, 2001.

J. Zarka. Généralisation de la théorie du potentiel plastique multiple en viscoplasticité. *Journal of the Mechanics and Physics of Solids*, 20:179–195, 1972.

A. Zeghadi, S. Forest, A.-F. Gourgues, and O. Bouaziz. Cosserat continuum modelling of grain size effects in metal polycrystals. *Proc. Appl. Math. Mech.*, 5:79–82, 2005.

A. Zeghadi, S. Forest, A.-F. Gourgues, and O. Bouaziz. Ensemble averaging stress–strain fields in polycrystalline aggregates with a constrained surface microstructure–Part 2: Crystal plasticity. *Philosophical Magazine*, 87:1425–1446, 2007a.

A. Zeghadi, F. Nguyen, S. Forest, A.-F. Gourgues, and O. Bouaziz. Ensemble averaging stress–strain fields in polycrystalline aggregates with a constrained surface microstructure–Part 1: Anisotropic elastic behaviour. *Philosophical Magazine*, 87:1401–1424, 2007b.

A. Ziegenbein, H. Neuhäuser, J. Thesing, R. Ritter, H. Wittich, E. Steck, and M. Levermann. Local plasticity of Cu–Al polycrystals - measurements and FEM simulation. *J. Phys. IV France*, 8:Pr8–407–412, 1998.

H. Zorski. Statistical theory of dislocations. *Int. J. Solids Structures*, 4: 959–974, 1968.